

**COMPARATIVE EVALUATION OF THE EFFECT OF
DIFFERENT SURFACE TREATMENTS ON THE
BIOACTIVITY OF ZIRCONIA – AN *IN VITRO* STUDY**

Dissertation Submitted to

THE TAMILNADU Dr. M.G.R. MEDICAL UNIVERSITY

In partial fulfilment for the Degree of

MASTER OF DENTAL SURGERY



BRANCH I

PROSTHODONTICS AND CROWN & BRIDGE

MAY 2018

THE TAMILNADU Dr. M.G.R MEDICAL UNIVERSITY
CHENNAI

DECLARATION BY THE CANDIDATE

I hereby declare that this dissertation titled "COMPARATIVE EVALUATION OF THE EFFECT OF DIFFERENT SURFACE TREATMENTS ON THE BIOACTIVITY OF ZIRCONIA – AN *IN VITRO* STUDY" is a bonafide and genuine research work carried out by me under the guidance of Dr. K. CHITRA SHANKAR, M.D.S., Professor, Department of Prosthodontics and Crown & Bridge, Ragas Dental College & Hospital, Chennai.

Date: 09.02.2018

Place: Chennai

A. Gayathree.

Dr. GAYATHREE ALAGIRISWAMY,

Post Graduate Student,

Department of Prosthodontics and Crown &
Bridge,

Ragas Dental College & Hospital,

Chennai.

CERTIFICATE


This is to certify that the dissertation titled “**COMPARATIVE EVALUATION OF THE EFFECT OF DIFFERENT SURFACE TREATMENTS ON THE BIOACTIVITY OF ZIRCONIA – AN *IN VITRO* STUDY**” is a bonafide record work done by **Dr. GAYATHREE ALAGIRISWAMY** under our guidance and to our satisfaction during her postgraduate study period between **2015 – 2018**.

This dissertation is submitted to **THE TAMILNADU Dr. M.G.R. MEDICAL UNIVERSITY**, in partial fulfilment for the Degree of **MASTER OF DENTAL SURGERY – PROSTHODONTICS AND CROWN & BRIDGE, BRANCH I**. It has not been submitted (partial or full) for the award of any other degree or diploma.

Guided by:



Dr. K. CHITRA SHANKAR, M.D.S.,
Professor,
Department of Prosthodontics and
Crown & Bridge,
Ragas Dental College & Hospital,
Chennai.



Dr. N.S. AZHAGARASAN, M.D.S.,
Principal, Professor and Head,
Department of Prosthodontics and
Crown & Bridge,
Ragas Dental College & Hospital,
Chennai.

PROFESSOR
DEPT. OF PROSPHODONTICS
RAGAS DENTAL COLLEGE & HOSPITAL
2/102, EAST COAST ROAD,
UTHANDI, CHENNAI - 119.

Dr. N.S. AZHAGARASAN, MDS,
PRINCIPAL AND PROFESSOR & HOD,
DEPARTMENT OF PROSTHODONTICS AND CROWN & BRIDGE
RAGAS DENTAL COLLEGE AND HOSPITAL
2/102, EAST COAST ROAD, UTHANDI,
CHENNAI - 600 119.

**THE TAMILNADU Dr. M.G.R MEDICAL UNIVERSITY
CHENNAI**

PLAGIARISM CERTIFICATE

This is to certify the dissertation titled “**COMPARATIVE EVALUATION OF THE EFFECT OF DIFFERENT SURFACE TREATMENTS ON THE BIOACTIVITY OF ZIRCONIA – AN *IN VITRO* STUDY**” of the candidate **Dr. GAYATHREE ALAGIRISWAMY** for the award of **MASTER OF DENTAL SURGERY in BRANCH I – PROSTHODONTICS AND CROWN & BRIDGE.**

On verification with the urkund.com website for the purpose of plagiarism check, the uploaded thesis file from introduction to conclusion contains **2 percentage** of plagiarism, as per the report generated and it is enclosed in Annexure – VII.

Date: 08.02.2018

Place: Chennai

A. Gayathree

Dr. GAYATHREE ALAGIRISWAMY
Post Graduate Student,
Department of Prosthodontics and crown
& bridge,
Ragas Dental College and Hospital,
Chennai

Chitra Shankar

Dr. K. CHITRA SHANKAR, M.D.S.,
Guide,
Department of Prosthodontics and Crown &
Bridge
Ragas Dental College and Hospital,
Chennai.

**PROFESSOR
DEPT. OF PROSPHODONTICS
RAGAS DENTAL COLLEGE & HOSPITAL
2112, EAST COAST ROAD,
CHENNAI - 600 019.**



RAGAS DENTAL COLLEGE & HOSPITAL

(Unit of Ragas Educational Society)

Recognized by the Dental Council of India, New Delhi

Affiliated to The Tamilnadu Dr. M.G.R. Medical University, Chennai

2/102, East Coast Road, Uthandi, Chennai - 600 119. INDIA.

Tele : (044) 24530002, 24530003-06. Principal (Dir) 24530001 Fax : (044) 24530009


TO WHOM SO EVER IT MAY CONCERN

Date: 27.01.2018

Place: Chennai

From
The Institutional Review board
Ragas Dental College & Hospital
Uthandi
Chennai- 600119

The dissertation topic titled "**COMPARATIVE EVALUATION OF THE EFFECT OF DIFFERENT SURFACE TREATMENTS ON THE BIOACTIVITY OF ZIRCONIA- AN INVITRO STUDY**" submitted by **Dr.GAYATHREE ALAGIRISWAMY** has been approved by the Institutional Ethics Board of Ragas Dental College & Hospital.


DR. N.S AZHAGARASAN, MDS,
Member Secretary,
Institutional Ethics Board,
Ragas Dental College & Hospital
Uthandi, Chennai - 600119



ACKNOWLEDGEMENT

I am privileged to have joined the department of prosthodontics and I take this opportunity to thank all those who have been a source of support and help throughout the postgraduate program.

*. I am deeply indebted to **Professor Dr. N. S. Azhagarasan, M.D.S., Principal and Head of the Department,** Department of Prosthodontics and Crown & Bridge, Ragas Dental College & Hospital, Chennai, for his conscientious encouragement, solicitude inspiration and constant motivation. I am extremely grateful to him for providing heartfelt support throughout my postgraduate programme and I have successfully overcome many difficulties with his personal attention. He has been a great counsel throughout the duration of this course and has impacted my life in many ways. He is a great rolemodel and very caring and considerate towards students and a very good human being.*

*I am extremely indebted to my **guide Professor Dr. K. Chitra Shankar M.D.S.,** for her wonderful suggestions, motivation, encouragement and personal attention which provided a good and smooth basis for the progress of this research. She has spared a lot of her valuable time right from the synopsis of this project to the final result. Her impeccable writing skills along with her alacrity, cogency and creativity has given a great shape to this dissertation. The guidance, constructive criticism, patience, perseverance and help rendered by her had benefited me enormously throughout this degree program. I am mesmerised by her explicit attention to detail and accuracy and am privileged*

to have got her as a guide for this project. She is a great rolemodel and a source of inspiration to all. I take this opportunity to say heartfelt thanks for the great guidance and help without which this study would not have been possible.

*I would love to sincerely thank **Dr. S. Jayakrishnakumar, M.D.S. Dr. Vallabh Mahadevan, M.D.S., Dr. Vidhya J, M.D.S.,** for sparing their valuable time critiquing my work, helping me with my dissertation and providing a great source of encouragement and support during the most difficult times.*

*I would like to sincerely thank **Dr. Hariharan Ramakrishnan, M.D.S., Dr. Hariharan Ramasubramanian, M.D.S., and Dr. M. Saravanakumar M.D.S.,** for great source of inspiration and support with my seminars, library dissertation and clinical work, and **Dr. Raja Ganesh, M.D.S., Dr. Harish Gopal M.D.S., Dr. Kamakshi, M.D.S., Dr. Rahmath Shameem, M.D.S., Dr. Manoj Kumar Sundar, M.D.S., Dr. Mahadevan, M.D.S.,** for their valuable suggestions, support and help given throughout my postgraduate course. It wouldn't be good on my part if I don't acknowledge the help of non-teaching staff in the prosthodontics section for their help with sterilization and routine day to day work. I would like to thank **Mrs. Kripa, Mrs. Sabeera, Mrs. Selvi and Mrs Sivamani** for their patience and help during critical times and **Mr. Madhan** for his technical support.*

*I would like to wholeheartedly thank Professor **Dr. K. Ramasamy,** Vice-chancellor of Tamil Nadu Agricultural University for permitting me to conduct basic experiments of this study in the centre for Plant Molecular Biology and*

Biotechnology with the support of Directors and Professors of Centre for Plant Molecular Biology and Biotechnology.

*I am extremely thankful to **Dr. Deepanandan M.D.S.**, Professor and Head, Department of Oral-Maxillo Facial Surgery, Sri Ramakrishna Dental College, Coimbatore and **Dr. Geetha Deepanandan M.D.S.**, Ezhil Dental clinic for their support in providing dental equipments used in this research. I greatly appreciate for their guidance and valuable support during this study.*

*I would like to thank **Mr. Kumaraguruparan, Mr. Raman and Mr.Senthilkumar P**, Vitalium dental laboratory, Chennai for providing the zirconia samples. I would like to extend my thanks to **Dr. Pon Pandiyan**, Professor and Head and **Dr. Rajendrakumar**, Associate Professor, Department of Nanoscience and Technology, Bharathiar University, Coimbatore for helping with the XRD, Profilometer, Contact angle goniometry, SEM and EDX analysis. I express my sincere thanks to the research scholars **Mr. Divagar, Mrs. Rebekah Gladys, Miss. Deepthy and Mr. Dinesh** for their help in the abovementioned analysis.*

*I wish to thank **Dr. P. Biji**, Associate Professor and **Mr. Karthikeyan**, Research scholar of Department of Nanoscience and Technology, PSG institute of Advanced studies, Coimbatore for helping me with AFM analysis.*

*I wholehearted express my heartfelt thanks to **Dr. Suganthan and Dr. Pragadeesh of TNAU** for their constant support and timely help in conducting the experiments and preparation of simulated body fluid. I am extremely grateful to **Dr. Suman, and Dr. Radhika**, Centre for Ocean Research,*

Sathyabama University, Chennai for helping me with ICP-MS technology used in the study.

*I wish to thank Professor **Dr. Duraisamy, Professor and Head** of the Department of Physical Sciences and Information Technology, TNAU for help with statistical analysis and **Mr. Thavamani** of **Scribbles India** for his valuable time in helping with final printouts of this dissertation.*

*It would not be justifiable on my part if I do not acknowledge the help of my senior batchmates **Dr. Ambedkar, Dr. Pavankumar Vaddempudi, Dr. Revathi D, Dr. Sherin Grace Babu, Dr. Mahalakshmi B, Dr. Arul Kumar N,** my very supportive batchmates, **Dr. Abinaya S, Dr. Ashwini Sukanya GU, Dr. Janani D, Dr. Priyadarshini T, Dr. Sethu Raman R** for being very understanding and caring, my junior batchmates **Dr. Jency Sara George, Dr. Maniamuthu R** for being supportive throughout the course and for sparing their valuable time helping me with my dissertation work, **Dr. Ashish M, Dr. Badimela Arjun, Dr. Samin Hallaj Mogadam, Dr. Manimala Murthy, Dr. Yasmin fathima, Dr Aishwarya, Dr Surabhi halder** for their timely help and continuous support during the past couple of years. I would like to specially thank my friend, **Dr. Aparnna Dayanidhi** for her constant support, encouragement and help throughout the postgraduate program.*

*This journey would not have been possible without the support of my family. I am grateful to my father **Mr A.R Alagiriswamy**, mother **Dr. S. Krishnaveni**, brother **Mr. Manjunaath O.A**, my sister-in-law **Dr. Suganya***

Anandaraman and the little one Mas. Sharvaa, for their love, sacrifice, constant support and encouragement during this course.

*Last but not the least, I thank **God Almighty** for the blessings, courage and grace endowed upon me.*

CONTENTS

S.No.	TITLE	PAGE No.
1.	INTRODUCTION	01
2.	REVIEW OF LITERATURE	09
3.	MATERIALS AND METHODS	19
4.	RESULTS	35
5.	DISCUSSION	50
6.	CONCLUSION	68
7.	SUMMARY	72
8.	BIBLIOGRAPHY	74

LIST OF TABLES

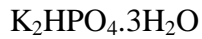
TABLE No.	TITLE	PAGE No.
1	Basic values and mean of surface roughness (nm) of representative samples of Groups I, II & III (n=1/Group), measured at 4 distinct areas per sample by 3D Atomic Force Microscopy (AFM)	37
2	Comparative evaluation of mean surface roughness (Sa in nm) between Groups I, II and III for overall significance by One-Way Analysis of Variance (ANOVA)	38
3	Comparative evaluation of mean surface roughness (Sa in nm) between Groups I, II and III by Multiple Post-hoc Tukey's HSD test	39
4	Basic values and mean of contact angles (degrees) denoting wettability as measured using contact angle goniometry for representative samples of Groups I, II and III (n=5/Group)	40
5	Comparative evaluation of the surface wettability between the mean contact angles of Groups I, II and III for overall significance by One-Way Analysis of Variance (ANOVA)	41
6	Comparative evaluation of mean contact angle measurements between Groups I, II and III by Multiple Post-hoc Tukey's HSD test	42
7	Basic values and mean pre-immersion calcium content (Reference value in mg/L) in Simulated Body Fluid (SBF) obtained by Inductively Coupled Plasma Mass Spectrometry (ICP-MS)	43

8	Basic values and mean of post-immersion calcium content (mg/L) in SBF of Group I (Untreated) samples obtained by Inductively Coupled Plasma Mass Spectrometry (ICP-MS)	44
9	Basic values and mean of post-immersion calcium content (mg/L) in SBF of Group II (Sandblasted) samples obtained by Inductively Coupled Plasma Mass Spectrometry (ICP-MS)	45
10	Basic values and mean of post-immersion calcium content (mg/L) in SBF of Group III (UVP) samples obtained by Inductively Coupled Plasma Mass Spectrometry (ICP-MS)	46
11	Comparative evaluation of the difference between the pre-immersion calcium content (Reference value) and the mean post-immersion calcium content obtained for Groups I, II & III respectively, using student's paired 't' test	47
12	Comparative evaluation of post-immersion calcium content in SBF between Groups I, II and III for overall significance by One-Way Analysis of Variance (ANOVA)	48
13	Comparative evaluation of mean post-immersion calcium content in SBF between Groups I, II and III by Multiple Post-hoc Tukey's HSD test	49

ANNEXURE I
METHODOLOGY – OVERVIEW

ANNEXURE II
LIST OF FIGURES

Fig. No.	TITLE
Fig. 1a &1b	: Universal light cure modeling paste
Fig. 2a	: Manufacturer package of yttria-stabilized zirconia blank
Fig. 2b	: Yttria-stabilized zirconia blank
Fig. 3a	: Silicon carbide emery paper - 600 grit
Fig. 3b	: Silicon carbide emery paper - 800 grit
Fig. 3c	: Silicon carbide emery paper - 1000 grit
Fig. 3d	: Silicon carbide emery paper - 1200 grit
Fig. 4	: Alumina powder 50 µm for sandblasting
Fig. 5	: Customised deionised water
Fig. 6	: Petri plate
Fig. 7	: 30 watts Ultraviolet lamp
Fig. 8a	: Sodium chloride, NaCl
Fig. 8b	: Sodium hydrogen carbonate, NaHCO ₃
Fig. 8c	: Potassium chloride, KCl
Fig. 8d	: Di-potassium hydrogen phosphate trihydrate,



- Fig. 8e** : Magnesium chloride hexahydrate, $MgCl_2 \cdot 6H_2O$
- Fig. 8f** : Calcium chloride, $CaCl_2$
- Fig. 8g** : Sodium Sulphate, Na_2SO_4
- Fig. 8h** : Tris-hydroxymethyl aminomethane, $(HOCH_2)_3CNH_2$
- Fig. 8i** : Hydrochloric acid, HCl
- Fig. 9** : Artery forceps
- Fig. 10** : Sandpaper mandrel
- Fig. 11** : Tweezer
- Fig. 12** : Desiccator
- Fig. 13** : Plastic beaker
- Fig. 14** : Laboratory thermometer
- Fig. 15** : Volumetric flask (1 L)
- Fig. 16** : Graduated polypropylene test tubes
- Fig. 17** : Conical centrifuge tube rack
- Fig. 18** : Light curing unit
- Fig. 19** : Copy milling machine
- Fig. 20** : Sintering unit
- Fig. 21** : Dental Micromotor
- Fig. 22** : Sandblasting unit
- Fig. 23** : Digital Ultrasonic cleaner
- Fig. 24** : UV laminar flow hood

- Fig. 25** : X-ray Diffractometer
- Fig. 26a** : Set up for Multimode Scanning Probe Microscopy (Atomic Force Microscopy) unit
- Fig. 26b** : Main unit of AFM
- Fig. 27** : Contact Angle Goniometer
- Fig. 28a** : Set up for Field Emission Scanning Electron Microscopy (FEI Quanta – 250 FEG) with Energy Dispersive X-ray Spectroscopy
- Fig. 28b** : Main unit of SEM
- Fig. 29** : Analytical Weighing Balance
- Fig. 30** : Magnetic Stirrer with hot plate
- Fig. 31** : pH tester
- Fig. 32** : Inductively coupled Plasma Mass Spectrometer (ICP-MS)
- Fig. 33** : Bacteriological Incubator
- Fig. 34a** : Disc made from universal light cure modeling paste
- Fig. 34b** : Light curing the modelling paste for 12 minutes
- Fig. 34c** : Light cured millable resin disc
- Fig. 34d** : Copy-milling of zirconia blank
- Fig. 34e** : Close up view of the resin pattern
- Fig. 34f** : Zirconia sample before sintering
- Fig. 34g** : Zirconia sample after sintering at 1500°C for 8 hours

- Fig. 34h** : Zirconia sample
- Fig. 35a** : Zirconia disc samples (10x10 mm with 2mm thickness)
- Fig. 35b** : Schematic Representation of zirconia discs
- Fig. 36** : Emery Treatment of zirconia samples
- Fig. 37a** : Group I (Untreated)
- Fig. 37b** : Group II (Sandblasted)
- Fig. 37c** : Group III (UVP)
- Fig. 38** : Sandblasting with Alumina powder(50 μ m) for Group II samples
- Fig. 39a** : Ultrasonic cleaning in progress
- Fig. 39b** : Samples placed in the ultrasonic bath
- Fig. 40a** : Test samples placed in the laminar flow hood for UVP
- Fig. 40b** : Group III samples being subjected to UVP in laminar flow hood
- Fig. 41** : Test samples of Group I, Group II & Group III (n=11/Group) after respective surface treatments
- Fig. 42** : Test samples of Groups I, II & III stored in Desiccator for further analysis
- Fig. 43** : Zirconia test sample placed on the platform of X- Ray Diffractometer for analysis
- Fig. 44** : Zirconia test sample placed on AFM for analysis
- Fig. 45a** : One μ l of water placed on platform of goniometer for contact angle measurement

- Fig. 45b** : Water droplet on test sample
- Fig. 45c** : Image of contact angle measurement recorded
- Fig. 46a** : Gold sputtered test samples of Groups I, II and III for SEM-EDX analysis
- Fig. 46b** : Zirconia test sample placed on SEM for analysis
- Fig. 47a** : SBF solution being prepared over the magnetic stirrer with hotplate and with pH tester in place
- Fig. 47b** : pH tester showing pH 7.4 for the SBF solution
- Fig. 48** : Freshly prepared Simulated Body Fluid (SBF) stored in an airtight container
- Fig. 49a** : Immersion of a test sample in SBF solution in a graduated test tube
- Fig. 49b** : Close-up view of test sample from Fig. 46a
- Fig. 50a** : Group I (Untreated) test samples in SBF (n=10)
- Fig. 50b** : Bird's eye view of Group I (Untreated) test samples
- Fig. 51a** : Group II (Sandblasted) test samples in SBF (n=10)
- Fig. 51b** : Bird's eye view of Group II (Sandblasted) test samples
- Fig. 52a** : Group III (UVP) test samples in SBF (n=10)
- Fig. 52b** : Bird's eye view of Group III (UVP) test samples
- Fig. 53** : Incubation of test samples at 36.5°C
- Fig. 54a** : Test samples in desiccator after immersion in SBF
- Fig. 54b** : Test samples in desiccator with lid
- Fig. 55** : Analysis of calcium content in SBF using ICP-MS

ANNEXURE – III

ANALYSIS OF SURFACE CHARACTERISTICS OF UNTREATED AND SURFACE TREATED REPRESENTATIVE SAMPLES

Fig. No.	TITLE
Fig. 56a:	Representative X-Ray Diffractogram (XRD) of Group I (Untreated) test sample
Fig. 56b:	Representative X-Ray Diffractogram (XRD) of Group II (Sandblasted) test sample
Fig. 56c:	Representative X-Ray Diffractogram (XRD) of Group III (UVP) test sample
Fig. 57a:	Representative 2D image of surface of Group I (Untreated) test sample
Fig. 57b:	Representative 2D image of the surface of Group II (Sandblasted) test sample
Fig. 57c:	Representative 2D image of surface of Group III (UVP) test sample
Fig. 58a:	Representative 3D image of surface roughness of Group I (Untreated) test sample
Fig. 58b:	Representative 3D image of surface roughness of Group II (Sandblasted) test sample
Fig. 58c:	Representative 3D image of surface roughness of Group III (UVP) test sample

- Fig. 59a:** Representative contact angle measurement image of Group I (Untreated) test sample
- Fig. 59b:** Representative contact angle measurement image of Group II (Sandblasted) test sample
- Fig. 59c:** Representative contact angle measurement image of Group III (UVP) test sample
- Fig. 60a:** Representative photomicrograph of surface topography of Group I (Untreated) test sample under 5000x magnification
- Fig. 60b:** EDX spectrum of surface elemental analysis graph of Group I (Untreated) test sample
- Fig. 61a:** Representative photomicrograph of surface topography of Group II (Sandblasted) test sample under 5000x magnification
- Fig. 61b:** EDX spectrum of surface elemental analysis graph of the Group II (Sandblasted) test sample
- Fig. 62a:** Representative photomicrograph of surface topography of Group III (UVP) test sample under 5000x magnification
- Fig. 62b:** EDX spectrum of surface elemental analysis graph of the Group III (UVP) test sample

ANNEXURE IV
LIST OF GRAPHS

BAR GRAPHS FOR SURFACE ROUGHNESS AND WETTABILITY DATA

GRAPH. No.	TITLE
1.	Comparative evaluation of mean surface roughness (Sa in nm) between Groups I, II and III
2.	Basic values and mean of contact angle measurements (degrees) for Group I (Untreated) test samples
3.	Basic values and mean of contact angle measurements (degrees) for Group II (Sandblasted) test samples
4.	Basic values and mean of contact angle measurements (degrees) for Group III (UVP) test samples
5.	Comparative evaluation of mean contact angle measurements between Groups I, II and III

ANNEXURE V
LIST OF GRAPHS
BAR GRAPHS FOR BIOACTIVITY DATA

GRAPH.	TITLE
No.	
6.	Basic values and mean of pre-immersion Ca-content (Reference value in mg/L) in Simulated Body Fluid (SBF)
7.	Basic values and mean of post-immersion Ca-content (mg/L) in SBF of Group I (Untreated) samples
8.	Basic values and mean of post-immersion Ca-content (mg/L) in SBF of Group II (Sandblasted) samples
9.	Basic values and mean of post-immersion Ca-content (mg/L) in SBF of Group III (UVP) samples
10.	Comparative evaluation of the difference between the pre-immersion calcium content (Reference value) and the mean post-immersion calcium content obtained for Groups I, II and III respectively
11.	Comparative evaluation of mean post-immersion Ca-content in SBF between Groups I, II and III

ANNEXURE – VI

ANALYSES OF SURFACE CHARACTERISTICS OF UNTREATED AND SURFACE TREATED TEST SAMPLES AFTER 3 WEEKS IMMERSION IN SBF

FIG. No.	TITLE
Fig. 63a :	Representative X-Ray Diffractogram of Group I (Untreated) test sample
Fig. 63b :	Representative X-Ray Diffractogram of Group II (Sandblasted) test sample
Fig. 63c :	Representative X-Ray Diffractogram of Group III (UVP) test sample
Fig. 64a :	Representative photomicrograph of surface topography of Group I (Untreated) test sample under 5000x magnification
Fig. 64b :	EDX spectrum of surface elemental analysis of the Group I (Untreated) test sample
Fig. 65a :	Representative photomicrograph of surface topography of Group II (Sandblasted) test sample under 5000x magnification
Fig. 65b :	EDX spectrum of surface elemental analysis of the Group II (Sandblasted) test sample
Fig. 66a :	Representative photomicrograph of surface topography of Group III (UVP) test sample under 5000x magnification
Fig. 66b :	EDX spectrum of surface elemental analysis of the Group III (UVP) test sample

ANNEXURE-VII

PLAGIARISM REPORT

Introduction

INTRODUCTION

Developments in clinical prosthodontics are driven by the introduction of new dental materials and processing technologies.^{1,3,4,7,10,30,45} The research in implant biomaterials is surging since past few decades due to a continuous increase in the aging population, who demand increasingly functional and aesthetic prosthodontic replacements.^{25,44,50,52} The criteria for a restorative material to be termed as a 'biomaterial' is that it has to be biocompatible with excellent aesthetic and mechanical properties.^{1,19,52,60} Titanium is an excellent implant biomaterial that has been used for the past several decades with appreciable success.^{3,4,36,50,74} Despite this, research in titanium alternatives for use as implant biomaterials is increasing.^{1,3,4,7,14,30,50,52} In response to the high demand for highly aesthetic, metal-free and biocompatible implant biomaterials, zirconia ceramics are the most frequently researched non-metallic implant biomaterial alternative due to their excellent aesthetics, biocompatibility, soft tissue stability, low plaque accumulation, and bone-like colour.^{1,7,14,25,38,44,52,54,58,60}

Zirconia, the metal dioxide (ZrO_2), was identified in 1789 by the German chemist Martin Heinrich and exists in three different crystal forms depending on the temperatures.^{1,7,19,21,54} Zirconia adopts a monoclinic (m) structure at room temperature and transforms into the tetragonal phase (t) at 1170°C, followed by a cubic phase (c) at 2370°C.^{21,43,44,50,54} Tetragonal zirconia has superior mechanical

properties but has a tendency to revert to monoclinic phase at room temperature, which is known as low temperature degradation (LTD).^{1,15,18,21,28,30,43,44,54} To prevent transformation to monoclinic phase and to ensure preservation of the mechanical properties, stabilizers like yttria, ceria, are added to retain the tetragonal polycrystalline form.^{1,14,19,30} This is also referred to as yttria stabilized zirconia or Y-TZP. Despite addition of stabilizing elements, zirconia is a bioinert material^{10,18,33,58} and this aspect may impact its osseointegration potential.^{22,33,42} Hence, studies focusing on surface treatments of zirconia to render the surface more receptive to osseointegration and apatite formation have gained significance.^{18,22,48} However, t-m phase conversions after certain surface treatments that can deleteriously affect the longevity of zirconia as an implant biomaterial has also been reported,^{1,15,43,80} and hence ascertaining maintenance of the tetragonal phase following any type of surface treatment of zirconia is crucial in bioactivity studies. Various reports are available stating the importance of surface topography and characteristics, such as, surface roughness and wettability on the extent of bioactivity of zirconia,^{1,3,47,48,50} following different surface treatments. Wettability has been suggested as a key parameter that impacts the chain of processes associated with osseointegration.^{12,46,59,67,68,75,78} The surface topography and elemental composition is also thought to influence the maintenance of the tetragonal phase as well as affect its bioactivity. Thus, bioactivity studies also typically include surface characteristics investigations comparing untreated and

treated zirconia surfaces to explain the bioactivity.^{18,48,64,65,75} Methods like XRD, AFM, contact angle goniometry, SEM-EDX are employed by researchers to assess crystal phase, roughness, wettability, topography and elemental composition, respectively.

Several reports have summarized different additive and subtractive surface modification methods to improve surface properties of zirconia implant biomaterials and the improvement in bone bonding achieved due to the same as compared to untreated surfaces.^{3,26,27,29,50,52,65} These include, air-borne particle abrasion^{9,22,28,55,65}, acid etching with different acids and concentrations^{18,22,47,71} airborne particle abrasion and acid etching^{9,65}, calcium apatite coatings^{52,55,58}, bioactive glass infiltration^{33,66}, Er,Cr: YSGG laser application,^{37,47} and ultra-violet light photofunctionalization (UVP)^{12,49,59,67,68,75} with promising results.

Airborne particle abrasion known as sandblasting technique has been used to increase surface roughness of zirconia^{2,9,13,15,22,28,37,48}, that has been shown to positively impact osseointegration in cell culture studies.^{9,22,48,56,65} One concern that is often mentioned is that, sandblasting could result in damage to the zirconia surface, thereby altering the vital surface characteristics. Airborne-particle abrasion with alumina particles lesser than 100 μm in size has been identified as a key factor in achieving an optimum surface roughness to enhance biological response of osteoblasts without causing structural damage to zirconia.^{9,22,48,57,65,66}

Recently, researchers have turned their focus on the development of UV Photofunctionalization (UVP) for surface modification of zirconia as a simple and inexpensive surface treatment to enhance the osseointegration potential.^{12,49,59,67,68,75} Studies have shown that UV treatment makes the zirconia surface "superhydrophilic" in addition to reducing the hydrocarbon contamination of surfaces, which improves its bioactivity. There are studies focusing on the behaviour of UVP treated zirconia in controlled cell culture and protein adsorption studies, with encouraging results.^{8,38,67,68}

"Bioactivity" is one of the characteristics of an implant material which allows it to form a bond with living tissue.^{3,18,34} Various approaches have been suggested to evaluate the bioactivity of implant surfaces such as *in vitro* (laboratory),^{18,33,65} *in vivo* (clinical trials)^{31,58,62,63} and *ex vivo* analyses.^{33,48} *In vitro* testing includes osteoblastic cell culture, Simulated Body Fluid (SBF) analysis and protein adsorption assays and has been used to mimic *in vivo* conditions, thereby decreasing time, cost and regulatory issues⁴ and it can be manipulated by researchers in a controlled manner.^{4,9,27,29,38,42,48}

Studies have recommended the use of *in vitro* bioactivity tests such as, immersion of synthetic materials into solutions like Simulated Body Fluid (SBF), that replicate the mineral content of human plasma.^{35,39,63,69} The calcium and phosphorus content in SBF form apatite precipitation on these biomaterials to varying extents, depending on the material, their surface characteristics, duration

of immersion environment, etc.^{1,69,72,73} Thus, immersion in SBF can aid to predict *in vivo* behaviour of a potential implant biomaterial. *In vitro* testing of bioactivity in SBF has also minimized the requirement of animal studies.^{38,35,39,62}

Calcium content analysis of the SBF solution by Inductively Coupled Plasma Mass Spectrometry (ICP-MS) both prior to and after immersion of samples has been recommended as a reliable method to assess the apatite precipitation, that indicates its bioactivity.^{18,41,69,70,72} Cell culture and protein adsorption studies exploring the bioactive potential of sandblasting and UVP surface treatments on zirconia are available in the literature.^{5,8,9,29,38,65,66,67,72,75,78,81} However, bioactivity studies focusing on the ability of sandblasting and UVP surface treatments of zirconia in inducing apatite precipitation using SBF are lacking. Surface characteristics such as, type of crystal phase, topography and elemental composition may undergo alterations after exposure to the SBF environment and can impact the longevity as well as indicate bioactivity of zirconia biomaterial. Thus, studying these characteristics aid in correlation of bioactivity results and are frequently employed as an adjunct in such studies.^{32,48,59,73,75,79}

In light of the above, the aim of the present *in vitro* study was to evaluate and compare the effects of two different surface treatments, namely, sand blasting and UV Photofunctionalization (UVP) on the bioactivity of zirconia. The null hypothesis of the present study was that these two surface treatments will not have any significant difference on the bioactivity of zirconia.

The objectives of the present study included:

1. To evaluate the type of crystal phase (monoclinic/tetragonal/cubic) on representative samples of untreated zirconia (Group I), zirconia sample treated by sandblasting with alumina (Group II), and zirconia sample treated by UV Photofunctionalization (Group III) by X-Ray Diffractometry (XRD).
2. To evaluate qualitatively and quantitatively on representative samples, the surface roughness of untreated zirconia (Group I), zirconia samples treated by sandblasting with alumina (Group II), and zirconia samples treated by UV Photofunctionalization (Group III) by 3-D Atomic Force Microscopy (AFM).
3. To compare the surface roughness of untreated zirconia samples (Group I), zirconia samples treated by sandblasting with alumina (Group II), and zirconia samples treated by UV Photofunctionalization (Group III) with respect to each other.
4. To evaluate the wettability (hydrophilicity) of untreated zirconia samples (Group I), zirconia samples treated by sandblasting with alumina (Group II), and zirconia samples treated by UV Photofunctionalization (Group III) by contact angle goniometry.
5. To compare the wettability (hydrophilicity) of untreated zirconia samples (Group I), zirconia samples treated by sandblasting with alumina (Group II), and zirconia samples treated by UV Photofunctionalization (Group III) with respect to each other.

6. To evaluate qualitatively and quantitatively, the surface characteristics and elemental composition, of representative samples of untreated zirconia (Group I), zirconia samples treated by sandblasting with alumina (Group II), and zirconia samples treated by UV Photofunctionalization (Group III), employing Scanning Electron Microscopy coupled with Energy Dispersive X-ray Spectroscopy (SEM-EDX) respectively.
7. To assess the calcium-ion content in freshly-prepared Simulated Body Fluid (SBF) prior to immersion of the test samples, by performing Ca-Simulated Body Fluid (Ca-SBF) analysis employing Inductively Coupled Plasma Mass Spectrometry (ICP-MS).
8. To evaluate the bioactivity of untreated zirconia samples (Group I), by performing post-immersion Ca-Simulated Body Fluid (Ca-SBF) analysis employing Inductively Coupled Plasma Mass Spectrometry (ICP-MS), following a 3 weeks immersion period.
9. To evaluate the bioactivity of zirconia samples treated by sandblasting with alumina (Group II), by performing post-immersion Ca-Simulated Body Fluid (Ca-SBF) analysis employing Inductively Coupled Plasma Mass Spectrometry (ICP-MS), following a 3 weeks immersion period.
10. To evaluate the bioactivity of zirconia samples treated by UV Photofunctionalization (Group III), by performing post-immersion Ca-

- Simulated Body Fluid (Ca-SBF) analysis employing Inductively Coupled Plasma Mass Spectrometry (ICP-MS), following a 3 weeks immersion period.
11. To compare the mean post-immersion Ca-content in SBF of all the three test groups with the pre-immersion Ca-content of Simulated Body Fluid (SBF), to assess calcium depletion (bioactivity).
 12. To compare the bioactivity of zirconia samples obtained by two different surface treatments (Groups II & III) with respect to the untreated samples (Group I) and to each other.
 13. To evaluate the type of crystal phase (monoclinic/tetragonal/cubic) on representative samples of untreated zirconia (Group I), zirconia sample treated by sandblasting with alumina (Group II), and zirconia sample treated by UV Photofunctionalization (Group III) by X-ray Diffractometry (XRD) following a 3 weeks immersion period.
 14. To evaluate qualitatively and quantitatively, the post-immersion surface topography and elemental composition of representative samples of untreated zirconia (Group I), zirconia samples treated by sandblasting with alumina (Group II), and zirconia samples treated by UV Photofunctionalization (Group III), by Scanning Electron Microscopy coupled with Energy Dispersive X-ray Spectroscopy (SEM-EDX) respectively.

Review of Literature

REVIEW OF LITERATURE

Uchida *et al* (2001)⁶⁹ investigated the apatite-forming ability of zirconia gels with different amorphous, tetragonal/ monoclinic structures in Simulated Body Fluid (SBF). Zirconia gel with an amorphous structure formed only a small amount of apatite on its surface, after 14 days immersion in SBF, whereas gels with tetragonal or monoclinic structures were fully covered with apatite within 14 days of immersion. They concluded that specific arrangements of Zr-OH groups in tetragonal/monoclinic zirconia were effective in inducing apatite nucleation.

Uchida *et al* (2002)⁷⁰ investigated the induction of an apatite forming ability on a nano-composite of a ceria-stabilized tetragonal zirconia polycrystals (Ce-TZP) and alumina (Al_2O_3) polycrystals via chemical treatment with aqueous solutions of H_3PO_4 , H_2SO_4 , HCl and NaOH. They concluded that the composite was shown to form a bonelike apatite layer when immersed in a simulated body fluid due to formation of Zr-OH surface functional groups.

Borges *et al* (2003)¹¹ reported through Scanning Electron Microscopy (SEM) evaluation, that the air-abrasion with $50\ \mu\text{m}$ Al_2O_3 for 5s at 4-bar pressure was not able to create irregularities on the surface of In-Ceram Zirconia.

Oyane *et al* (2003)⁵¹ conducted experiments to revise conventional SBF (c-SBF) to prepare new SBFs, namely revised SBF (r-SBF), ionised SBF (i-SBF) and modified SBF (m-SBF) with ion concentrations equal to or closer to those of blood plasma and reported that the r-SBF and i-SBF are less stable than

the c-SBF and m-SBF in terms of changes in ion concentrations relative to storage period. They concluded that m-SBF was optimal for in vitro bioactivity assessment of artificial materials and for biomimetic production of bone-like apatite.

Liu *et al* (2006)⁴² in their study fabricated zirconium oxide thin films on silicon wafers using a filtered cathodic arc system and the surface composition of the zirconium oxide thin films characterized by Atomic Force Microscopy (AFM), X-ray diffraction (XRD), Rutherford Backscattering Spectrometry (RBS) and transmission electron microscopy (TEM) revealed change in their nanostructure. The bioactivity assessed after soaking in simulated body fluids indicated formation of apatite due to nanostructured surface of ZrO₂ thin films which was conducive for favourable bioactivity and cytocompatibility.

Bachle *et al* (2007)⁹ investigated the osteoblastic response to airborne particle abraded and acid-etched zirconia polycrystal (Y-TZP) with different surface topographies using CAL72 osteoblast-like cells. The surface roughness of Y-TZP was increased by airborne particle abrasion and additionally by acid etching. No statistically significant differences were found between average roughness (R_a) and maximum peak-to-valley height (R_{p-v}) values of airborne particle abraded and acid-etched Y-TZP and SLA titanium. Whereas the cell proliferation assay revealed statistically significant greater values at day 3 for surface-treated Y-TZP suggesting that roughened Y-TZP is an appropriate substrate for the proliferation and spreading of osteoblastic cells.

Della Bona *et al* (2007)¹⁹ characterized the microstructure, composition and physical properties of a glass-infiltrated alumina/zirconia-reinforced ceramic (IZ) and the effect of surface treatment such as sandblasting with 25 μ m Al₂O₃ particles for 15 s, HF-etching with 9.5% hydrofluoric acid for 90 and SC-blasting with 30mm aluminum oxide particles modified by silica (silica coating) for 15s on topography. They concluded that an increase in the roughness (Ra) of In-Ceram Zirconia (from 207 nm to 1000 nm) was due to the use of 25 μ m Al₂O₃ air-abrasion at a distance of 10 mm for 15 s, at a pressure of 2.8 bars through quantitative and qualitative analyses using the respective equipments.

Ferguson *et al* (2008)²³ conducted in vivo studies in sheep evaluating titanium and zirconia implants by exposing to 6 different surface treatments including sand blasting and acid etching. They concluded that there were no differences in surface treatments between Ti and zirconia implants by comparing peri-implant bone density and removal torque for a period of 2, 4, and 8 weeks after implantation.

Casucci *et al* (2009)¹³ evaluated the effect of airborne particle abrasion with 125 μ m Al₂O₃ along with other surface treatments of zirconia ceramic. Ceramic discs surfaces were analysed by atomic force microscopy (AFM) for average surface roughness and for bi-dimensional surface characterization with scanning electron microscope (SEM) on a nanometric scale. Statistical analysis indicated that ceramic surface treatments significantly influenced surface topography and roughness (p<0.001).

Han *et al* (2008)²⁹ evaluated pure ZrO₂ films roughened by micro-arc oxidation and concluded that enhanced hydrophilicity and bioactivity upon irradiation with UV treatment at a wavelength of 300-400nm.

Wang *et al* (2010)⁷² reported that a monoclinic zirconia coating with a nanostructural surface prepared on the Ti–6Al–4V substrate by an atmospheric plasma-spraying technique enhanced bone-like apatite precipitation on the surface of the coating after soaking in SBF for 6 days, indicating excellent bioactivity in vitro due to zirconia coating. Morphological observation and the cell proliferation test demonstrated that osteoblast-like MG63 cells could attach, adhere and proliferate well on the surface of zirconia.

Dehestani *et al* (2012)¹⁸ evaluated zirconia after its surface treatment with 5M H₃PO₄ and alternate soaking of zirconia in calcium chloride/sodium hydrogen phosphate solutions. Both surface treatments resulted in change of surface characteristics as revealed by XPS and XRD and enhanced formation of hydroxyapatite indicating the bioactivity potential of zirconia.

Hallman *et al* (2012)²⁸ evaluated the effect of different blasting pressures and airborne particle composition and size on phase transformation and surface morphological change of yttria-stabilized tetragonal polycrystalline zirconia (Y-TZP). Specimens sintered at 1350 °C for 2 h were abraded with 50 μm and 110 μm alumina at pressures of 1, 1.5, 2, 2.5, 3 and 3.5 bar. The Y-TZP was characterized using XPS, FESEM and XRD and t–m phase transformation were observed after air abrasion process. They concluded that the extent of morphological change and t–m phase transformation of abraded surface

depended on the blasting pressures and size of abrasive particle. The abrasion of the ceramic surface with 50 μm or 110 μm alumina airborne particle at pressures of 2.5 or 1.5 bar, respectively, was regarded as the optimum blasting condition.

Queiroz *et al* (2012)⁵⁷ evaluated Y-TZP surface after different airborne particle abrasion protocols using alumina and silica with sintered and polished seventy-six Y-TZP ceramic blocks. By analysing surface topography and statistical analysis, they concluded that the sandblasting protocols using alumina particles were dependent on application duration, particle size and pressure and they influenced the topographic pattern and amplitude of the roughness parameters.

Watanabe *et al* (2012)⁷⁵ studied the roughened effects of sandblasting and acid-etching converting the discs of TZP “superhydrophilic”, a significant decrease of surface carbon and an enhanced initial attachment of mouse osteoblast-like cells (MC3T3-E1) upon UV treatment.

Chintapalli *et al* (2013)¹⁵ evaluated commercial grade 3Y-TZP specimens after sandblasting using different particle sizes (110 μm and 250 μm) and pressures (2 and 4bar) for 10s for phase transformation using X-ray diffraction. They concluded that sandblasting induced monoclinic volume fraction is in the range of 12-15% on the surface and the subsurface damage was found to be larger in specimens sandblasted with large particles.

Noro *et al* (2013)⁴⁹ evaluated different surface treatments such as alumina blasting and acid etching, oxygen (O₂) plasma, ultraviolet (UV) light

and hydrogen peroxide treatment. Several types of surface topography were produced by alumina blasting and acid etching with hydrofluoric acid. Alumina blast /acid etching as well as O₂ plasma and UV treatment, greatly increased the surface wettability, resulting in super hydrophilicity. The results showed a remarkable decrease in carbon content and the introduction of hydroxyl groups were responsible for the observed superhydrophilicity, which plays an important role in osseointegration.

Han *et al* (2014)²⁹ compared nanocomposite 3Y TZP, CpTi for their surface characteristics such as surface roughness (Ra), surface wettability and surface morphology through FESEM analysis. Surface roughness and morphology were almost similar and found statistically significant. Bioactivity by using cell attachment, cell morphology and ALP activity exhibited similar cell viability.

Abi-Rached *et al* (2014)² evaluated the effect of airborne-particle abrasion protocols on the surface roughness, wettability, and morphology of an yttria-stabilized tetragonal zirconia polycrystal ceramic by taking 7 groups with a total of 140 Lava zirconia specimens. Their surfaces were abraded with airborne-particles of different sizes. i.e. No treatment (control), 50- μ m, 120- μ m, 250- μ m Al₂O₃ particles and 30- μ m, 110- μ m and 120- μ m silica-coated Al₂O₃ particles. Statistical analyses (ANOVA) indicated no significant difference among the groups concerning wettability. The control group exhibited the lowest mean roughness value (Ra=0.35 μ m)) and 250- μ m Al₂O₃

particles showed highest (Ra 1.13 μm). No correlation ($r_s = -0.09$; $P = 0.27$) was found between the 2 dependent variables.

Ewais *et al* (2014)²² evaluated three novel surface treatments namely, and low pressure particle abrasion (LPPA), selective infiltration etching treatment (SIE) and fusion sputtering (FS) by taking 45 zirconia discs while non-treated surface served as control. They concluded that the effects of surface treatments on roughness, topography, hardness, and porosity of implants varied on three treatments. There were significant differences between all groups regarding surface roughness ($p < 0.01$). SEM and AFM revealed a nanoporous surface characteristic of SIE and FS resulted in the creation of surface micro beads, while LPPA resulted in limited abrasion of the surface.

Yang *et al* (2014)⁷⁸ evaluated smooth and rough zirconia disks for enhancing its biocompatibility with human gingival fibroblasts (HGFs) by UV treatment for 24h by analysing the surface morphology, wettability, elemental composition by SEM, Goniometer and XPS respectively. For bioactivity, the cultured HGFs' adhesive density, morphology, proliferation, and collagen synthesis were measured on different time points from 3 h to 7 days. They concluded that after UV treatment, contact angles and C/O ratio in both types of zirconia. After UV light treatment, cells initial spreading areas and perimeters were nearly tripled on disks. Cell adhesion and Cell proliferation were all significantly changed on UV-treated disks and UV treatment on rough zirconia had a positive effect on behaviour of HGFs.

Mohammed *et al* (2015)⁴⁶ had compared wettability of four types of implants valuated four original screw-type implants (One grit-blasted/acid-etched; one anodically oxidized titanium; one zirconia and one polyetheretherketone implant) after exposure to mixture of UVA and UVC for 40 min. Samples were treated by UV-A (382 nm) and UV-C (260 nm), respectively. All implants were surface characterized by SEM and contact angle measurements. Unexposed implants were hydrophobic (CA >90°) while UV treated implants with anatase coating became superhydrophilic (CA<5°). The anodized titanium and the zirconia implants were considerably hydrophilic (CA=34° and 27°, respectively) and the PEEK implants slightly (CA=79°) hydrophilized. The wettability changes strongly dependent on the specific material and its surface which in turn contribute for bioresponses.

Tuna *et al* (2015)⁶⁷ evaluated the effect of ultraviolet light (UV) treatment on the surface characteristics of two types of zirconia (Zr1 and Zr2) with smooth (m) and roughened (r) surfaces by treating with UV light for 15 min. Though SEM and AFM revealed quantitative and qualitative differences between the roughened and smooth surfaces due to UV treatment, UV treatment did not induce any topographic changes of the tested surfaces (p>0.05). All UV-treated samples showed a significant surface elemental content change with a decrease of carbon by 43-81%, an increase of oxygen by 19-45%, and an increase of zirconia by 9-41%. Upon UV treatment, a slight /no change in phase transformation was observed with respect to Zr1 and Zr2. The average contact

angles were between 56.4° and 69° before and 2.5° and 14.1° after UV treatment changing the hydrophobic status to hydrophilic status ($p < 0.0001$).

Tuna *et al* (2015)⁶⁸ examined the effect of UV treatment on the response of primary human alveolar bone-derived osteoblasts (PhABO) (bioactivity) by selecting disks of two zirconia-based materials (smooth, rough). Cell area and perimeter were significantly larger on all UV-treated surfaces ($p < 0.05$). The proliferation activity was significantly higher on roughened UV-treated surfaces than on untreated samples ($p < 0.05$). They concluded that UV pre-treatment of zirconia surfaces changed their physicochemical properties and improved their attractiveness against PhABO, resulting in faster healing and better bone-to-implant contact of zirconia implants *in vivo*.

Brezavšček *et al* (2016)¹² evaluated smooth and rough zirconia-based disks and cylindrical implants by treating with UV light for 15 min and subsequent placement in rat femurs. They concluded that UV treatment decreased the amount of surface carbon and converted the hydrophobic surface to superhydrophilic and enhanced the osteoconductive capacity of zirconia-based materials by *in vivo* histomorphometry.

Kenawy *et al* (2016)³⁴ evaluated silicon-zirconia based glass prepared by sol-gel method where SiO_2 was substituted by ZrO_2 with different values ($x = 0, 2, 4, 6, 8$ and 10wt %). XRD, FTIR, SEM (EDX) studies were done before and after soaking of the material in SBF. They concluded that increasing ZrO_2 content in the glass composition increased the growth of HA layer on glass

surfaces soaked in SBF and led to enhance the bioactivity of the glasses indicating that zirconia material plays an important role in enhancing osseointegration.

Ke *et al* (2017)³³ evaluated the surface properties, in vitro bioactivity and cell behaviour of Y-TZP using XRD, SEM-EDX, Raman Spectroscopy, cell culture studies and immersion in SBF. A bone-like apatite was formed on the entire surface of zirconia by immersion in SBF and cell culture studies revealed that surface modification of Y-TZP could promote bioactivity by cell adhesion and differentiation.

Nguyen *et al* (2017)⁴⁸ investigated the surface properties and initial cell response of bioactive glass infiltrated zirconia before and after sandblasting by taking four groups comprising 100 zirconia specimens. Groups include untreated zirconia (ZR), sandblasted zirconia (ZS), glass infiltrated zirconia (ZG), and sandblasted glass infiltrated zirconia (ZGS). They concluded that after sandblasting, the ZGS group had the highest surface roughness ($R_a = 1.24 \mu\text{m}$) with enhanced osteoblast cells response and indicated that sandblasting method can improve the mechanical properties of bioactive glass infiltrated zirconia with better osteoblast cell response.

Roy *et al* (2017)⁵⁹ have characterized the physicochemical changes occurring in ZrO_2 after UVC irradiation. XRD analysis had indicated that UVC treatment did not affect the crystalline structure of ZrO_2 but reduced the contamination and converted the surfaces “superhydrophilic” leading to adsorption of proteins thus enhancing the bioactivity.

Materials and Methods

MATERIALS AND METHODS

The present *in vitro* study was conducted to evaluate and compare the effects of two different surface treatments, namely, air-borne particle abrasion or sandblasting and UV Photofunctionalization (UVP) on the bioactivity of zirconia.

The following materials, instruments, equipments and methodology were employed in the present study:

Materials used:

- Universal light cure modeling paste (Kuss dental S L, Spain) (Fig. 1a & 1b)
- Yttria-stabilized, zirconia ceramic blank (Ceramill, AMANN GIRRBACH, Austria) (Fig.2a & 2b)
- Silicon Carbide emery papers - 600, 800, 1000, 1200 grit sizes (Norton Brazil) (Fig. 3a, 3b, 3c & 3d)
- Alumina powder - 50 μm (Deldent Ltd., Israel) (Fig. 4)
- Customized deionised water (CPMB, TNAU, India) (Fig. 5)
- Petri plate (Tarsons Industries Pvt Ltd., India) (Fig. 6)
- 30 watts Ultraviolet Lamp (Philips, Holland) (Fig. 7)
- ❖ SBF Chemicals (Merck & Co., Mumbai, India) (Fig. 8a to 8i):
 - Sodium chloride, NaCl (Fig. 8a)
 - Sodium hydrogen carbonate, NaHCO₃ (Fig. 8b)
 - Potassium chloride, KCl (Fig. 8c)
 - Di-potassium hydrogen phosphate trihydrate, K₂HPO₄.3H₂O (Fig. 8d)

- Magnesium chloride hexahydrate, $\text{MgCl}_2 \cdot 6\text{H}_2\text{O}$ (Fig. 8e)
- Calcium chloride CaCl_2 , (Fig. 8f)
- Sodium sulphate Na_2SO_4 , (Fig. 8g)
- Tris-hydroxymethyl amino methane, $(\text{HOCH}_2)_3\text{CNH}_2$ (Fig. 8h)
- 1.0M HCl (Fig. 8i)

Instruments used:

- Artery forceps (Sirag Dental Co., Chennai, India) (Fig. 9)
- Sandpaper Mandrel (Sirag Dental Co., Chennai, India) (Fig. 10)
- Tweezer (Dibya Industries, India) (Fig. 11)
- Desiccator (Borosil, India) (Fig. 12)
- 1L Plastic beaker (Tarsons Industries Pvt. Ltd., India) (Fig. 13)
- Laboratory thermometer (GH Zeal Ltd., England) (Fig. 14)
- 1L Plastic Volumetric Flask (Tarsons Industries Pvt. Ltd., India) (Fig. 15)
- Graduated polypropylene tubes (Tarsons products Pvt. Ltd., India) (Fig. 16)
- Conical centrifuge tube rack (Tarsons products Pvt Ltd., India) (Fig. 17)

Equipments used:

- Light curing unit (Baistra, United States) (Fig. 18)
- Copy-milling machine (Ceramill, Austria) (Fig. 19)
- Sintering unit (VITA Zyrcomat, VITA Zahnfabrik, Germany) (Fig. 20)
- Dental micromotor unit (Marathon, Korea) (Fig. 21)
- Sandblasting unit (Delta, Chennai, India) (Fig. 22)
- Digital ultrasonic cleaner (Beijing ultrasonic Co., China) (Fig. 23)

- UV laminar flow hood (Marks, Mumbai, India) (Fig. 24)
- X-ray Diffractometer (Ultima IV, Rigaku Corporation, Japan) (Fig. 25)
- Multimode Scanning Probe Atomic Force Microscope (NTEGRA Aura, NT-MDT, Russia) (Fig. 26a & 26b)
- Contact Angle Goniometer (DSA 20E, Kruss, Hamburg, Germany) (Fig. 27)
- Field Emission Scanning Electron Microscope (FEI Quanta – 250, Thermo Fisher Scientific, USA) coupled with Energy Dispersive X-ray Spectroscopy (SEM-EDX) (Bruker Corporation, USA) (Fig. 28a & Fig. 28b)
- Analytical Balance (CAS New Zealand Pvt Ltd., NZ) (Fig. 29)
- Magnetic Stirrer with hot plate (Remi Elektrotechnik Ltd., India) (Fig. 30)
- pH tester (Eco Ltd, India) (Fig. 31)
- Inductively Coupled Plasma Mass Spectrometer (ICP-MS) (Agilent Technologies, USA) (Fig. 32)
- Bacteriological Incubator (Scigenics Biotech Pvt ltd., India) (Fig. 33)

Description of equipments employed in the study:

1. X-Ray Diffractometer (Fig. 25):

X-ray diffraction is a unique technique in determination of the type of crystal phase and is based on constructive interference of monochromatic X-rays on a crystalline sample. A typical diffractometer consists of a source of radiation, a monochromator to choose the wavelength, slits to adjust the shape

of the beam, a detector to monitor the diffracted radiation, a semitransparent beam stop to prevent damage to the apparatus by blocking the non-diffracted primary beam. The semitransparent beam stop determine the radiation absorbed by the sample and its intensity. With the intensity formed at different theta levels based on the crystal phases, peaks are formed, which indicate the type of phases present in the given sample.

2. Atomic Force Microscope (AFM) (Fig. 26a & 26b):

Atomic Force Microscope (NTEGRA Aura, NT-MDT, Russia) is an advanced scanning probe microscope (SPM) specifically used to create images of surfaces and structures on a nanoscale. The AFM consists of a cantilever made of silicon or silicon nitride with a sharp tip (probe) at its end, which is used to scan back and forth the specimen surface. When the tip is brought into proximity of a sample surface (noncontact mode), electrostatic forces between the tip and the sample lead to a deflection of the cantilever and the sample is raster scanned resulting in 2D and 3D high resolution images of surface topography and also quantify surface roughness.

3. Contact Angle Goniometer (Fig. 27):

Universal Goniometer DSA 20E (Kruss, Hamburg, Germany) is used to investigate interfacial properties (surface free energy, wettability, surface/interfacial tension) of solid-solid, solid-liquid and liquid-liquid interface. It has software controlled electronic syringes to eject known volume of liquids on a solid surface. The contact angle is measured by static sessile-drop technique by dropping 1 μ l of water on the surface of a sample kept in the

centre of the base platform. The contact angles (right and left) between the water drop and the sample is captured using a high-resolution camera and displayed in the computer using specific software.

4. Field Emission Scanning Electron Microscope (FESEM) Coupled with Energy Dispersive X-Ray Spectroscopy (EDX) (Fig. 28a & Fig. 28b):

The Scanning Electron Microscope uses a beam of highly energetic electrons (1KeV, 1MeV) from an electron gun to examine objects on a very fine scale (0.2nm onwards), resulting in higher magnification of the image (5X to 300000X). The electrons are focused into a narrow beam and scanned across a sample in a grid pattern and detectors record the image from the sample. Nonconductive samples in the electron microscope will build up surface charge, reducing image quality. The sample is sputter coated with gold to remove the surface charge and loaded in the specimen chamber. The centre of the sample is brought into focus and its image recorded.

Energy-dispersive X-ray spectroscopy (EDX) works on the fundamental principle that each element has an atomic structure allowing a unique set of peaks on its electromagnetic emission spectrum. To stimulate the emission of characteristic X-rays from a sample, a high energy beam of charged particles (electrons) is focused onto the sample. The number and energy of the X-rays emitted from a sample is measured by an energy-dispersive spectrometer. As the energies of the X-rays are characteristic of the differences in the atomic structure of the emitting element, the elemental composition and percentage in a sample is obtained.

5. Inductively Coupled Plasma Mass Spectrometer (ICP-MS) (Fig. 32):

Inductively Coupled Plasma Mass Spectrometer detects metals and several non-metals at low concentrations (parts per quadrillion). This is achieved by ionizing the sample with inductively coupled plasma and the resulting ions are separated and quantified using a mass spectrometer. The Inductively Coupled Plasma (ICP) is sustained in a torch consisting of three quartz concentric tubes. The end of this torch is placed inside an induction coil supplied with a radio-frequency electric current. A flow of argon gas is introduced between the two outermost tubes and an electric spark is applied for a short time to introduce free electrons into the gas stream. These electrons interact with the radio-frequency magnetic field of the induction coil and are accelerated first in one direction, then the other, as the field changes at high frequency. The accelerated electrons collide with argon atoms, resulting in the argon atom to part with one of its electrons, which is accelerated by the rapidly changing magnetic field. Another flow of gas is introduced to pass through the centre of the plasma. The sample is introduced into the central tube with consistent droplet sizes using a nebulizer and the atoms of the sample ionize after evaporation forming singly charged ions, whose concentrations are measured at mg/litre levels using software.

METHODOLOGY

The methodology adopted in this study is described under the following sections:

I. Obtaining test samples

1. Customizing test samples
2. Grouping of test samples
3. Surface treatment procedures

II. Surface characteristic analyses of representative test samples of each test group

1. Crystal phase analysis by X-Ray Diffractometry (XRD)
2. Surface roughness analysis by Atomic Force Microscopy (AFM)
3. Wettability (hydrophilicity) evaluation by Contact Angle Goniometry
4. Surface topographic and elemental analysis by Scanning Electron Microscopy coupled with Energy Dispersive X-ray Spectroscopy (SEM-EDX)

III. Bioactivity test

1. Preparation of Simulated Body Fluid (SBF)
2. Pre-immersion Ca-content analysis in SBF (Ca-SBF analysis)
3. Immersion of test samples in SBF
4. Post-immersion Ca-content analysis in SBF (Ca-SBF analysis)

IV. Surface characteristic analyses of representative post-immersion test samples of each test group

1. Crystal phase analysis by XRD

2. Surface topographic and elemental analysis by Scanning Electron Microscopy coupled with Energy Dispersive X-ray Spectroscopy (SEM-EDX)

V. Data tabulation and statistical analysis

DETAILED DESCRIPTION OF METHODOLOGY

I. Obtaining Test Samples

1. Customizing test samples: (Fig. 34a to Fig. 36)

A customized resin pattern resembling a disc of 12mm x 4mm dimensions, with an extension tag of 6mm x 6mm x 4mm dimensions was manually molded using universal light cure modeling paste (Kuss dental SL, Spain) (Fig. 1a & 1b) to fabricate a prototype with slightly higher dimensions than the final dimensions of the test sample, to compensate for the sintering shrinkage (Fig. 34a). It was cured in a light cure unit (Baistra, United States) (Fig. 7) for 12 minutes (Fig. 34b) to obtain a resin prototype, which could be replicated during the milling process (Fig. 34c). The prototype was secured beneath the tracing arm with an attached tracing tool. The zirconia blank (Figs. 2a, 2b) (AMANN GIRRBACH, Austria), was secured in its slot beneath the milling arm with an attached milling tool. The tracing tool passes over the prototype and the milling tool duplicates these movements (Fig. 34d), to produce a copy-milled sample (Fig. 34f). The copy-milled samples were then sintered for 8 hours at 1500°C to obtain zirconia samples of 10 mm diameter x 2mm thickness with an extension tag of 4mm x 4mm x 2mm (Fig. 34g, 34h). In

this manner, thirty three customised samples (Figs. 35a & 35b) were obtained by copy-milling and sintering of the zirconia blank.

All the samples were subjected individually to finishing with emery papers of successive grit sizes. Each sample was held with an artery forceps (Sirag Dental Co., Chennai) (Fig. 4), by holding the extension tag and ground for 15 seconds (Norton, Brazil) (Fig. 3) using 600, 800, 1000, 1200 grit sizes, respectively, starting from 600 and progressing finally to 1200 grit size using a sandpaper mandrel attached to a dental micromotor (Marathon, Korea) (Fig. 10) at a low speed, to ensure baseline homogeneity of surface texture of all test samples (Fig. 36) prior to grouping and surface treatments. The samples were then cleaned with sterile de-ionized water (CPMB, TNAU, India) (Fig. 11) and air-dried.

2. Grouping of Test Samples: (Fig. 37a to Fig. 37c)

The samples were assigned to three test groups designated as Group I, II and III depending on the type of surface treatment (n=11/Group):

Group I (Untreated): comprised of test samples (n=11), that were not subjected to any surface treatment (Fig. 37a).

Group II (Sandblasted): comprised of test samples (n=11), that were subjected to sandblasting with 50 μ m alumina (Fig. 37b).

Group III (UVP): comprised of test samples (n=11), that were subjected to surface treatment with UV Photofunctionalization (UVP) (Fig. 37c).

3. Surface treatment procedures: (Fig. 38 to Fig. 42)

Group II samples were held with an artery forceps (Sirag Dental Co., Chennai, India) (Fig. 3) and blasted with 50 μ m alumina particles (Deldent Ltd, Israel) (Fig. 10) at a distance of 10mm at an angle of 90° at 2.5 bar pressure for 15 seconds (Fig. 38). After blasting, the samples were cleaned using an ultrasonic cleaner (Beijing Ultrasonic Co., China) (Fig. 15) for a duration of 15 minutes in de-ionised water to remove the alumina particles (Fig. 39a & Fig. 39b).

Group III samples were subjected to Ultraviolet Photofunctionalization (UVP). Ultraviolet C type of irradiation was employed by placing the samples in a petri-plate (Fig. 6) and placing the petri-plate inside the laminar flow hood (Marks, Mumbai, India) (Fig. 24) of the UV chamber at a distance of 4 cms from the light source for 15 minutes (Fig. 40a & Fig. 40b). All the samples of the 3 test groups (Fig. 41) were subsequently marked, dried and stored in a desiccator (Borosil, India) (Fig. 17) until further testing (Fig. 42).

II. Surface characteristic analyses of representative test samples of each test group

1. Crystal phase analysis by X-Ray Diffractometer (XRD) (Groups I, II and III; n=1/Group): (Fig. 43)

X-Ray Diffractometer (XRD) (Ultima IV, Rigaku Corporation, Japan) (Fig. 25) was used to detect the type of crystal phase present on representative samples of untreated and treated test groups. The diffractograms were obtained using Cu- α radiation at 40kv and 200mA (Refer Results section;

Fig. 56a to Fig. 56c). XRD spectra were collected over a 2θ range between $20-80^\circ$ at the scan speed of $3^\circ/\text{minute}$ and 0.02° stepsize. The peak intensity and the type of crystal phase (t/m) present was recorded automatically.

2. Surface roughness analysis by Atomic Force Microscopy (AFM) (Groups I, II and III; n=1/Group): (Fig. 44)

Atomic Force Microscopy (NTEGRA Aura from NT-MDT, Russia) (Fig. 26a & Fig. 26b) was used to detect surface roughness of representative samples of untreated and treated test groups. The test samples were analysed in 4 areas of each sample of each group, by keeping the cantilever tip of the equipment in non-contact mode. Subsequently, $5\mu\text{m} \times 5\mu\text{m}$ images with 256×256 pixels were taken with a scan rate of 0.5Hz , to obtain both 2D and 3D images (Refer Results section; Fig. 57a to Fig. 58c). The analysis also gave numeric values for surface roughness (S_a) at nanoscale levels for each group.

3. Wettability (hydrophilicity) evaluation by Contact Angle Goniometry (Groups I, II and III; n=5/Group): (Fig. 45a to Fig. 45c)

Universal goniometer DSA 20E (Kruss, Hamburg, Germany) (Fig. 21) was used to detect surface wettability of representative samples of untreated and treated groups. The surface wettability (hydrophilicity) was examined by static sessile-drop technique using $1\mu\text{l}$ H_2O . Five contact angle values were obtained for each sample (Refer Results section; Fig. 59a to Fig. 59c) and the sample mean was obtained. Five samples per test group were analyzed and the overall mean contact angle of each group was recorded.

4. Surface topographic and elemental analysis by Scanning Electron Microscopy coupled with Energy Dispersive X-ray Spectroscopy (SEM-EDX) (Groups I, II and III; n=1/Group): (Fig. 46a & 46b)

The surface topography and surface elemental composition of untreated and treated samples were analysed by Field Emission Scanning Electron Microscopy (Thermo Fisher Scientific, USA) coupled with Energy Dispersive X-ray Spectroscopy (Bruker Corporation, USA) (Fig. 22).

The samples for SEM analysis were gold-coated using auto fine coaters and observed with Scanning Electron Microscope (SEM) at 5000x magnification and representative photomicrographs obtained for all test groups (Refer Results section; Fig. 60a, Fig. 61a & Fig. 62a). EDX spectrum analysis yielded automated calculation of atomic and weight percentage of elemental composition of all three test groups (Refer Results section; Fig. 60b, Fig. 61b & Fig. 62b).

III. Bioactivity test

1. Preparation of Simulated Body Fluid (SBF): (Fig. 47a to Fig. 48)

A custom-made solution was used to assess the bioactivity of test samples and was prepared as per guidelines given by Kokubu T and Takadama H (2006).³⁹ To prepare 1000 ml of SBF, 700 ml of de-ionised water (CPMB, TNAU, India) (Fig. 12) was taken in a 1L plastic beaker (Tarsons Products Pvt Ltd., India) (Fig. 24) and set on magnetic stirrer with hotplate (Remi Elektrotechnik Ltd., India) (Fig. 30). The water in the beaker was heated

to $36.5\pm 1.5^{\circ}\text{C}$ under stirring and the temperature was maintained using a laboratory thermometer (GH Zeal Ltd., England) (Fig. 25). The SBF was prepared by dissolving the prescribed quantities of chemicals, weighed in an electronic balance (CAS New Zealand Pvt Ltd., NZ) (Fig. 26) and added to de-ionised water at $36.5\pm 1.5^{\circ}\text{C}$ in the following sequential order (Fig. 23a – 23i):

1. NaCl (8.035 g),
2. NaHCO₃ (0.355 g),
3. KCl (0.225 g),
4. K₂HPO₄·3H₂O (0.311 g),
5. MgCl₂·6H₂O (0.311 g),
6. 1.0M - HCl (39ml),
7. CaCl₂ (0.292 g),
8. Na₂SO₄ (0.072 g),
9. Tris - hydroxymethyl aminomethane, (HOCH₂)₃CNH₂ (6.118 g), and
10. 1.0M - HCl (0 - 5ml).

During the preparation of SBF, chemicals were added one by one after the preceding one was completely dissolved. After dissolving the chemicals one by one from 1st to 8th in de-ionised water, the temperature of the solution was set at $36.5\pm 1.5^{\circ}\text{C}$ using the thermometer and volume was made up to 900ml with de-ionised water. The pH tester electrode was then dipped into the solution to check the pH of the solution before addition of the 9th reagent (Tris). After checking the pH, Tris was added incrementally taking careful note of the pH and temperature change. When the pH had risen to 7.45 ± 0.01 , further addition of Tris was stopped and the 10th reagent, 1M HCl was dropped to lower pH to 7.42 ± 0.01 . The process of addition of Tris and 1M HCl was repeated until the whole amount of Tris was dissolved and finally the pH was adjusted to 7.4 by addition of 1M HCl with the temperature being maintained at $36.5\pm 1.5^{\circ}\text{C}$ (Fig. 47a & Fig. 47b). The pH electrode was removed, rinsed with de-ionised water and the washings were added to the solution. The pH adjusted solution was

poured into 1L plastic volumetric flask (Tarsons India Pvt Ltd., India) (Fig. 26) and the volume was made up to one litre using de-ionised water after the temperature of the solution dropped to 20°C. The SBF thus prepared was refrigerated in an airtight container (Fig. 48) until further use, to prevent precipitation of the constituents.

2. Pre-immersion Ca-content analysis in SBF (Ca-SBF analysis):

The Ca-content of the prepared SBF solution was evaluated. One ml volume of the prepared solution was kept in the counter of ICP-MS equipment (Agilent Technologies, USA) (Fig. 32) which then automatically computed the calcium content value. The procedure was repeated 4 times to obtain 4 values of the Ca-content in SBF and the mean value obtained, was taken as a pre-immersion Ca-content value in SBF or reference value and recorded for future use.

3. Immersion of test samples in SBF (Groups I, II and III; n=10 /Group)

(Fig. 49a to Fig. 54b)

25 ml of SBF was poured (Fig. 49a & Fig. 49b) into each of the 30 graduated polypropylene test tubes (Tarsons Products Pvt Ltd., India) (Fig. 27) labelled to indicate the test groups as well as sample numbers for identification (Figs. 50a, 50b, 51a, 51b, 52a & 52b). The samples of each test group were immersed one per test tube in the SBF (Fig. 49a & 49b) after warming the SBF to $36.5 \pm 1.5^\circ\text{C}$. The test tubes containing the samples were closed with their respective air-tight caps and incubated in an incubator (Scigenics Biotech, Chennai, INDIA) at $36.5 \pm 1.5^\circ\text{C}$ (Fig. 53). After incubation for 3 weeks, the samples were removed from SBF, washed gently with de-ionised water and dried in a desiccator (Fig.

54a & Fig. 54b), until further analysis by SEM-EDX. The SBF solution in each test tube was subjected to analysis of post-immersion Ca-content.

4. Post-immersion analysis of Ca-content in SBF (Ca-SBF analysis): (Fig. 55)

The SBF from each test tube containing one test sample of each test group was subjected to Ca-SBF analysis by ICP-MS, to assess Ca-content depletion, if any, in the SBF and thereby asserting the bioactivity of the test sample. The procedure for detecting the Ca-content in SBF was similar to that described previously for determining the pre-immersion Ca-content in SBF. These values were designated as the post-immersion Ca-content in SBF for each sample. The mean post-immersion Ca-content for each test group was obtained from these basic values of each test sample of the respective test group.

IV. Surface characteristic analyses of representative post-immersion test samples of each test group

1. Crystal phase analysis by X-Ray Diffractometer (XRD) (Groups I, II and III; n=1/Group):

X-Ray Diffractometer (XRD) was used to detect the type of crystal phase present on representative post-immersion test samples of untreated and treated groups. The procedure for obtaining the diffractograms (Refer Results section; Fig. 63a to Fig. 63c) was similar to that described previously in this section.

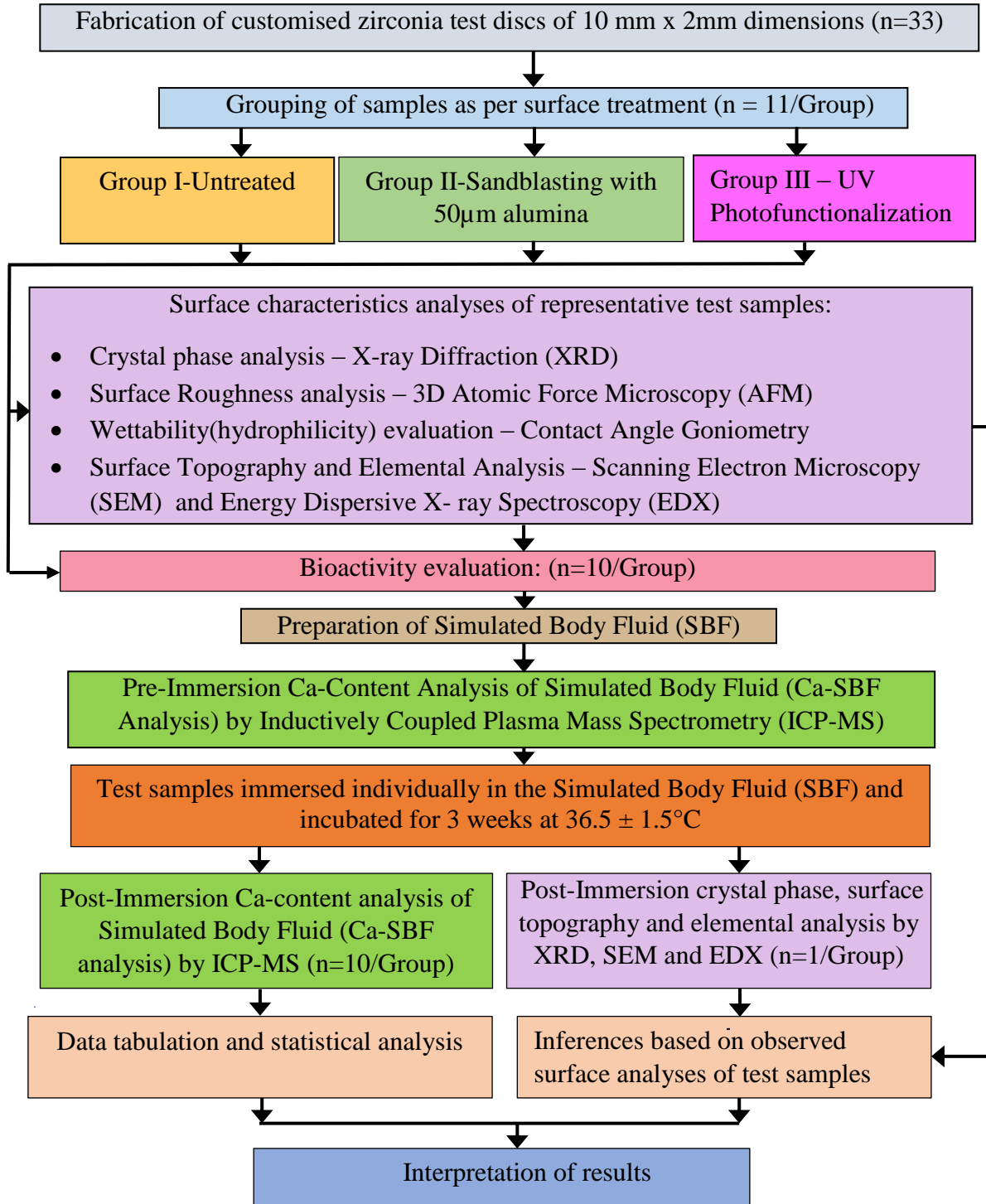
2. Surface topographic and elemental analysis by Scanning Electron Microscopy coupled with Energy Dispersive X-ray Spectroscopy (SEM-EDX) (Groups I, II and III; n=1/Group):

The surface topography and elemental composition of representative post-immersion untreated and treated samples were analyzed by SEM-EDX. The procedure for obtaining representative SEM photomicrographs (Refer Results section; Fig. 64a, Fig. 65a & Fig. 66a) and EDX spectrums (Refer Results section; Fig. 64b, Fig. 65b & Fig. 66b) were similar to that described previously in this section. The Ca/P ratio was calculated based on the atomic percentage of elements obtained by the EDX analysis.

V. Data tabulation and statistical analysis

The basic data and mean values obtained were tabulated and subjected to statistical analysis by SPSS software (SPSS for windows 16.0 SPSS Corp., Germany). One way ANOVA, Post-hoc Tukey's HSD analysis and Students' paired 't' test were done to compare the data obtained for statistical significance with respect to surface roughness, wettability and bioactivity of the three test groups.

ANNEXURE – I METHODOLOGY – OVERVIEW



Figures

ANNEXURE – II

FIGURES

MATERIALS EMPLOYED IN THE PRESENT STUDY

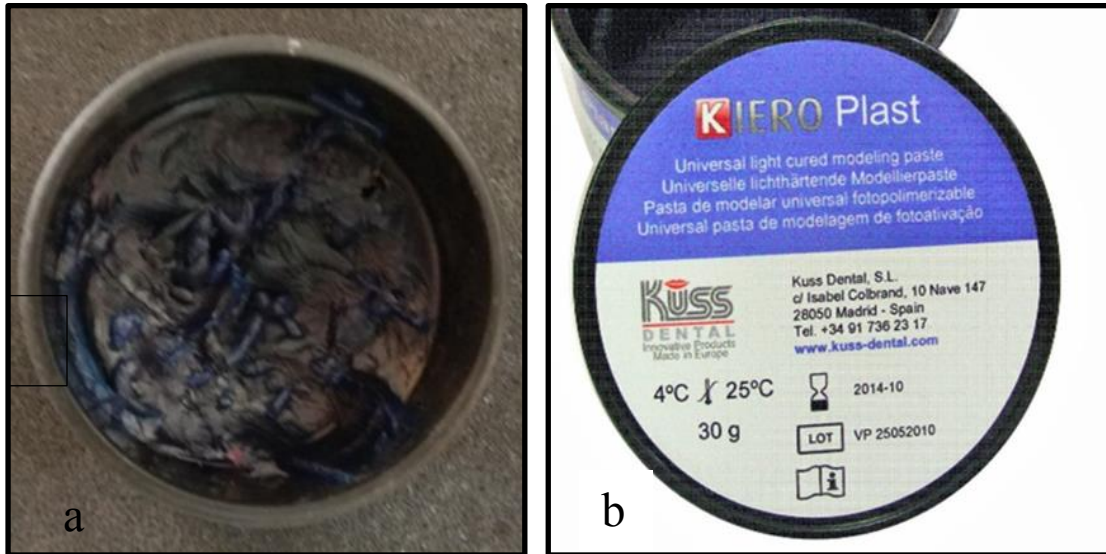
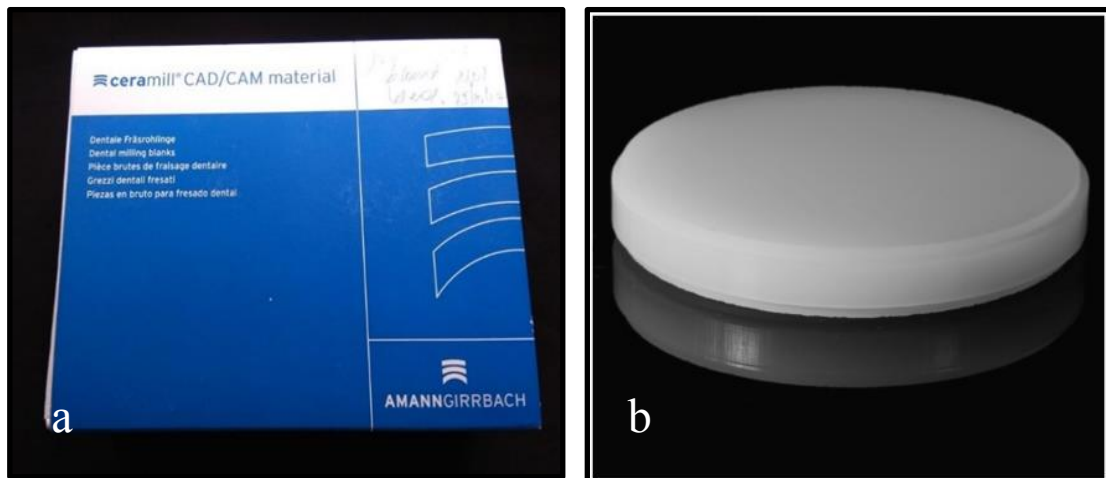


Fig. 1a & Fig. 1b: Universal light cure modeling paste



**Fig. 2a: Manufacturer package of Yttria-stabilized zirconia blank
2b: Yttria-stabilized zirconia blank**

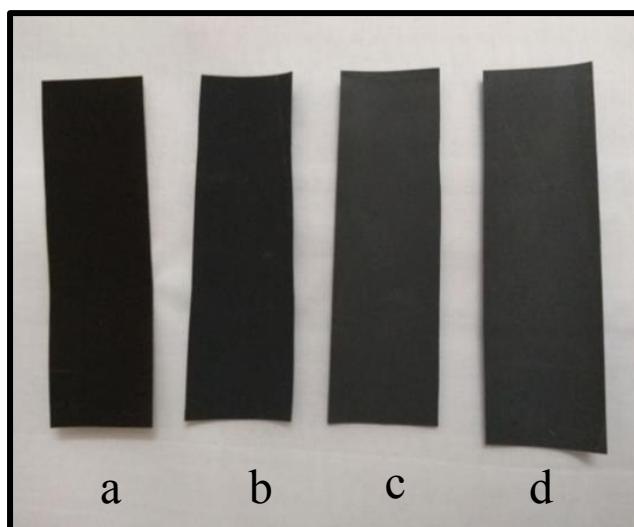


Fig. 3: Silicon carbide emery paper of successive grits:

- 3a. 600**
- 3b. 800**
- 3c. 1000**
- 3d. 1200**



Fig. 4: Alumina powder 50 μ m for sandblasting



Fig. 5: Customised deionised water



Fig. 6: Petri plate



Fig. 7: 30 watts Ultraviolet lamp



Fig. 8a to 8i: CHEMICALS EMPLOYED FOR SBF PREPARATION

Fig. 8a: Sodium chloride, NaCl

8b: Sodium hydrogen carbonate, NaHCO₃

8c: Potassium chloride, KCl

8d: Di-potassium hydrogen phosphate trihydrate K₂HPO₄·3H₂O

8e: Magnesium chloride hexahydrate, MgCl₂·6H₂O

8f: Calcium chloride, CaCl₂

8g: Sodium sulphate, Na₂SO₄

8h: Tris-hydroxymethyl aminomethane, (HOCH₂)₃CNH₂

8i: Hydrochloric acid, HCl

INSTRUMENTS USED IN THE PRESENT STUDY



Fig. 9: Artery forceps



Fig. 10: Sandpaper mandrel

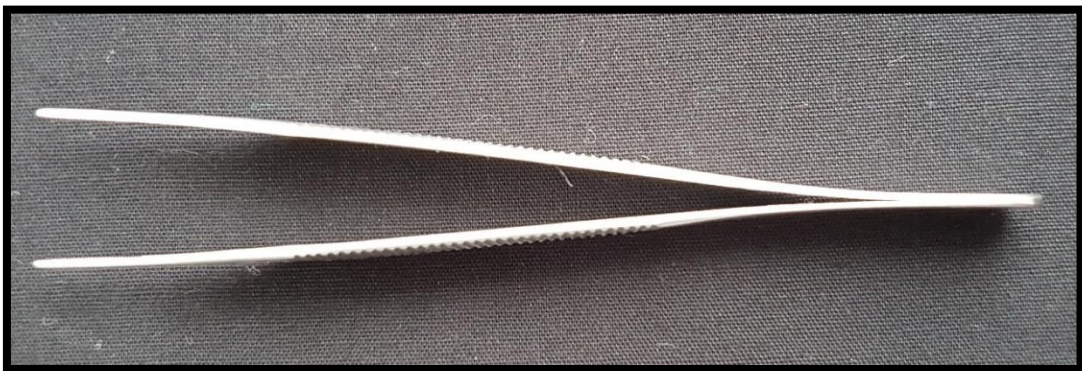


Fig. 11: Tweezer



Fig. 12: Desiccator



Fig. 13: Plastic beaker



Fig. 14: Laboratory thermometer



Fig. 15: Volumetric flask (1 L)



Fig. 16: Graduated polypropylene test tubes

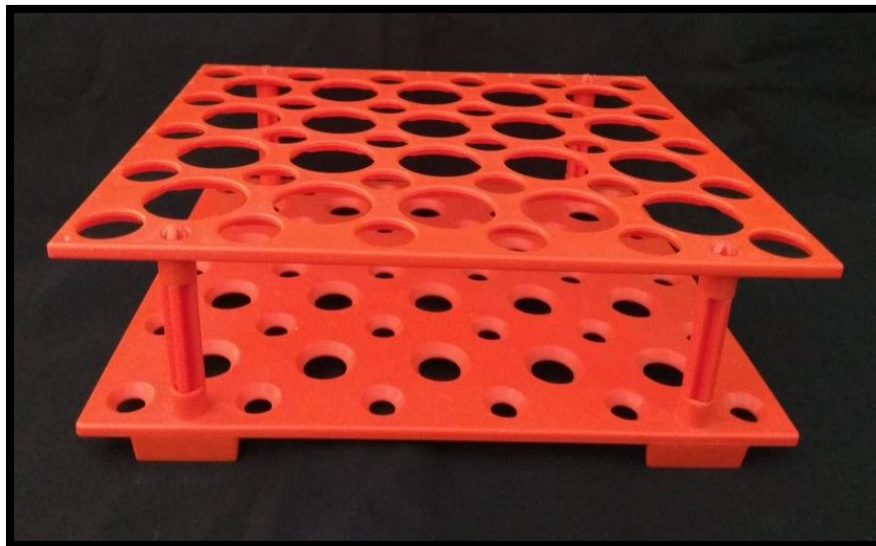


Fig. 17: Conical centrifuge tube rack

EQUIPMENTS USED IN THE PRESENT STUDY



Fig. 18: Light curing unit



Fig. 19: Copy-milling machine



Fig. 20: Sintering unit



Fig. 21: Dental Micromotor



Fig. 22: Sandblasting unit



Fig. 23: Digital Ultrasonic cleaner



Fig. 24: UV laminar flow hood



Fig. 25: X-ray Diffractometer



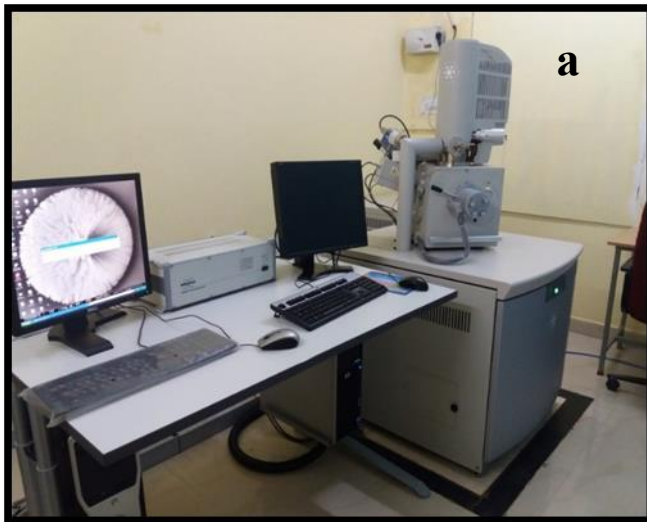
Fig. 26a: Set –up for Multimode Scanning Probe Microscopy (Atomic Force Microscopy) unit



Fig. 26b: Main unit of AFM



Fig. 27: Contact Angle Goniometer



**Fig. 28a: Set up for
Field Emission Scanning Electron Microscopy
(FEI Quanta – 250 FEG) with Energy
Dispersive X-ray Spectroscopy**



**Fig. 28b: Main unit of
SEM**



Fig. 29: Analytical Weighing Balance



Fig. 30: Magnetic Stirrer with hot plate



Fig. 31: pH tester



Fig. 32: Inductively coupled Plasma Mass Spectrometer (ICP-MS)



Fig. 33: Bacteriological Incubator

METHODOLOGY

I. OBTAINING TEST SAMPLES

1. Customizing test samples: (Fig. 34a to Fig. 36)

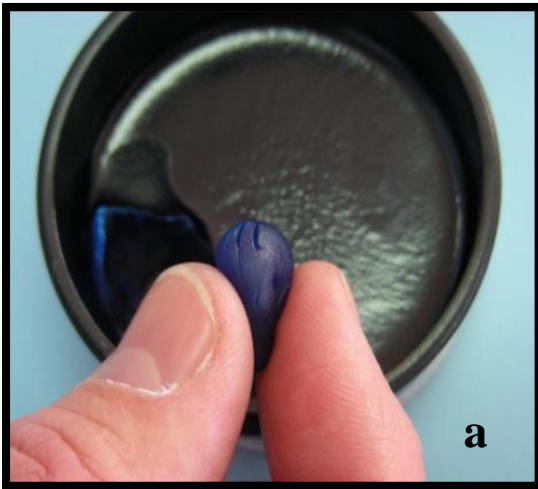


Fig. 34a: Disc made from universal light cure modeling paste



Fig. 34b: Light curing the modeling paste for 12 minutes



Fig. 34c: Light cured millable resin disc

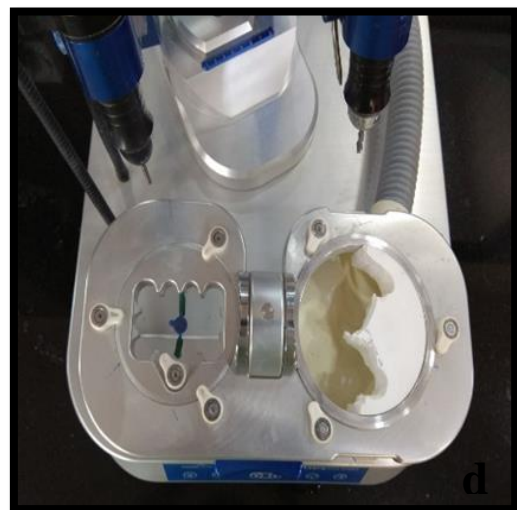


Fig. 34d: Copy- milling of zirconia blank

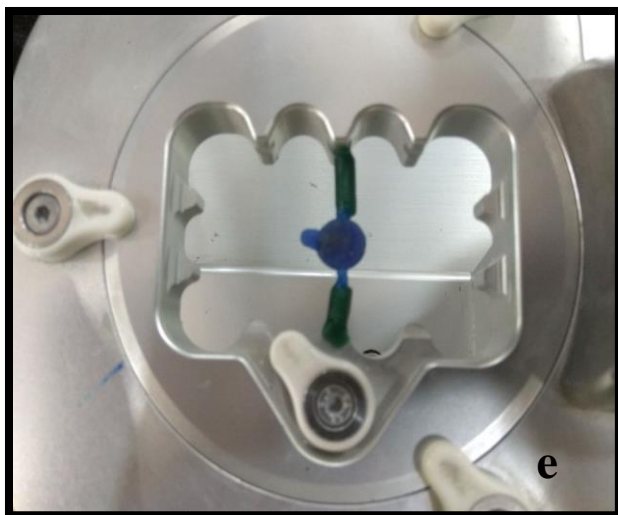


Fig. 34e: Close up view of the resin pattern



Fig. 34f: Zirconia sample before sintering



Fig. 34g: Zirconia sample after sintering at 1500°C for 8 hours



Fig. 34h: Zirconia sample sintering

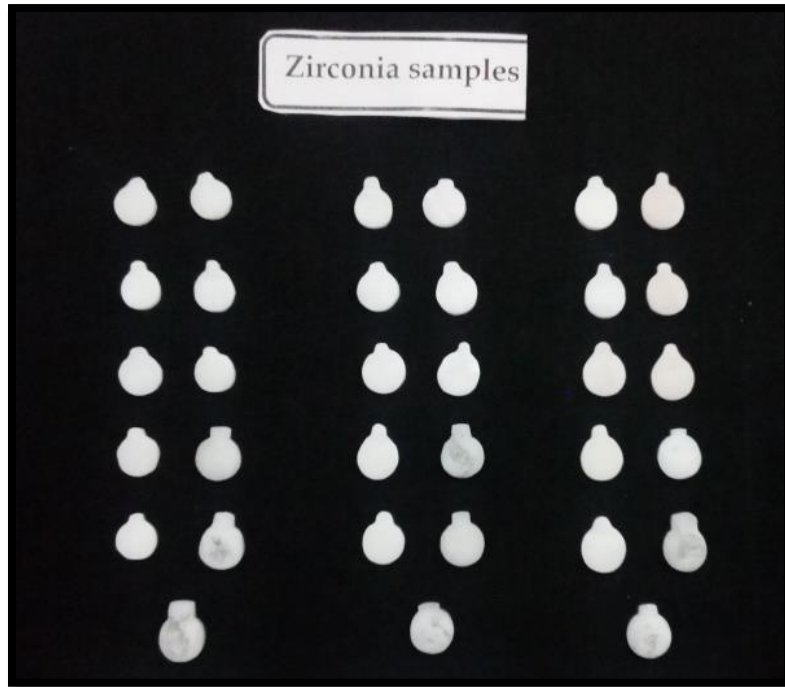


Fig. 35a: Zirconia disc samples (10x10 mm with 2mm thickness)

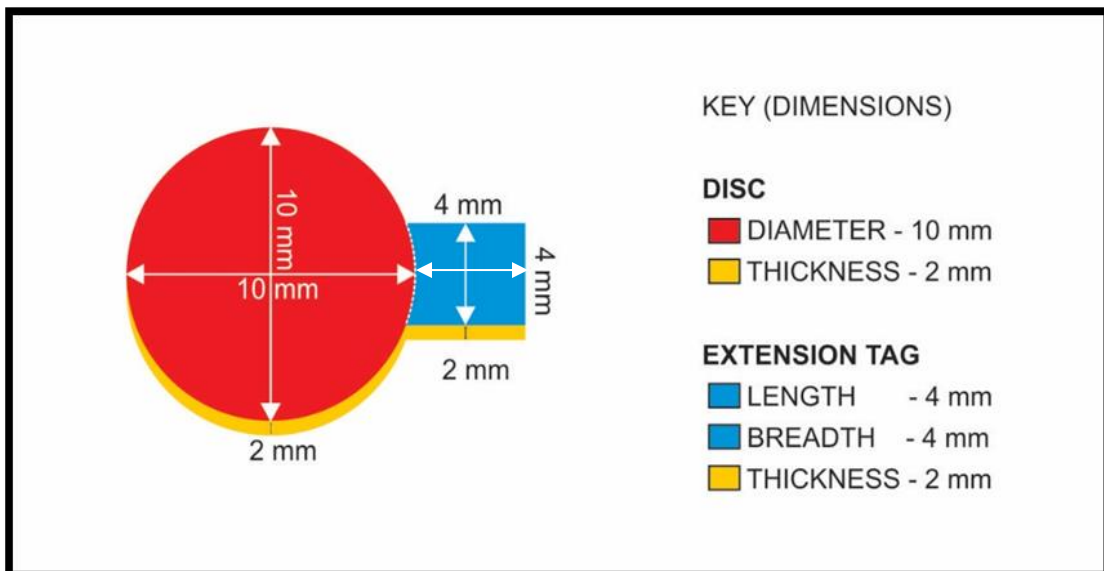


Fig. 35b: Schematic Representation of zirconia discs

Finishing of copy-milled samples

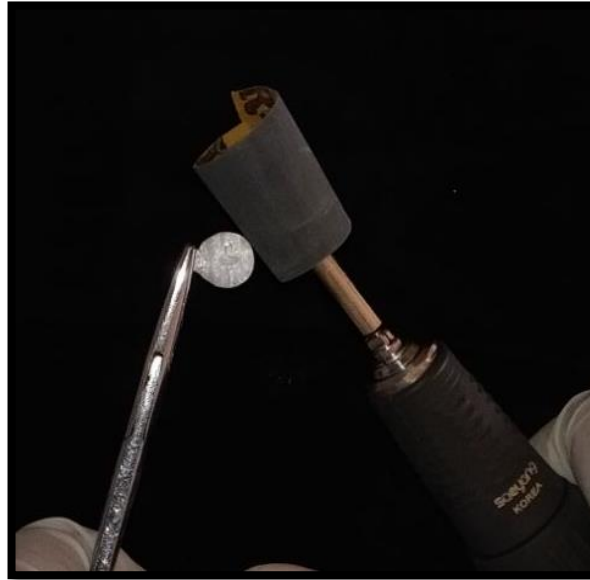


Fig. 36: Emery Treatment of Zirconia samples

2. Grouping of test samples (Fig. 37a to Fig. 37c)

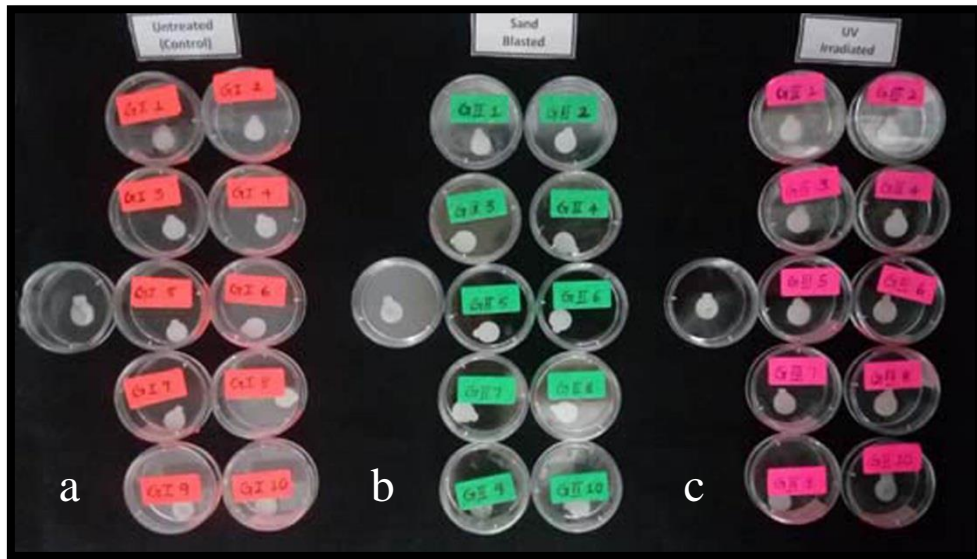


Fig. 37a: Group I
(Untreated)

37b: Group II
(Sandblasted)

Fig.37c: Group III
(UVP)

3. Surface treatment procedures (Fig. 38 to Fig. 42)

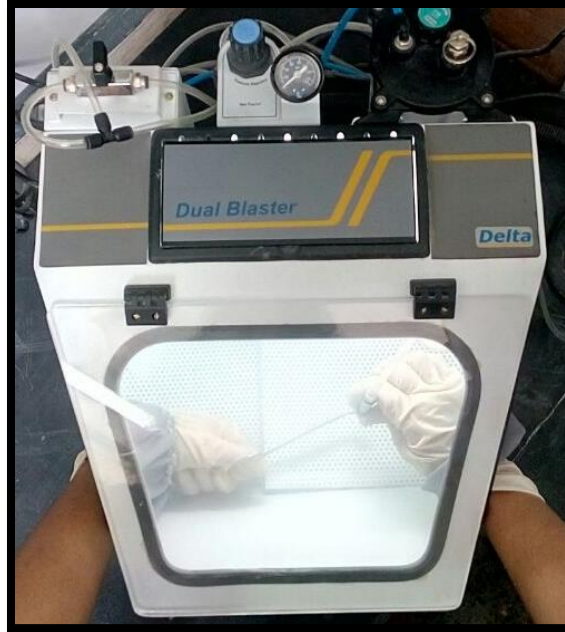


Fig. 38: Sandblasting with Alumina (50 μm) for Group II samples



Fig. 39a: Ultrasonic cleaning in progress



Fig. 39b: Samples placed in the ultrasonic bath

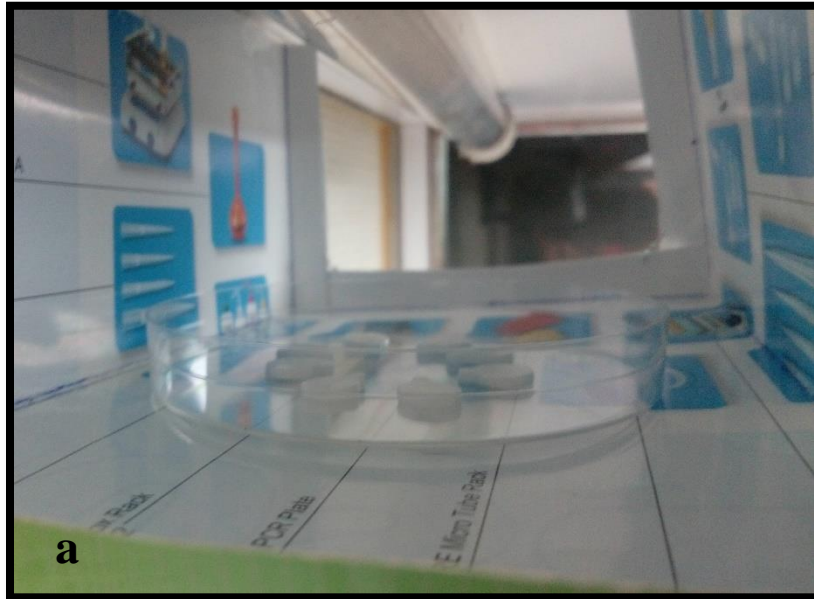


Fig. 40a: Test samples placed in the laminar flow hood for UVP



Fig. 40b: Group III samples being subjected to UVP in laminar flow hood

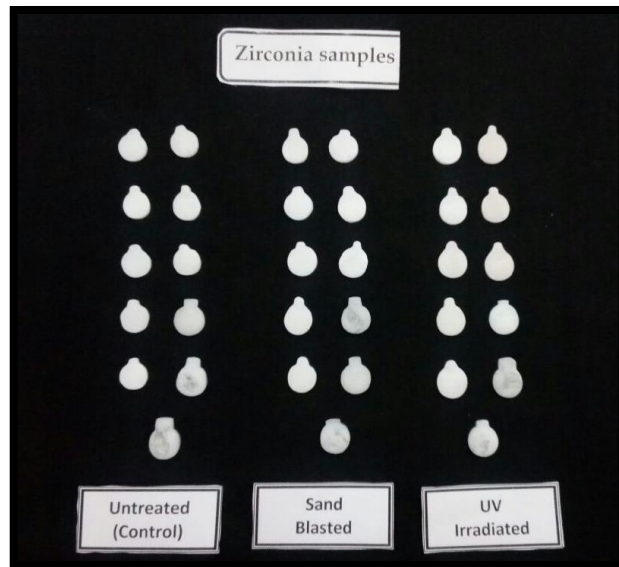


Fig. 41: Test samples of Group I, Group II & Group III (n=11/Group) after respective surface treatments



Fig. 42: Test samples of Groups I, II & III stored in Desiccator for further analysis

II. SURFACE CHARACTERISTICS ANALYSES OF TEST SAMPLES OF EACH TEST GROUP

1. Crystal phase analysis by X-Ray Diffractometry (XRD)

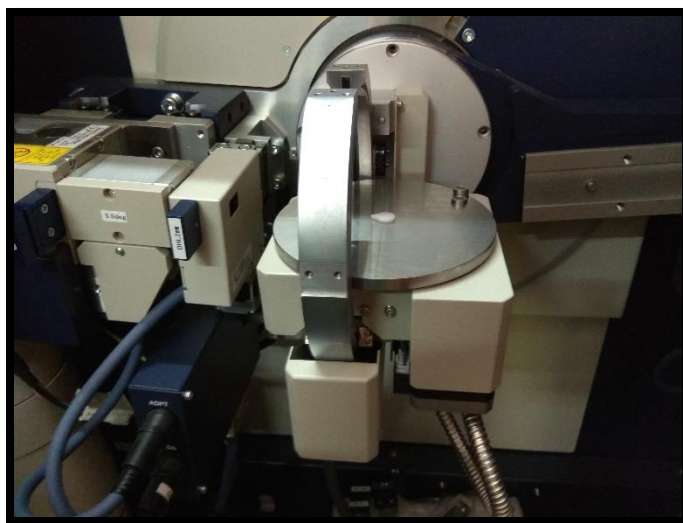


Fig. 43: Zirconia test sample placed on the platform of X- Ray Diffractometer for analysis

2. Surface roughness analysis by Atomic Force Microscopy (AFM)

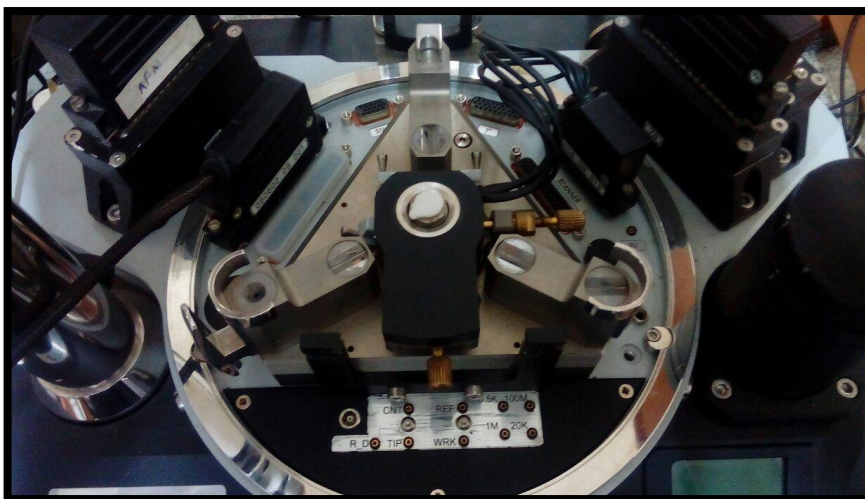


Fig. 44: Zirconia test sample placed on AFM for analysis

3. Wettability evaluation by contact angle goniometry



Fig. 45a: One μl of water placed on platform for contact angle measurement

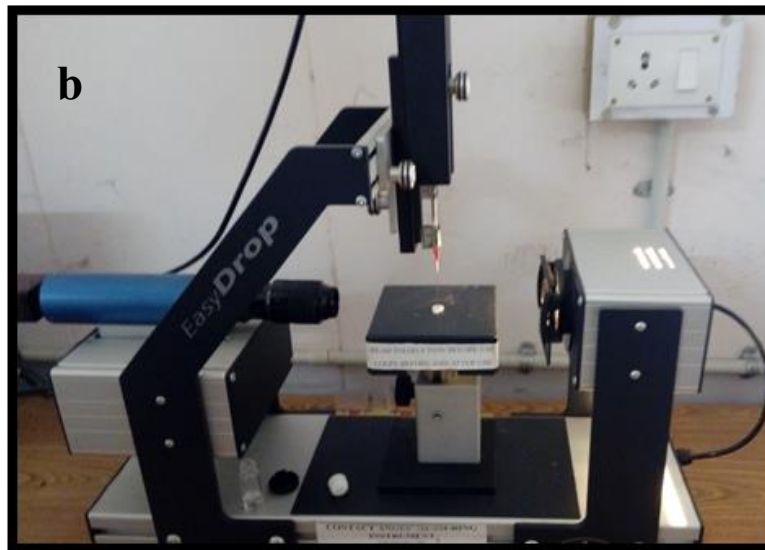


Fig. 45b: Water droplet on test sample

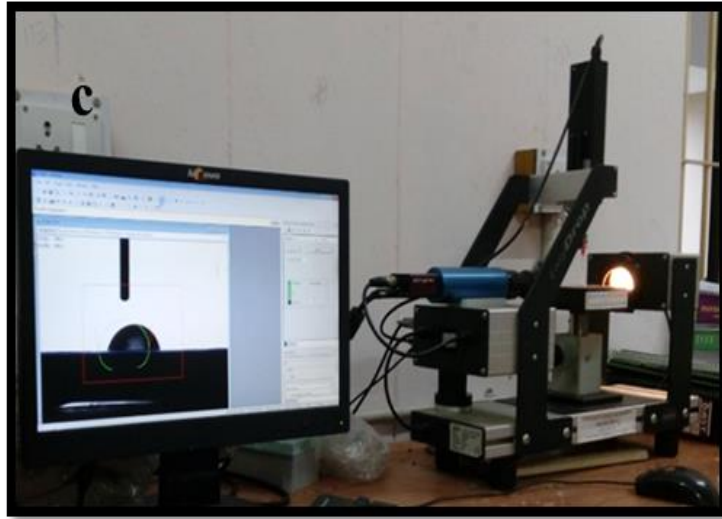


Fig. 45c: Image of contact angle measurement recorded

4. Surface topographic and elemental analysis by Scanning Electron Microscopy coupled with Energy Dispersive X-ray Spectroscopy (SEM-EDX) (Fig. 46a & Fig. 46b)



Fig. 46a. Gold sputtered test samples of Groups I, II and III for SEM – EDX analysis

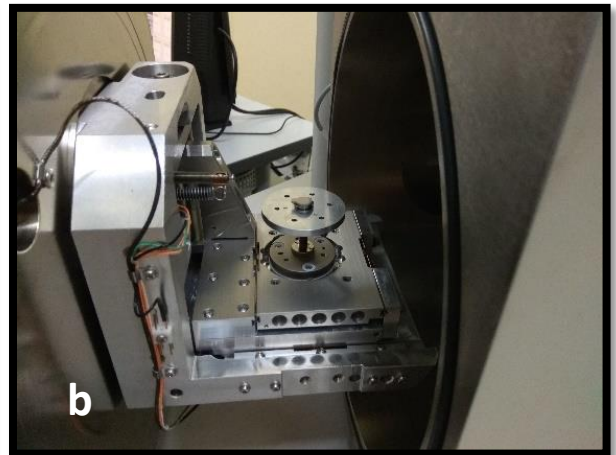


Fig. 46b. Zirconia test sample placed on SEM for analysis

BIOACTIVITY TEST

1. Preparation of Simulated Body Fluid (SBF) (Fig. 47a to Fig. 48)

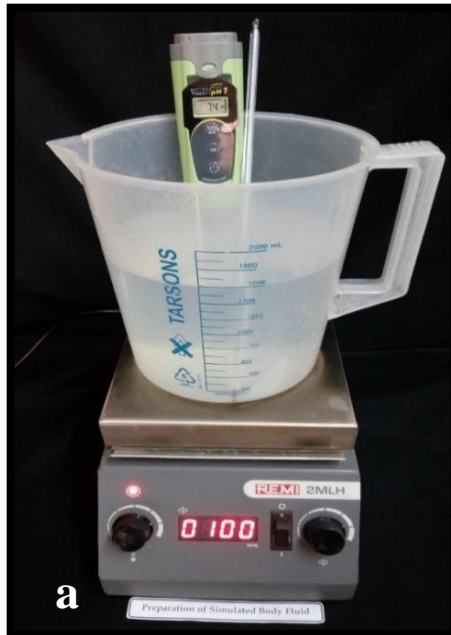


Fig. 47a: SBF solution being prepared over the magnetic stirrer with hotplate and with pH tester in place



Fig. 47b: pH tester showing pH 7.4 for the SBF solution



Fig. 48: Freshly-prepared Simulated Body Fluid (SBF) stored in an airtight plastic container

Immersion of test samples in SBF (Fig. 49a to Fig. 52b)



Fig. 49a: Immersion of a test sample in SBF solution in a graduated test tube

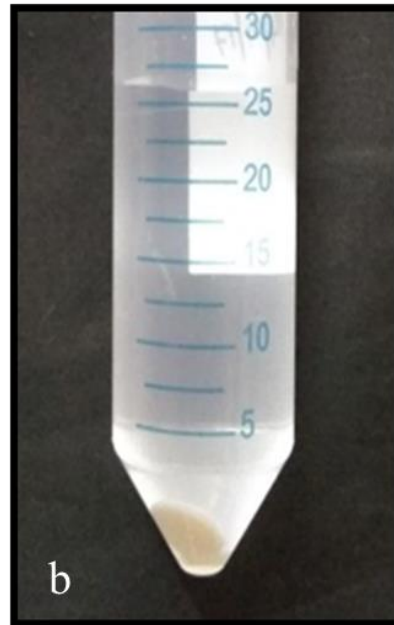


Fig. 49b: Close-up view of test sample from Fig. 46a



Fig. 50a: Group I (Untreated) test samples in SBF (n=10)

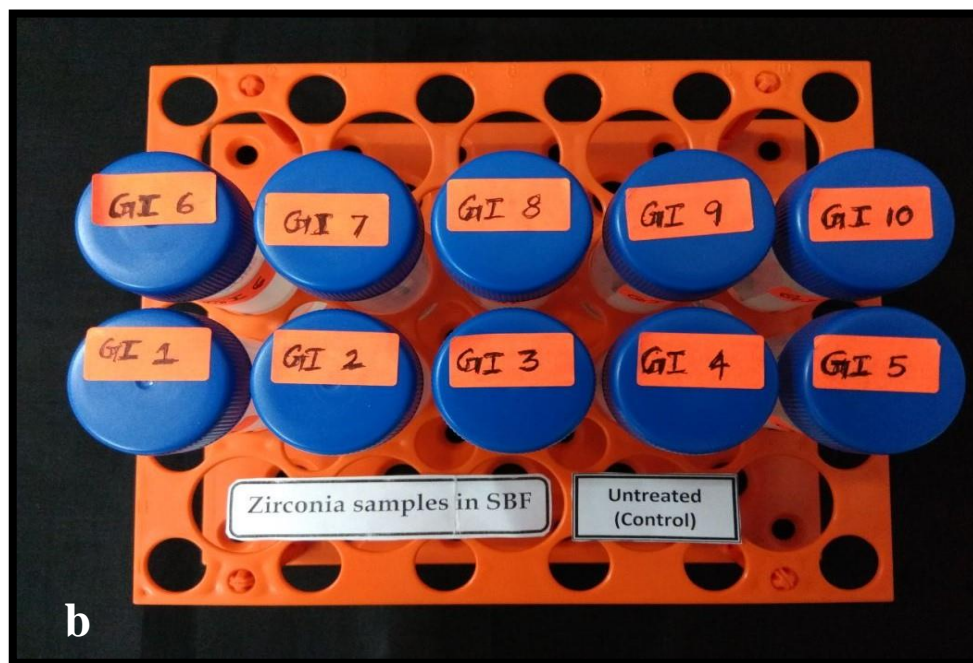


Fig. 50b: Bird's eye view of Group I (Untreated) test samples



Fig. 51a: Group II (Sandblasted) test samples in SBF (n=10)

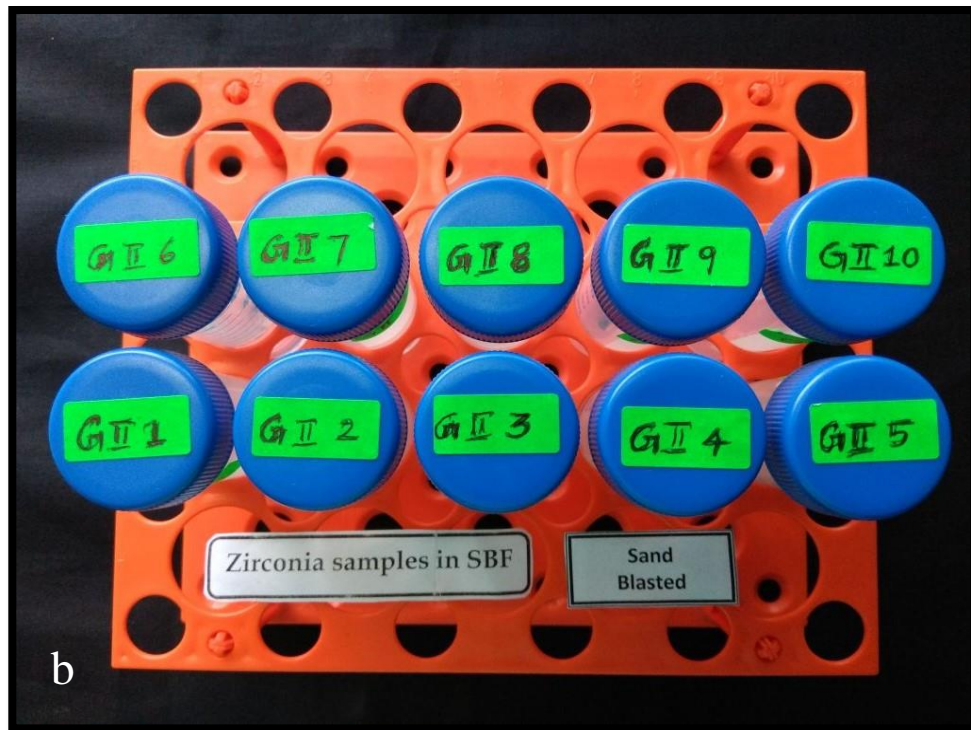


Fig. 51b: Bird's eye view of Group II (Sandblasted) test samples

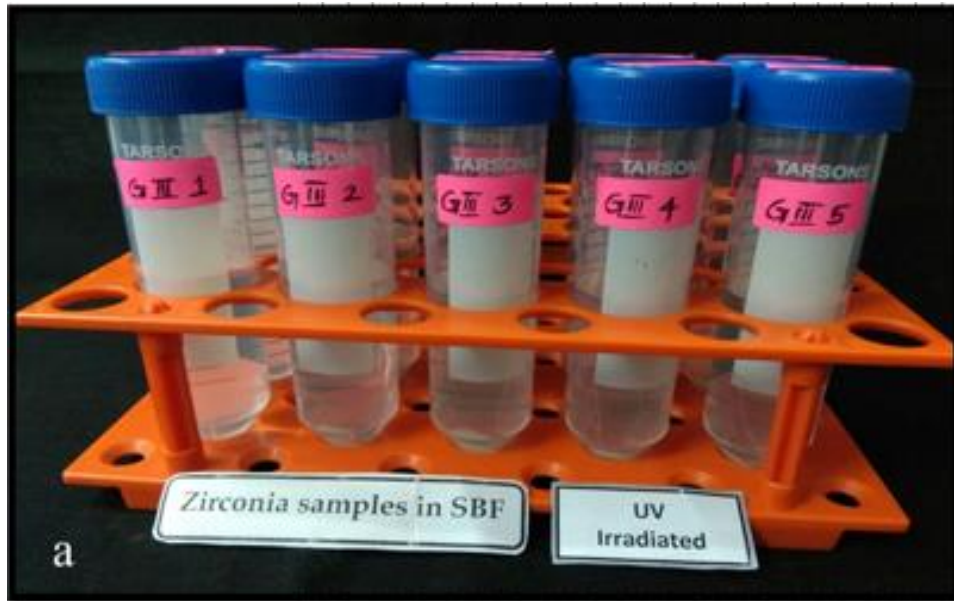


Fig. 52a: Group III (UVP) test samples in SBF (n=10)



Fig. 52b: Bird's eye view of Group III (UVP) test samples



Fig. 53: Incubation of test samples at 36.5°C

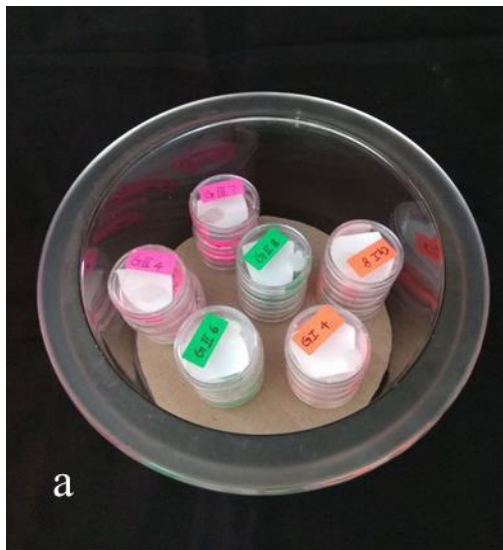


Fig. 54a: Test samples in desiccator after immersion in SBF

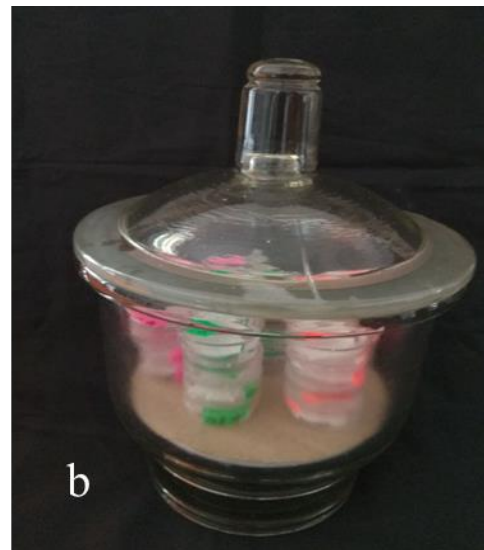


Fig. 54b: Test samples in desiccator with lid



Fig. 55: Analysis of calcium content in SBF using ICP-MS

Results

RESULTS

The aim of the present *in vitro* study was to evaluate and compare the effects of two different surface treatments, namely, sandblasting and UV Photofunctionalization on the bioactivity of zirconia. Thirty three zirconia test samples with dimensions of 10mm x 2mm were divided into 3 study groups each comprising of 11 samples. The study groups were designated as Groups I, II and III.

Group I samples were not subjected to any treatment (**Untreated**).

Group II samples were subjected to sandblasting with alumina (**Sandblasted**).

Group III samples were subjected to UV Photofunctionalization (**UVP**).

Representative test samples from each test group were subjected to analysis of surface characteristics after surface treatment, as follows:

- X-Ray Diffractometer (XRD) analysis to evaluate the type of surface crystalline phase (monoclinic/tetragonal/cubic) of zirconia (**Annexure III - Figs. 56a, 56b & 56c**).
- 3-D Atomic Force Microscopy (AFM) to evaluate and compare the surface roughness at the nanometre level (**Annexure III - Figs. 57a, 57b, 57c, 58a, 58b & 58c**), (**Tables 1 to 3**), (**Annexure IV - Graph 1**).
- Contact angle goniometry to evaluate and compare the wettability (**Annexure III - Figs. 59a, 59b & 59c**), (**Tables 4 to 6**), (**Annexure IV - Graph 2 to 5**).
- Scanning Electron Microscopy and Energy Dispersive X-ray Spectroscopy (SEM-EDX) to evaluate the surface topography and surface elemental composition (**Annexure III - Figs. 60a & 60b, 61a & 61b and 62a & 62b**).

The mean calcium content in freshly prepared Simulated Body Fluid (Ca-SBF) using Inductively Coupled Plasma Mass Spectrometry (ICP-MS) was measured and the reference value was obtained (**Table 7**), (**Annexure V - Graph 6**).

Ten samples of each test group were immersed individually in Simulated Body Fluid (SBF) for 3 weeks and Ca-SBF analysis of each test sample was analysed for bioactivity and the basic data and mean for each group were recorded and compared with the mean pre-immersion calcium content and between the test groups (**Tables 8 to 13**), (**Annexure V - Graphs 7 to 11**).

Representative test samples from each test group after immersion in SBF for 3 weeks were subjected to analysis of surface characteristics as follows:

- X-Ray Diffractometer (XRD) analysis to evaluate the type of surface crystalline phase (monoclinic/tetragonal/cubic) of zirconia (**Annexure VI - Figs. 63a, 63b & 63c**).
- Scanning Electron Microscopy and Energy Dispersive X-ray Spectroscopy (SEM-EDX) to evaluate the surface topography and the surface elemental composition respectively (**Annexure VI - Figs. 64a & 64b, 65a & 65b and 66a & 66b**).

All basic data and mean values obtained for each test group were tabulated and subjected to statistical analysis. The SPSS (SPSS for windows 16.0 SPSS Corp., Munich, Germany) software package was used for statistical analysis. One way ANOVA, Post-hoc Tukey's HSD analysis and students' paired 't' test were done to compare the data obtained for statistical significance with respect to surface roughness, wettability and bioactivity of the test groups.

ANNEXURE – III

ANALYSES OF SURFACE CHARACTERISTICS OF UNTREATED AND SURFACE TREATED REPRESENTATIVE TEST SAMPLES

A. SURFACE PHASE DIFFRACTOGRAMS OF UNTREATED AND SURFACE TREATED TEST SAMPLES OBTAINED BY X-RAY DIFFRACTOMETER (XRD)

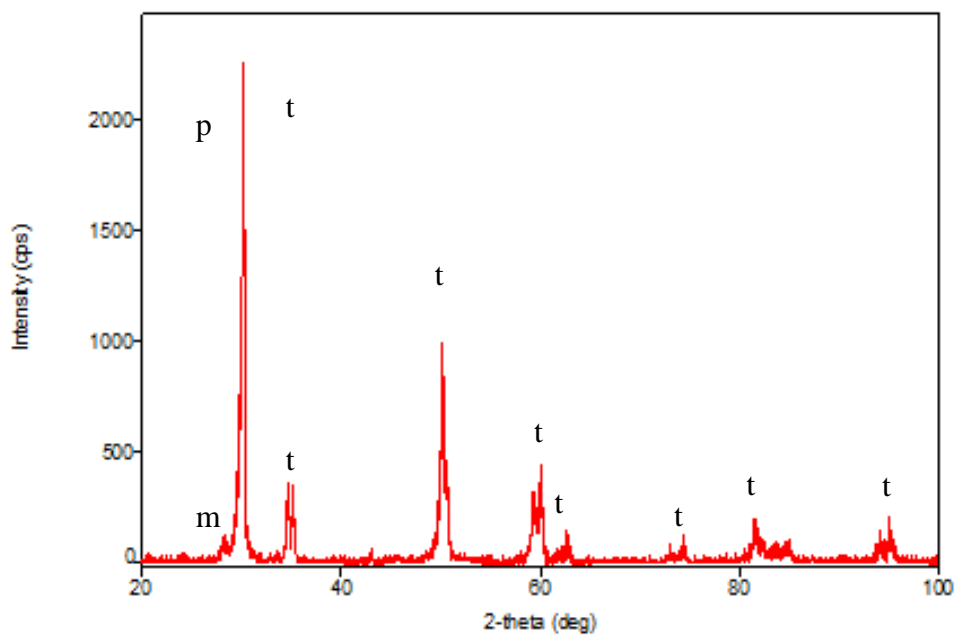


**Fig. 56a: Representative X-ray Diffractogram (XRD) of Group I
(Untreated) test sample**

Key

m = Monoclinic ZrO₂

t = Tetragonal ZrO₂

p = Highest peak of Tetragonal Phase observed at 30°

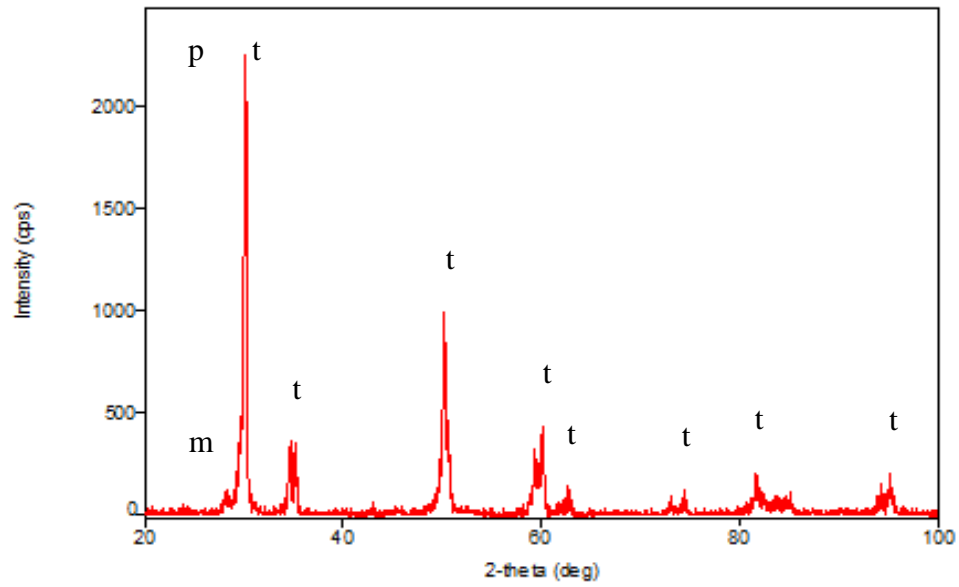


Fig. 56b: Representative X-Ray Diffractogram (XRD) of Group II (Sandblasted) test sample

Key

m = Monoclinic ZrO₂

t= Tetragonal ZrO₂

p= Highest peak of Tetragonal Phase observed at 30°

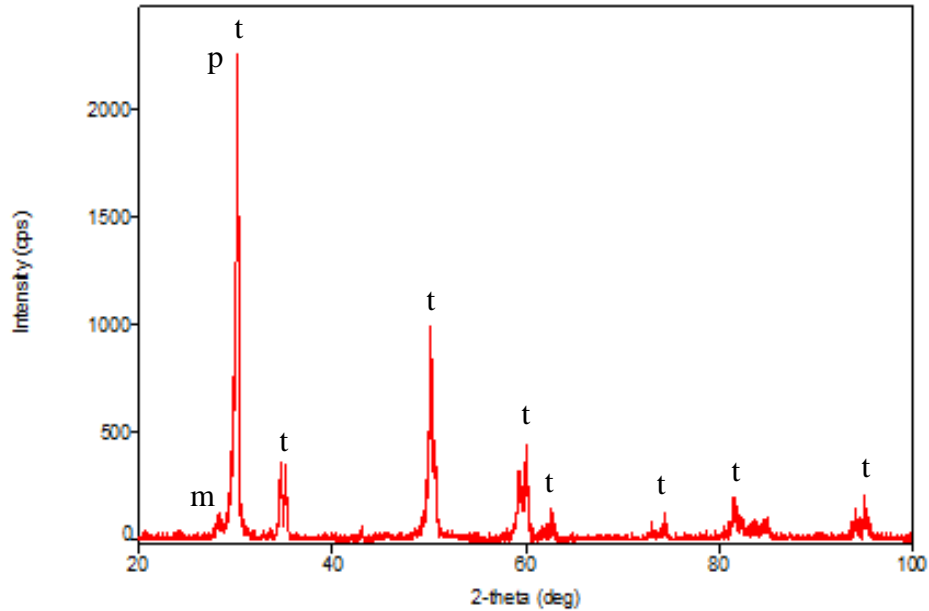


Fig. 56c: Representative X-Ray Diffractogram of Group III (UVP) test sample

Key

m = Monoclinic ZrO₂

t = Tetragonal ZrO₂

p = Highest peak of Tetragonal Phase observed at 30°

Overall Inference: X -Ray Diffractograms obtained for all the three test groups (Untreated, Sandblasted and UVP samples) revealed presence of predominantly tetragonal zirconia peaks, with negligible presence of monoclinic phase, indicating no crystal phase transformation occurring due to any of the surface treatments. The peak of the tetragonal phase was identified at 30° for all three test groups.

B. 2-D SURFACE ROUGHNESS IMAGES OF UNTREATED AND SURFACE TREATED TEST SAMPLES OBTAINED BY ATOMIC FORCE MICROSCOPY (AFM)

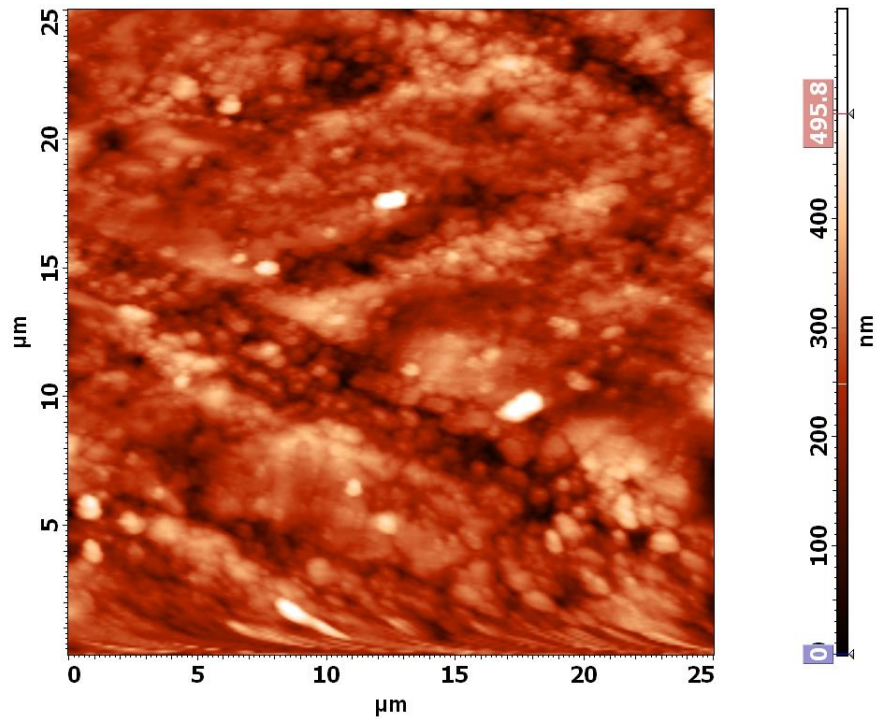


Fig. 57a: Representative 2D image of surface of Group I (Untreated) test sample

Inference: 2D image of Group I (Untreated) test sample showed a relatively uniform texture. Shallow grooves that were more or less uniform in depth and orientated in a grid-like pattern were observed across the sample surface.

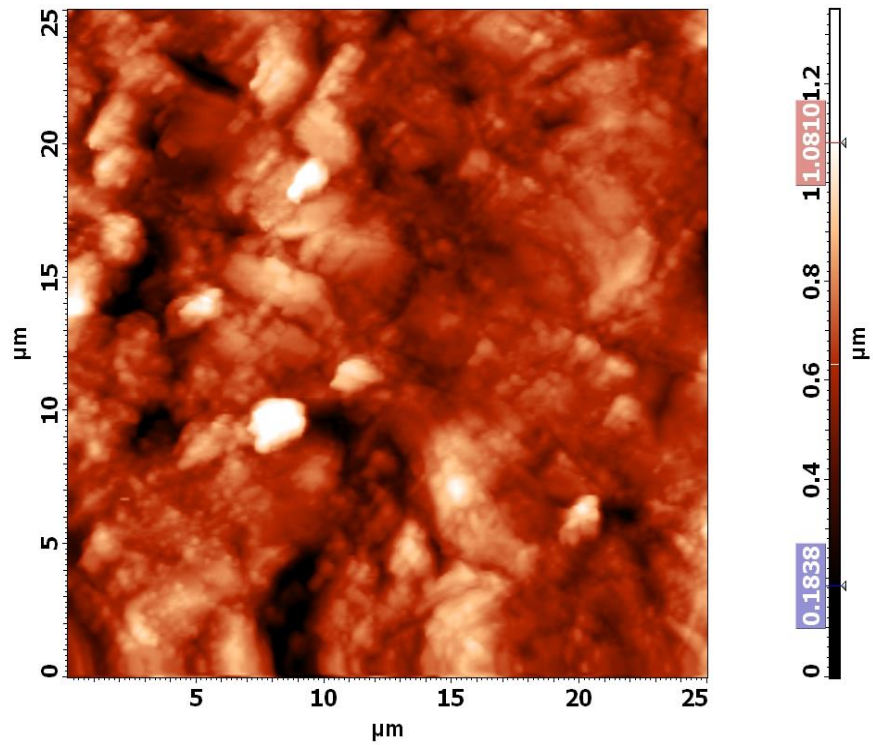


Fig. 57b: Representative 2D image of the surface of Group II (Sandblasted) test sample

Inference: 2D image of Group II (Sandblasted) test sample exhibited a non-uniform and irregularly roughened surface texture. Deep grooves of varying depths and orientation were observed across the sample surface.

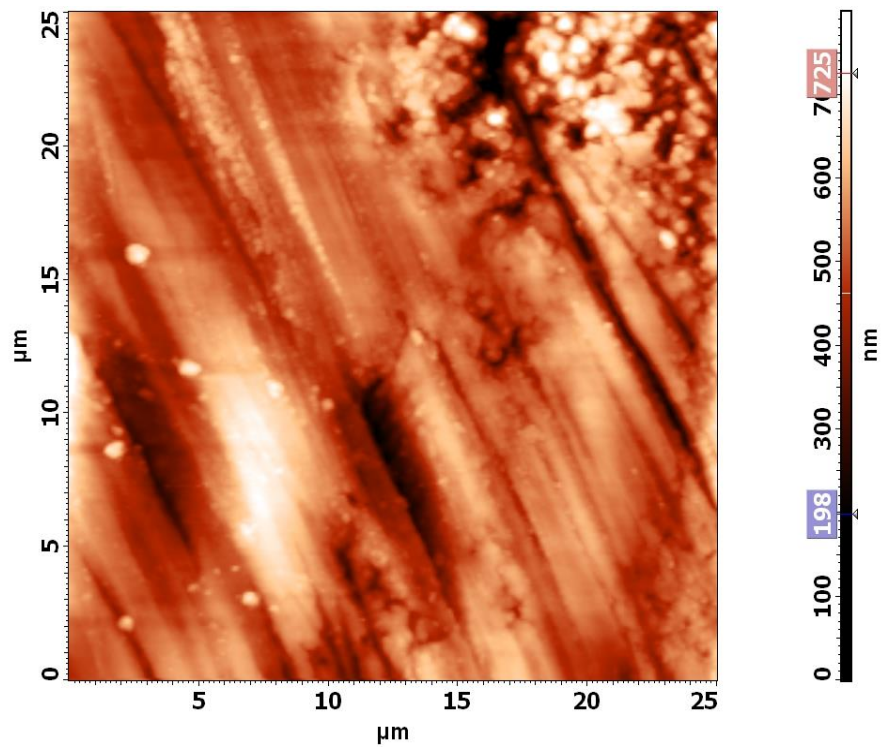


Fig. 57c. Representative 2D image of surface of Group III (UVP) test sample

Inference: 2D image of Group III (UVP) test sample revealed a uniformly roughened surface texture predominantly and an isolated non-uniform area. Grooves that were orientated predominantly parallel to each other were observed across the sample surface.

C. 3-D SURFACE ROUGHNESS IMAGES OF UNTREATED AND SURFACE TREATED TEST SAMPLES OBTAINED BY ATOMIC FORCE MICROSCOPY (AFM)

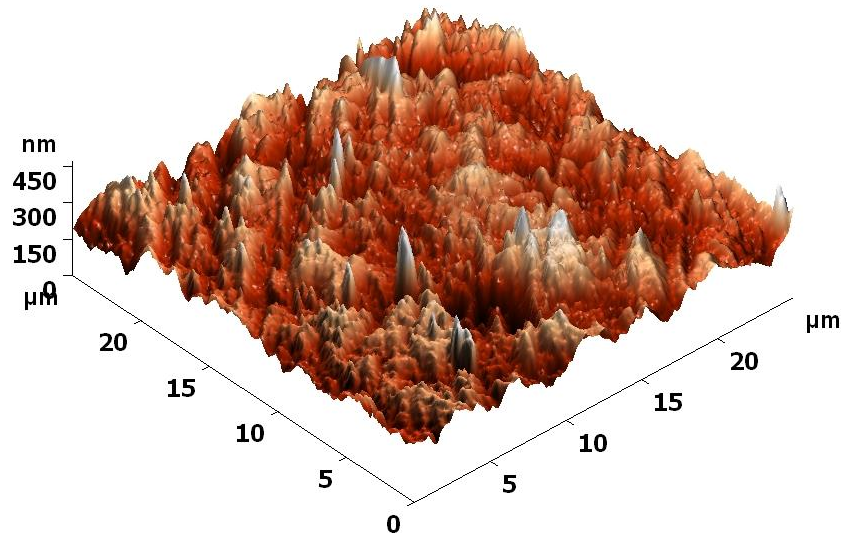


Fig. 58a: Representative 3D image of surface roughness of Group I (Untreated) test sample

Inference: Group I (Untreated) surface revealed a uniform appearance throughout with lesser number of shallow peaks and valleys, seen at isolated places on the sample surface. The average height of peaks and valleys was found to be 292.13 nm (Also refer Table 1).

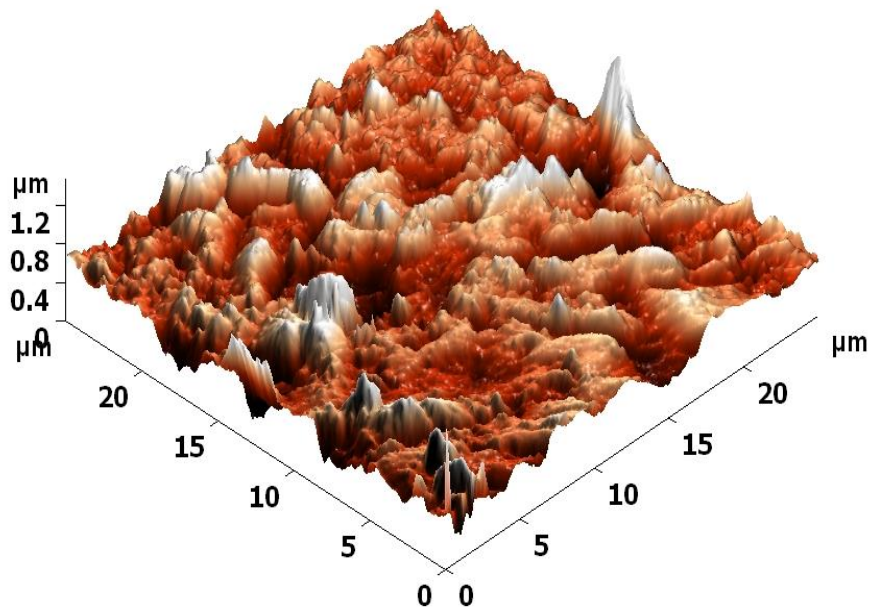


Fig. 58b: Representative 3D image of surface roughness of Group II (Sandblasted) test sample

Inference: Group II (Sandblasted) surface revealed a non-uniform texture, with greater number of very high and well defined peaks and valleys distributed throughout the sample surface. The average height of peaks and valleys was 764.06 nm (Also refer Table 1).

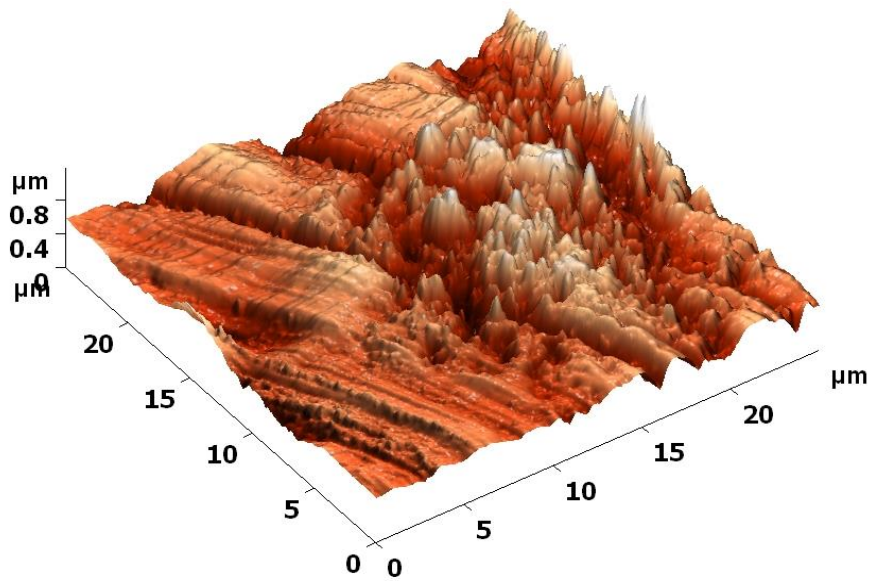
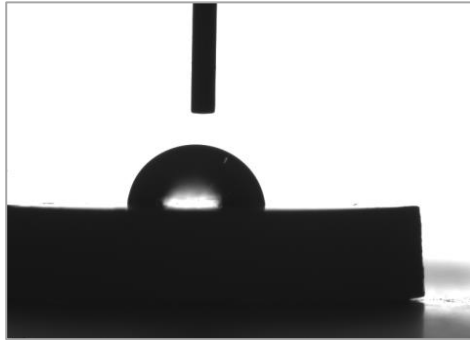


Fig. 58c: Representative 3D image of surface roughness of Group III (UVP) test sample

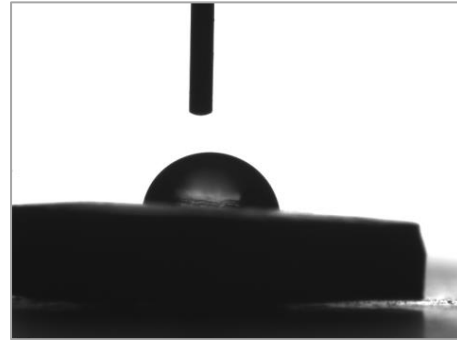
Inference: Group III (UVP) surface revealed a non-uniform texture of roughened plains with several deep grooves, along with areas of clustered peaks and valleys, which were well-defined. The average height of peaks and valleys was 541.65 nm (Also refer Table 1).

D. CONTACT ANGLE IMAGES OF UNTREATED AND SURFACE TREATED TEST SAMPLES OBTAINED BY CONTACT ANGLE GONIOMETRY



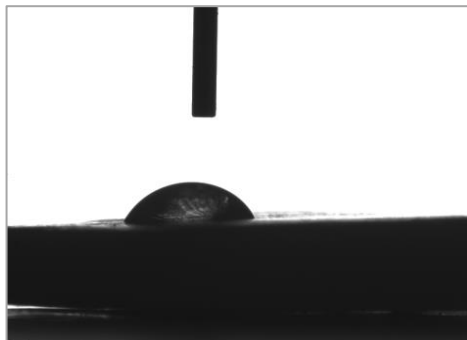
93.60° - 100.66°

Fig. 59a: Group I (Untreated)



82.76° - 91.30°

Fig. 59b: Group II (Sandblasted)



66.12° - 69.48°

Fig. 59c: Group III (UVP)

Fig. 59a, 59b & 59c: Contact angle measurements of Group I, Group II and Group III test samples

Inference: Contact angles ranged between 93.60° – 100.66° in Group I; 82.76° – 91.30° in Group II; 66.12° - 69.48° in Group III. The mean contact angles of Group I, Group II and Group III test samples were 98.26°, 86.77° and 68.03° respectively.

**E. TOPOGRAPHY AND ELEMENTAL COMPOSITION OF
UNTREATED AND SURFACE TREATED TEST SAMPLES
OBTAINED BY SCANNING ELECTRON MICROSCOPY (SEM) AND
ENERGY DISPERSIVE X-RAY SPECTROSCOPY(EDX)**

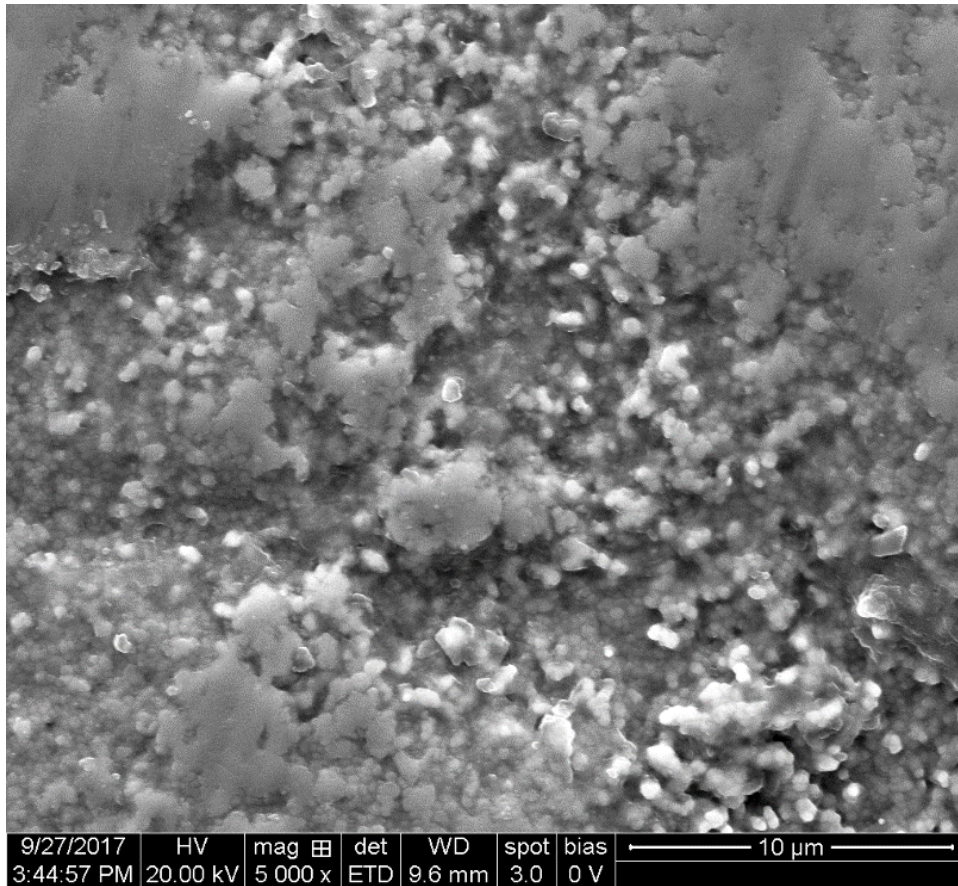


Fig. 60a: Representative photomicrograph of surface topography of the Group I (Untreated) test sample under 5000x magnification

Inference: SEM photomicrograph of Group I (Untreated) test sample showed presence of flattened areas interspersed with some patches of moderately roughened surface.

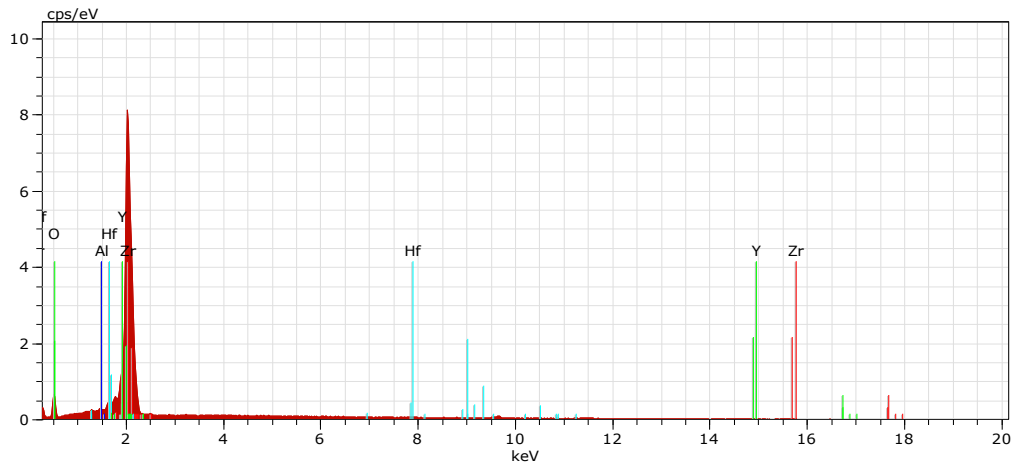


Fig. 60b: EDX spectrum of surface elemental analysis of the Group I (Untreated) test sample

El	AN	Series	unn. [wt.%]	C norm. [wt.%]	C Atom. [at.%]	CError(1Sigma) [wt.%]
Zr	40	L-series	67.01	69.69	40.26	2.58
O	8	K-series	15.74	16.37	53.59	2.58
Y	39	L-series	12.66	13.16	5.61	0.54
Hf	72	L-series	0.56	0.58	0.17	0.06
Al	13	K-series	0.19	0.20	0.38	0.04
Total:			96.15	100.00	100.00	

Inference: EDX spectrum of Group I (Untreated) test sample revealed surface elemental composition of Zirconium (40.26%), Oxygen (53.59%), Yttrium (5.61%), Hafnium (0.17%) and Aluminium (0.38%). The elements revealed by the EDX evaluation was similar to the composition mentioned by the manufacturer.

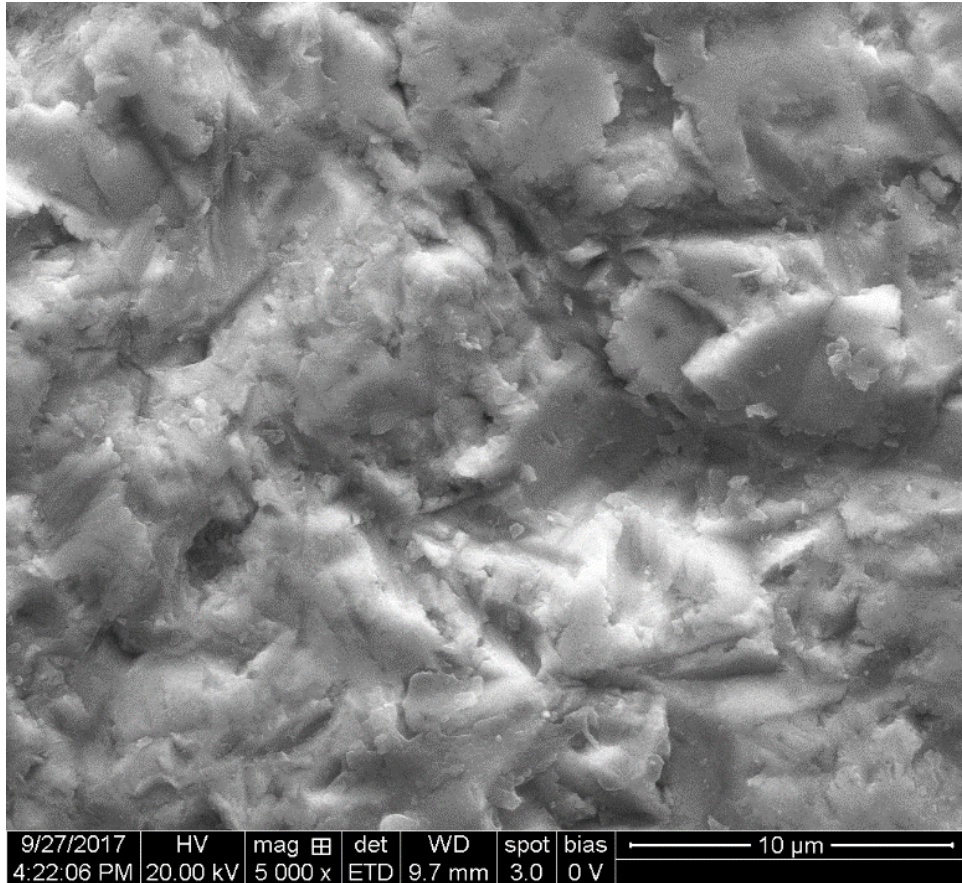


Fig. 61a: Representative photomicrograph of surface topography of Group II (Sandblasted) test sample under 5000x magnification

Inference: SEM photomicrograph of Group II (Sandblasted) test sample showed presence of irregular surface with accentuated peaks and depressions throughout the observed field. The irregularities observed were non-uniform in character. There was absence of flattened areas, unlike those observed with the Group I (Untreated) test sample.

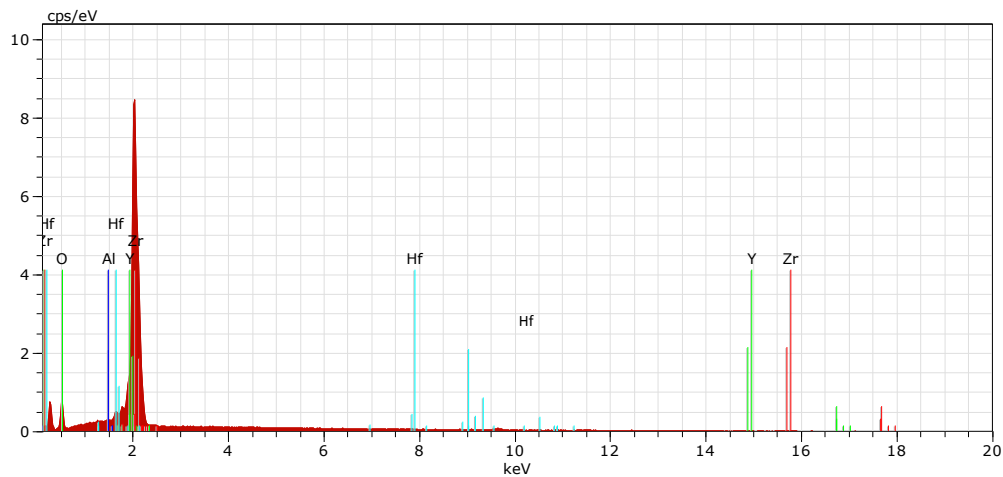


Fig. 61b: EDX spectrum of surface elemental analysis of the Group II (Sandblasted) test sample

El	AN	Series	unn. [wt.%]	C norm. [wt.%]	C Atom. [at.%]	C Error(1Sigma) [wt.%]
Zr	40	L-series	62.53	70.26	39.20	2.41
O	8	K-series	15.83	17.79	55.16	2.55
Y	39	L-series	10.01	11.25	5.28	0.43
Hf	72	L-series	0.52	0.59	0.16	0.06
Al	13	K-series	0.10	0.11	0.20	0.03
Total:			88.99	100.00	100.00	

Inference: EDX spectrum of Group II (Sandblasted) test sample revealed surface elemental composition of Zirconium (39.20%), Oxygen (55.16%), Yttrium (5.28 %), Hafnium (0.16%) and Aluminium (0.20 %), indicating that surface treatment with sandblasting did not alter the original surface elemental composition significantly.

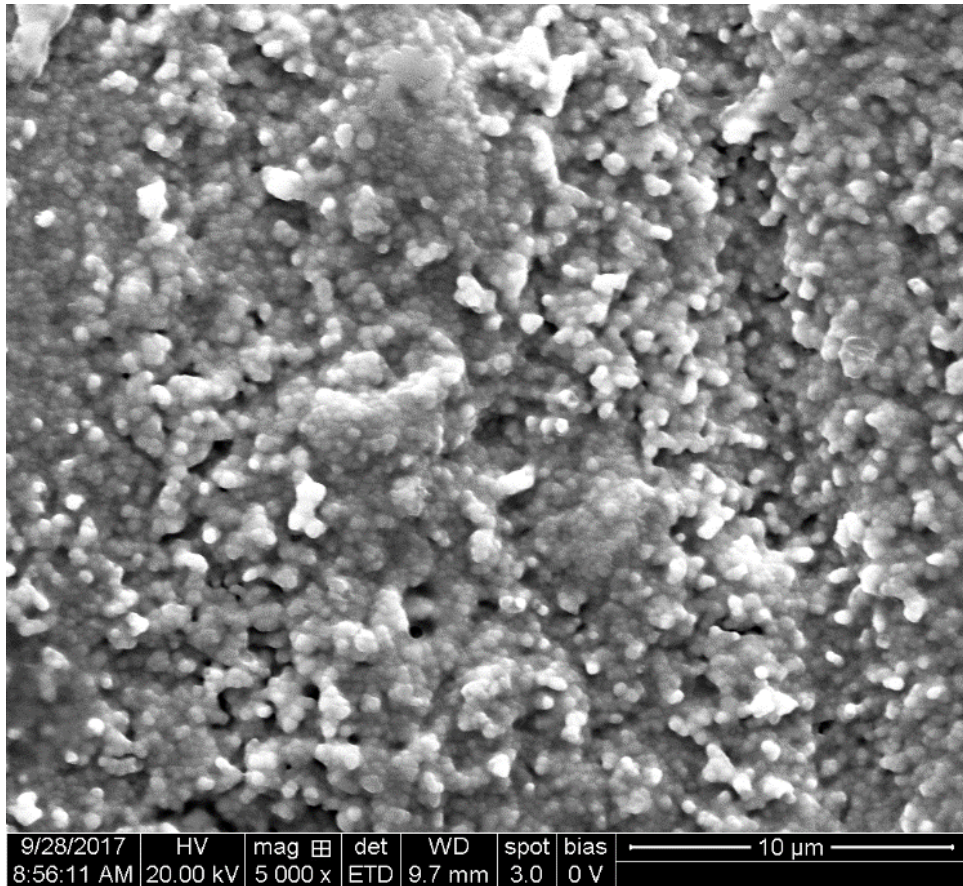


Fig. 62a: Representative photomicrograph of surface topography of Group III (UVP) test sample under 5000x magnification

Inference: SEM photomicrograph of Group III (UVP) test sample showed presence of uniformly roughened surface with a coral-like appearance throughout the observed field. The irregularities appeared more uniform in character and shallower, as compared to that of Group II (Sandblasted) sample. There was absence of flattened areas, unlike those observed with the Group I (Untreated) test sample.

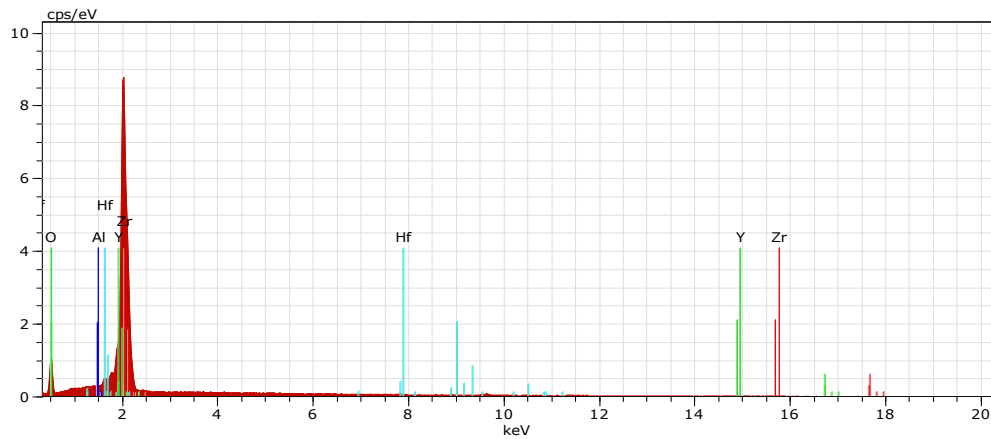


Fig. 62b: EDX spectrum of surface elemental analysis of the Group III (UVP) test sample

El	AN	Series	unn. [wt.%]	C norm. [wt.%]	C Atom. [at.%]	C Error(1Sigma) [wt.%]
Zr	40	L-series	59.48	66.13	32.66	2.29
O	8	K-series	19.58	21.77	61.31	2.99
Y	39	L-series	10.13	11.26	5.71	0.44
Hf	72	L-series	0.68	0.75	0.19	0.07
Al	13	K-series	0.07	0.08	0.13	0.03
Total:			89.94	100.00	100.00	

Inference: EDX spectrum of Group III (UVP) test sample revealed surface elemental composition of Zirconium (32.66%), Oxygen (61.31%), Yttrium (5.71%), Hafnium (0.19%) and Aluminium (0.13%), indicating that surface treatment with UVP did not alter the original surface elemental composition significantly.

Table 1: Basic values and mean of surface roughness (nm) of representative samples of Groups I, II & III (n=1/Group), measured at 4 distinct areas per sample by 3D Atomic Force Microscopy (AFM)

Groups	Average Roughness (Sa)			Average Values -Heights & Valleys (Sz)		
	#	Value (nm)	Mean (nm)	#	Value(nm)	Mean(nm)
Group I	1	42.62	41.83	1	303.00	292.13
	2	32.00		2	238.11	
	3	46.33		3	331.01	
	4	46.37		4	296.40	
Group II	1	89.80	115.65	1	697.81	764.06
	2	132.65		2	796.67	
	3	105.79		3	672.00	
	4	134.35		4	889.74	
Group III	1	90.19	102.43	1	498.56	541.65
	2	138.27		2	686.39	
	3	96.74		3	401.20	
	4	84.53		4	580.45	

- Areas per representative sample

Inference: The mean surface roughness of Group I (Untreated), Group II (Sandblasted) and Group III (UVP) test samples were **41.83nm**, **115.65nm** and **102.43nm** respectively. The average values of heights and valleys for Group I (Untreated), Group II (Sandblasted) and Group III (UVP) test samples were **292.13nm**, **764.06nm** and **541.65nm** respectively.

Table 2: Comparative evaluation of mean surface roughness (Sa in nm) between Groups I, II and III for overall significance by One-Way Analysis of Variance (ANOVA)

Test Groups	No. of Samples	Mean (nm)	p-Value
Group I	1	41.83	0.001**
Group II	1	115.65	
Group III	1	102.43	

**p-value < 0.01; highly significant

Inference: One-Way Analysis of Variance (ANOVA) revealed overall significant difference between the mean surface roughness values of the three test groups.

Table 3: Comparative evaluation of mean surface roughness (Sa in nm) between Groups I, II and III by Multiple Post-hoc Tukey's HSD test

Group	No. of Samples	Mean (nm)	p-value
Group I Vs Group II	1	41.83	0.001 **
	1	115.65	
Group I Vs Group III	1	41.83	0.004**
	1	102.43	
Group II Vs Group III	1	115.65	0.612
	1	102.43	

**p-value < 0.01; highly significant

Inference: Multiple comparisons using Post-hoc Tukey's HSD analysis showed statistically highly significant increase ($p < 0.01$) in mean surface roughness for both the surface treated groups (Group II and Group III), as compared to that of the untreated group (Group I). Group II (Sandblasted) showed a marginally higher increase in mean surface roughness as compared to that of Group III (UVP) that was found to be statistically insignificant ($p > 0.05$), indicating similar surface roughness achieved after both the surface treatments.

Table 4: Basic values and mean of contact angles (degrees) denoting wettability as measured using contact angle goniometry for representative samples of Groups I, II and III (n=5/Group)

Sample No.	Contact Angles (degrees)		
	Group I	Group II	Group III
1	100.62	87.66	66.12
2	100.66	89.04	68.84
3	99.98	82.76	68.44
4	93.60	83.12	69.48
5	96.48	91.30	67.30
Range	93.60-100.66	82.76-91.30	66.12-69.48
Mean	98.26	86.77	68.03
Standard Deviation	3.129	3.737	1.333
Standard Error	1.390	1.670	0.590

Inference: The contact angles of Group I (Untreated) were found to range between **93.60° to 100.66°**, with a mean of **98.26°**. The contact angles of Group II (Sandblasted) were found to range between **82.76° to 91.30°**, with a mean of **86.77°**. The contact angles of Group III (UVP) were found to range between **66.12° to 69.48°**, with a mean of **68.03°**.

Table 5: Comparative evaluation of the surface wettability between the mean contact angles of Groups I, II and III for overall significance by One-Way Analysis of Variance (ANOVA)

Test Groups	No. of Samples	Mean(in degrees)	p-Value
Group I	5	98.26	0.000**
Group II	5	86.77	
Group III	5	68.03	

**p-value < 0.01; highly significant

Inference: One-Way Analysis of Variance (ANOVA) revealed overall significant differences between the mean contact angles of the three test groups, indicating highly significant differences between their wettabilities (hydrophilicity).

Table 6: Comparative evaluation of mean contact angle measurements between Groups I, II and III by Multiple Post-hoc Tukey's HSD test

Group	No. of samples	Mean (in degrees)	p-value
Group I Vs Group II	5	98.26	0.000**
	5	86.77	
Group I Vs Group III	5	98.26	0.000**
	5	68.03	
Group II Vs Group III	5	86.77	0.000**
	5	68.03	

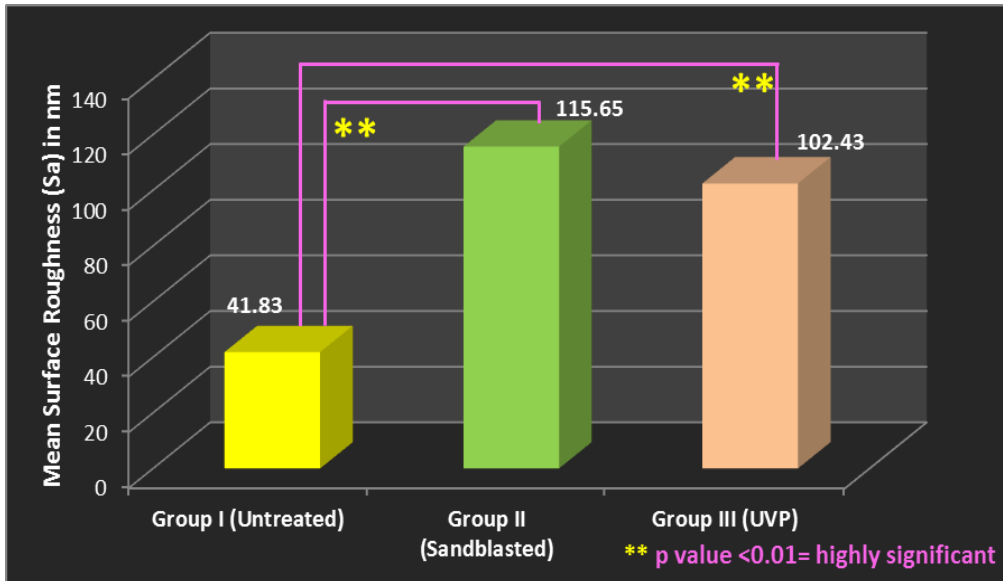
**p-value < 0.01; highly significant

Inference: Multiple comparisons using Post-hoc Tukey's HSD analysis showed statistically and highly significant decrease in mean contact angles for both the surface treated groups (Group II & Group III) as compared to that of untreated group (Group I), indicating increased wettability for both the surface treated groups ($p < 0.01$; highly significant). Group III showed significantly lesser mean contact angle than that for Group II, indicating superior wettability after UVP surface treatment as compared to sandblasting ($p < 0.01$; highly significant).

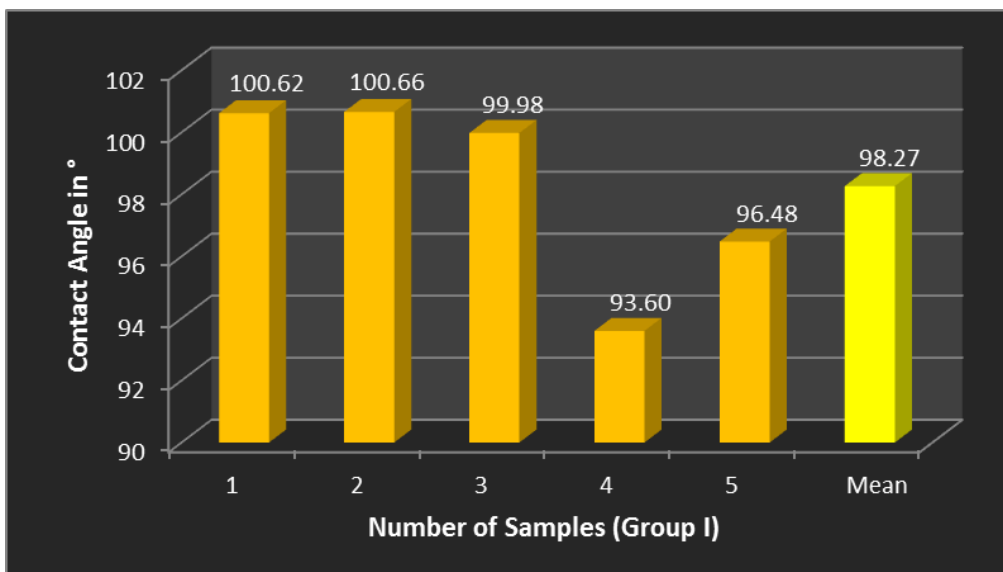
ANNEXURE IV

BAR GRAPHS FOR SURFACE ROUGHNESS & WETTABILITY DATA

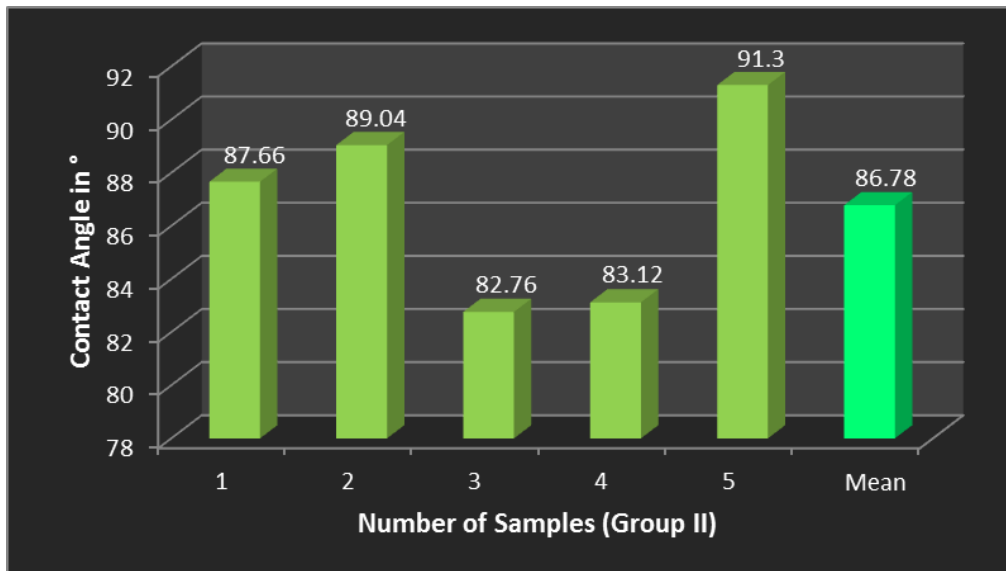
Graph 1: Comparative evaluation of mean surface roughness (Sa in nm) between Groups I, II and III



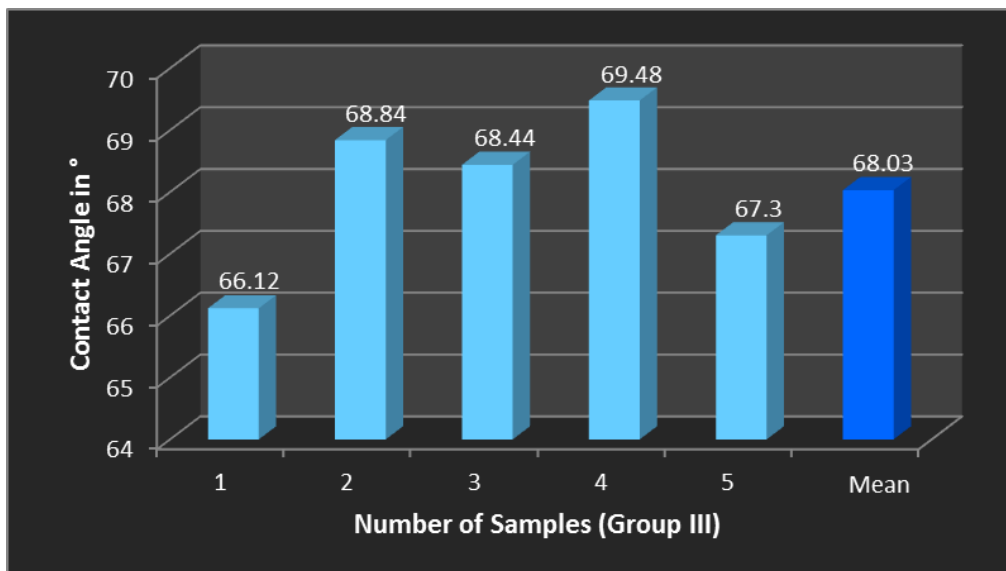
Graph 2: Basic values and mean of contact angle measurements (degrees) for Group I (Untreated)



Graph 3: Basic values and mean of contact angle measurements (degrees) for Group II (Sandblasted)



Graph 4: Basic values and mean of contact angle measurements (degrees) for Group III (UVP)



Graph 5: Comparative evaluation of mean contact angle measurements between Groups I, II and III

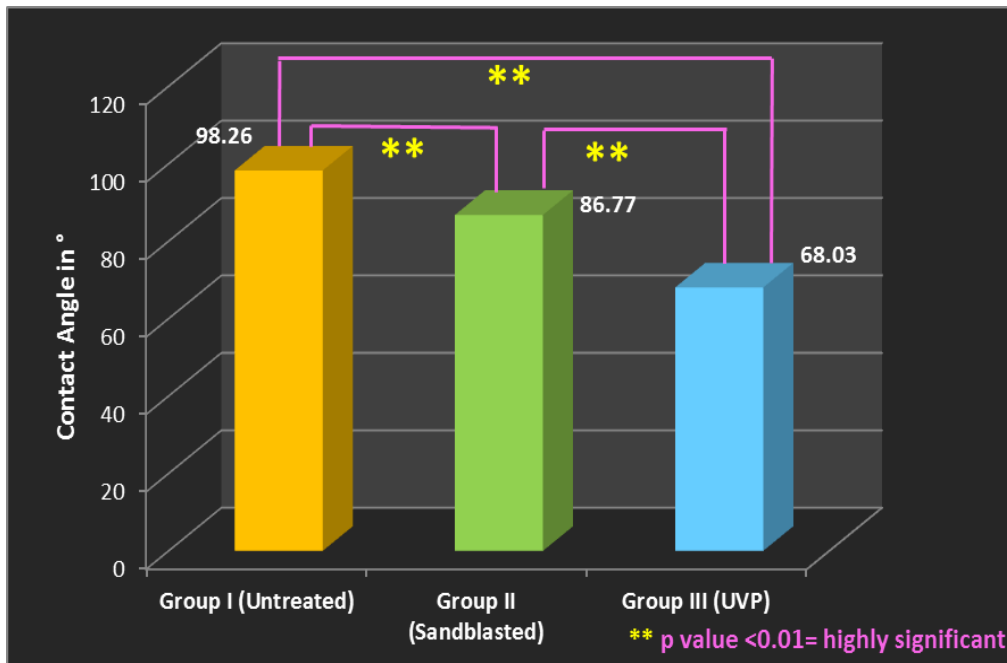


Table 7: Basic values and mean pre-immersion calcium content (Reference value in mg/L) in Simulated Body Fluid (SBF) obtained by Inductively Coupled Plasma Mass Spectrometry (ICP-MS)

Sample No.	Pre-Immersion calcium content in SBF (mg/L)
1	161
2	159
3	153
4	163
Mean	159

Inference: Ca-SBF analysis to detect calcium content in SBF prior to immersion of test samples revealed calcium content to be in the range of **153 mg/L to 163 mg/L** with a mean of **159 mg/L**. This mean value was considered as the pre-immersion reference value and used for comparing with the post-immersion calcium content in SBF obtained for the three test groups.

Table 8: Basic values and mean of post-immersion calcium content (mg/L) in SBF of Group I (Untreated) samples obtained by Inductively Coupled Plasma Mass Spectrometry (ICP-MS)

Sample No.	Calcium content in SBF in mg/L
GI 1	77
GI 2	64
GI 3	71
GI 4	67
GI 5	78
GI 6	68
GI 7	65
GI 8	66
GI 9	71
GI 10	74
Mean	70.10
Standard Deviation	4.95
Standard Error	1.56

Inference: The minimum calcium content of Simulated Body Fluid (SBF) in Group I (Untreated) was found to be **64 mg/L** (Sample no. 2), and the maximum calcium content was found to be **78 mg/L** (Sample no. 5). The mean calcium content was found to be **70.10 mg/L**.

Table 9: Basic values and mean of post-immersion calcium content (mg/L) in SBF of Group II (Sandblasted) samples obtained by Inductively Coupled Plasma Mass Spectrometry (ICP-MS)

Sample No.	Calcium content in SBF in mg/L
GII 1	72
GII 2	74
GII 3	53
GII 4	54
GII 5	60
GII 6	55
GII 7	56
GII 8	58
GII 9	54
GII 10	72
Mean	60.80
Standard Deviation	8.45
Standard Error	2.67

Inference: The minimum calcium content of Simulated Body Fluid (SBF) in Group II (Sandblasted) was found to be **53 mg/L** (Sample no. 3), and the maximum calcium content was found to be **74 mg/L** (Sample no. 2). The mean calcium content was found to be **60.80 mg/L**.

Table 10: Basic values and mean of post-immersion calcium content (mg/L) in SBF of Group III (UVP) samples obtained by Inductively Coupled Plasma Mass Spectrometry (ICP-MS)

Sample No.	Calcium content in SBF in mg/L
GIII 1	64
GIII 2	69
GIII 3	58
GIII 4	49
GIII 5	56
GIII 6	40
GIII 7	49
GIII 8	48
GIII 9	60
GIII 10	69
Mean	56.20
Standard Deviation	9.65
Standard Error	3.05

Inference: The minimum calcium content of Simulated Body Fluid (SBF) in Group III (UVP) was found to be **40 mg/L** (Sample no. 6), and the maximum calcium content was found to be **69 mg/L** (Sample nos. 2 & 10). The mean calcium content was found to be **56.20 mg/L**.

Table 11: Comparative evaluation of the difference between the pre-immersion calcium content (Reference value) and the mean post-immersion calcium content obtained for Groups I, II & III respectively, using student's paired 't' test

Pre-immersion calcium content in mg/L (Reference value)	Test Groups	Mean Post immersion calcium content in mg/L	Mean Difference of calcium content in mg/L	p-Value
159mg/L	Group I	70.10	88.90	0.039*
	Group II	60.80	98.20	
	Group III	56.20	102.80	

*p-Value < 0.05; significant

Inference: Student's paired 't'- test revealed significant reduction ($p < 0.05$) in the mean post- immersion calcium content of Groups I, II & III as compared to the pre-immersion calcium content (Reference value), indicating significant bioactivity for untreated as well as both the surface treated groups.

Table 12: Comparative evaluation of post-immersion calcium content in SBF between Groups I, II and III for overall significance by One-Way Analysis of Variance (ANOVA)

Test Groups	Number of samples	Mean	p-value
Group I	10	70.10	0.002**
Group II	10	60.80	
Group III	10	56.20	

**p-value < 0.01; highly significant

Inference: One way analysis of variance (ANOVA) revealed overall significant difference between the mean post-immersion calcium content values of three test groups ($p < 0.01$).

Table 13: Comparative evaluation of mean post-immersion calcium content in SBF between Groups I, II and III by Multiple Post-hoc Tukey's HSD test

Group	No. of samples	Mean	p-value
Group I Vs Group II	10	70.10	0.037*
	10	60.80	
Group I Vs Group III	10	70.10	0.002*
	10	56.20	
Group II Vs Group III	10	60.80	0.410
	10	56.20	

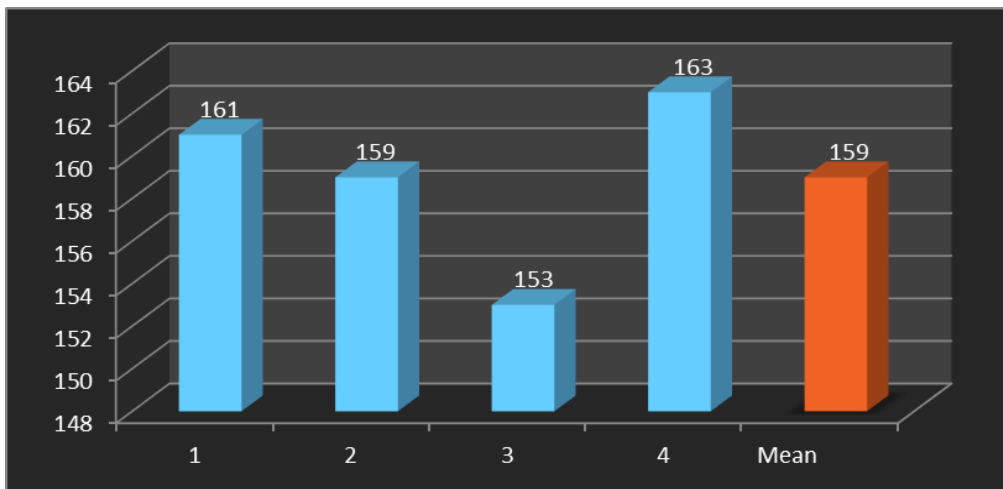
*p-value < 0.05; significant

Inference: Multiple comparisons using Post Hoc Tukey's HSD analysis showed statistically significant and greater decrease ($p < 0.05$) in the mean post-immersion calcium contents in SBF for both the surface treated groups (Groups II and III), as compared to that of the untreated group (Group I), indicating superior bioactivity for both the surface treated groups. Group III (UVP) showed lesser mean post-immersion calcium content in SBF as compared to that for Group II (Sandblasted). However, this was found to be statistically insignificant ($p > 0.05$), indicating similar bioactive behaviour in SBF with either surface treatments.

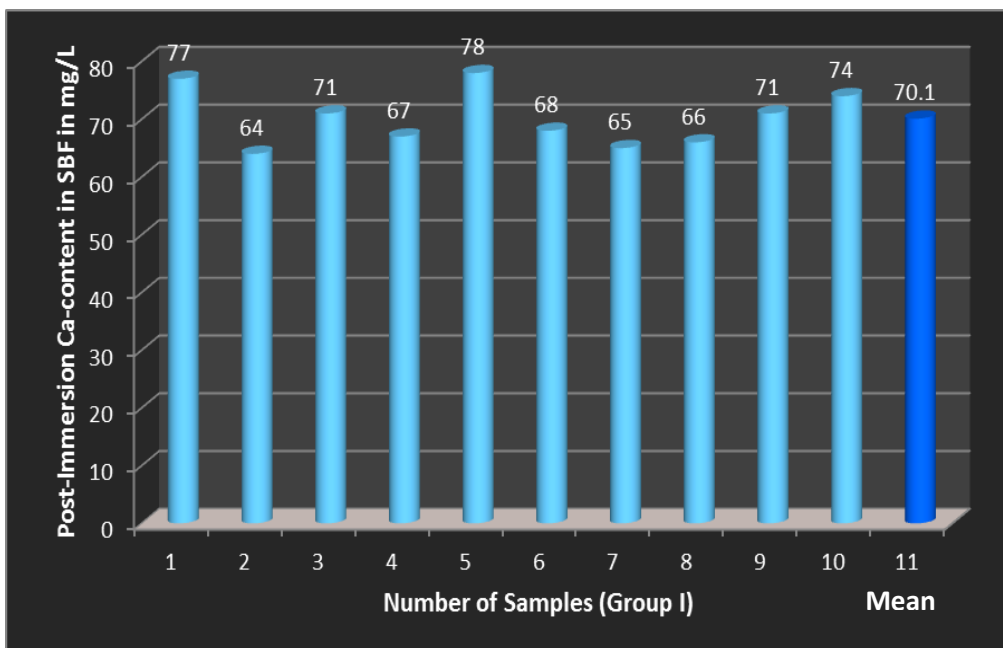
ANNEXURE V

BAR GRAPHS FOR BIOACTIVITY DATA

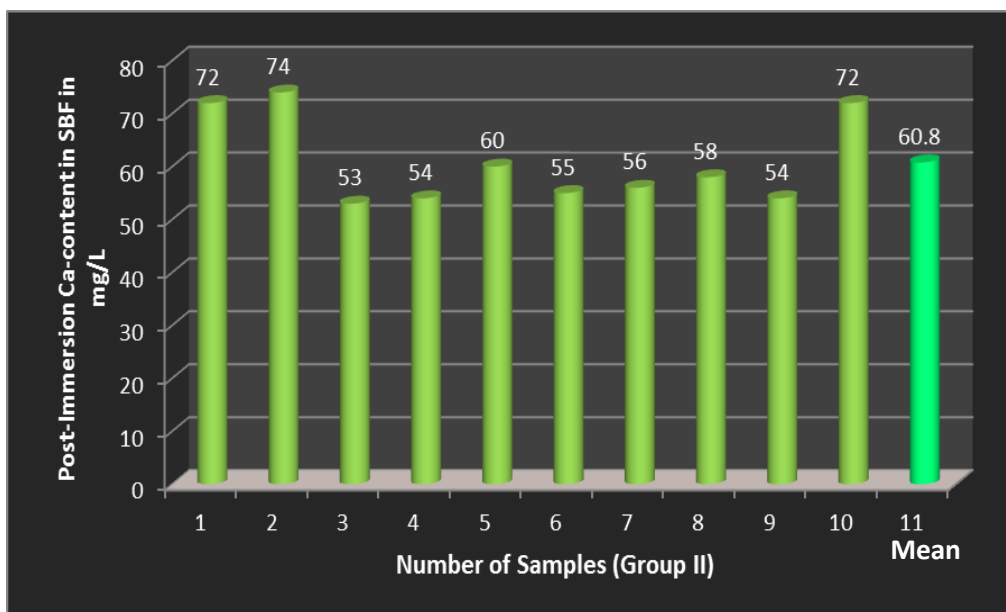
Graph 6: Basic values and mean pre-immersion Ca-content (Reference value in mg/L) in Simulated Body Fluid (SBF)



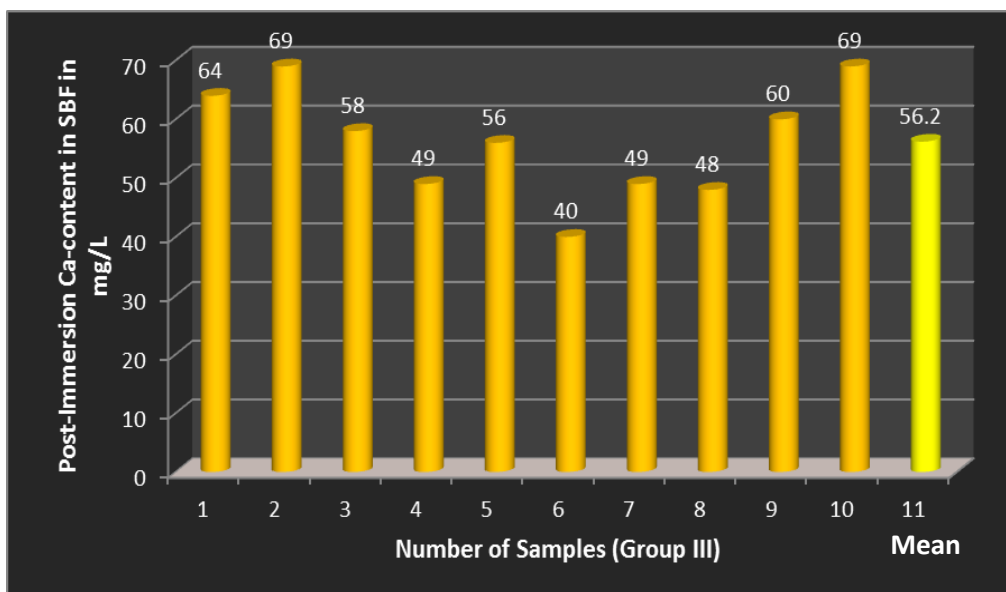
Graph 7: Basic values and mean of post-immersion Ca-content (mg/L) in SBF of Group I (Untreated) samples



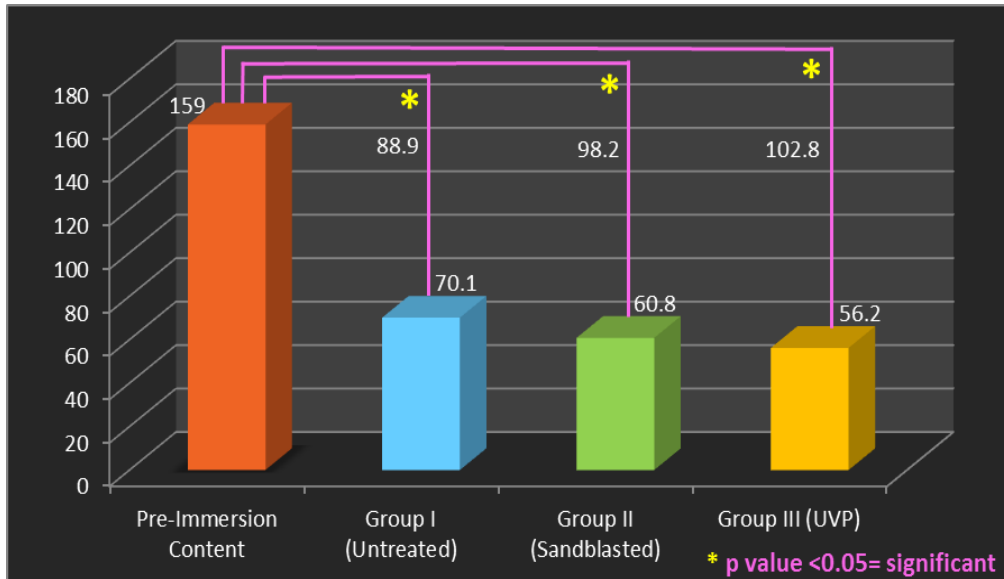
Graph 8: Basic values and mean of post-immersion Ca-content (mg/L) in SBF of Group II (Sandblasted) samples



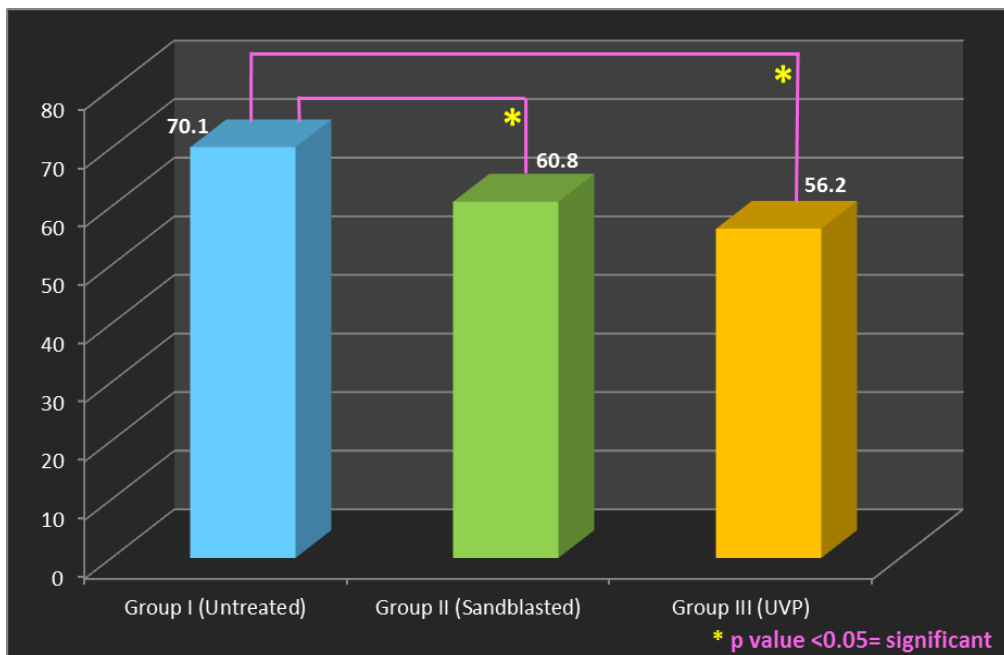
Graph 9: Basic values and mean of post-immersion Ca-content (mg/L) in SBF of Group III (UVP) samples



Graph 10: Comparative evaluation of the difference between the pre-immersion calcium content (Reference value) and the mean post-immersion calcium content obtained for Groups I, II & III respectively



Graph 11: Comparative evaluation of mean post-immersion Ca-content in SBF between Groups I, II and III



ANNEXURE – VI

ANALYSES OF SURFACE CHARACTERISTICS OF UNTREATED AND SURFACE TREATED TEST SAMPLES AFTER 3 WEEKS IMMERSION IN SBF

A. SURFACE PHASE DIFFRACTOGRAMS OF UNTREATED AND SURFACE TREATED TEST SAMPLES OBTAINED BY X-RAY DIFFRACTOMETER (XRD)

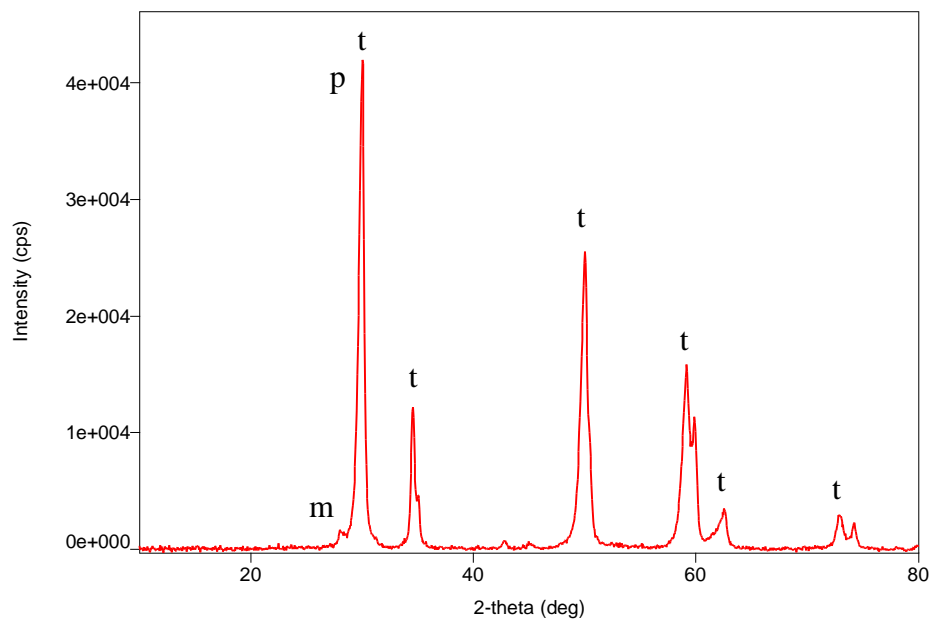


Fig. 63a: Representative X-Ray Diffractogram of Group I (Untreated) test sample

Key

m= Monoclinic ZrO₂

t = Tetragonal ZrO₂

p= Highest peak of Tetragonal Phase observed at 30°

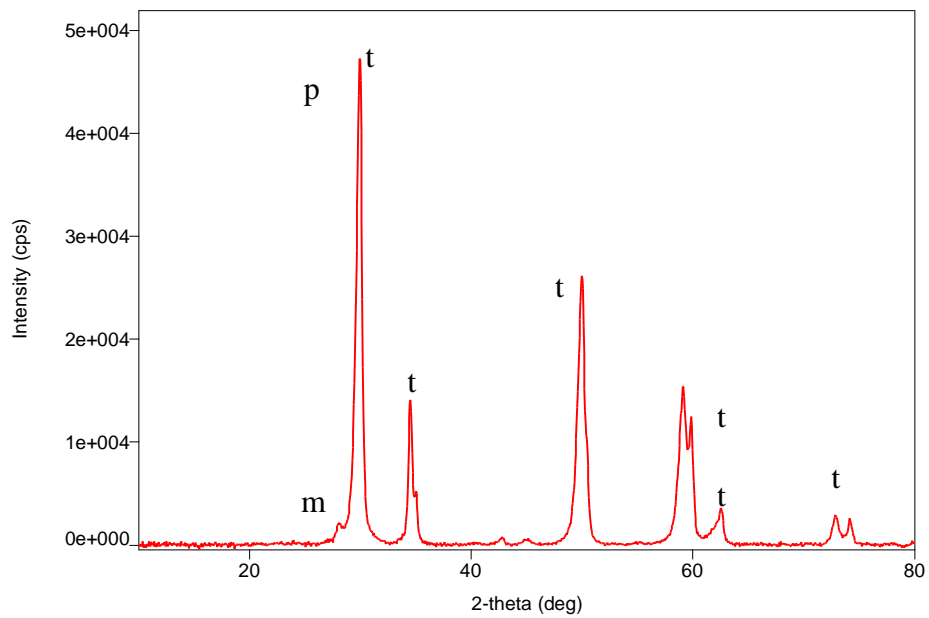


Fig. 63b: Representative X-Ray Diffractogram of Group II (Sandblasted) test sample

Key

m = Monoclinic ZrO₂

t= Tetragonal ZrO₂

p= Highest peak of Tetragonal Phase observed at 30°

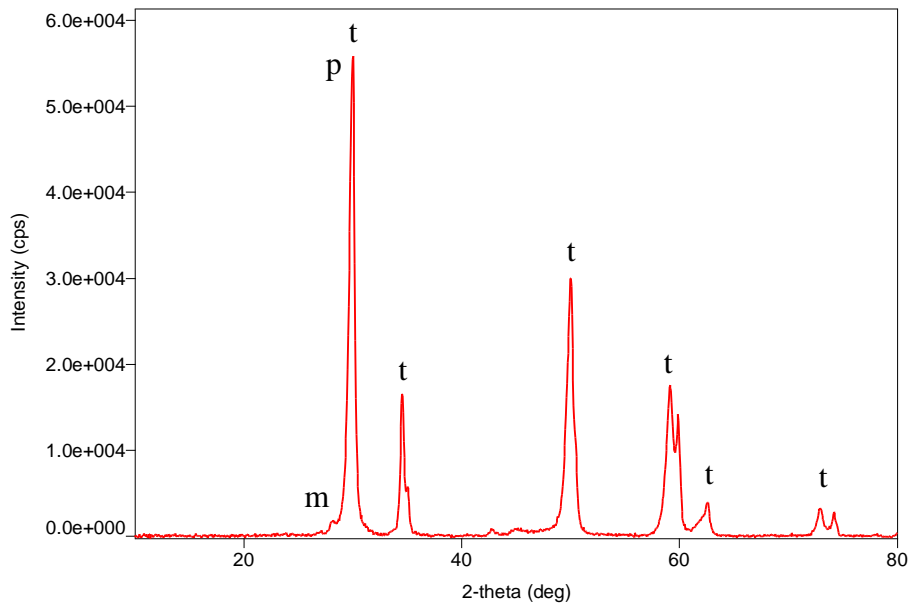


Fig. 63c: Representative X-Ray Diffractogram of Group III (UVP) test sample

Key

m = Monoclinic ZrO₂

t= Tetragonal ZrO₂

p= Highest peak of Tetragonal Phase observed at 30°

Overall Inference: X -Ray Diffractograms obtained for all the three test groups (Untreated, Sandblasted and UVP samples) revealed presence of predominantly tetragonal zirconia surface, with negligible presence of monoclinic phase, indicating no crystal phase transformation occurring due to immersion in SBF for 3 weeks. The peak of the tetragonal phase was identified at 30° for all three test groups.

B. QUALITATIVE ANALYSIS OF UNTREATED AND SURFACE TREATED TEST SAMPLES AFTER 3 WEEK IMMERSION IN SBF, BY SCANNING ELECTRON MICROSCOPY

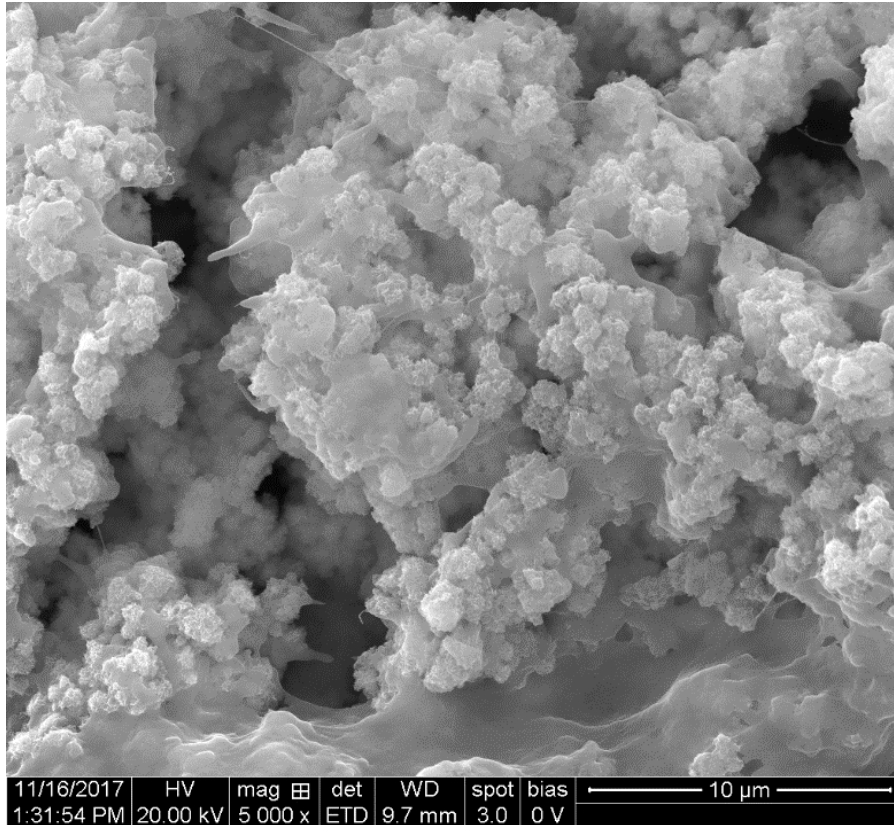


Fig. 64a: Representative photomicrograph of surface topography of Group I (Untreated) test sample under 5000x magnification

Inference: Three week post-immersion SEM photomicrograph of Group I (Untreated) test sample revealed presence of low precipitation of poorly-defined, discontinuous and scattered layer of bone-like apatite over the zirconia substrate. Uncovered, zirconia substrate is also visible at some locations.

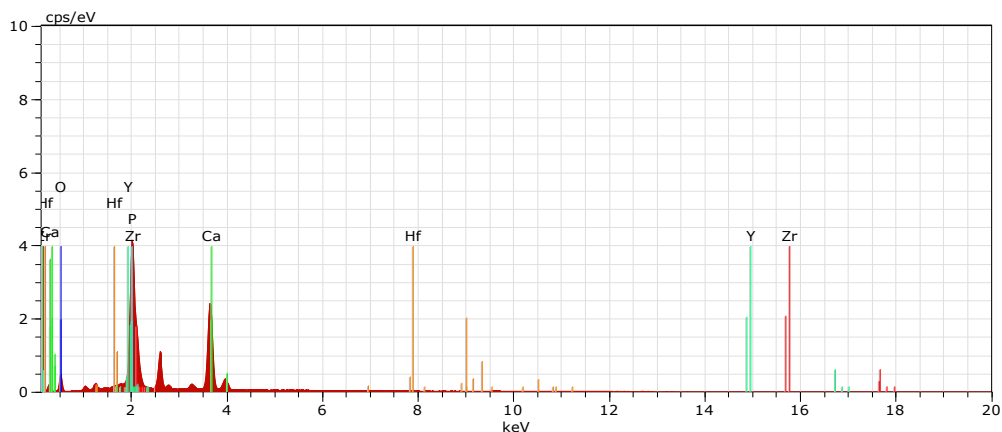


Fig. 64b: EDX spectrum of surface elemental analysis of the Group I (Untreated) test sample

El	AN	Series	unn. [wt.%]	C norm. [wt.%]	C Atom. [at.%]	C Error(1Sigma) [wt.%]
Zr	40	L-series	25.27	30.31	11.17	1.00
Ca	20	K-series	20.92	25.09	21.00	0.65
O	8	K-series	18.97	22.76	47.85	3.06
P	15	K-series	13.97	16.76	18.18	0.57
Y	39	L-series	3.73	4.48	1.69	0.19
Hf	72	L-series	0.50	0.60	0.11	0.06
Total:			83.36	100.00	100.00	Ca/P ratio=1.15

Inference: Three week post-immersion EDX spectrum of Group I (Untreated) test sample revealed surface elemental composition of Zirconium (11.17%), Calcium (21%), Oxygen (47.85%), Phosphorus(18.18%), Yttrium (1.69%) and Hafnium (0.11%), indicating that three week immersion in SBF did not substantially degrade the original surface elemental composition of zirconia. Presence of calcium and phosphorus elements is indicative of the formation of hydroxyapatite. The calcium-phosphorus ratio was **1.15**.

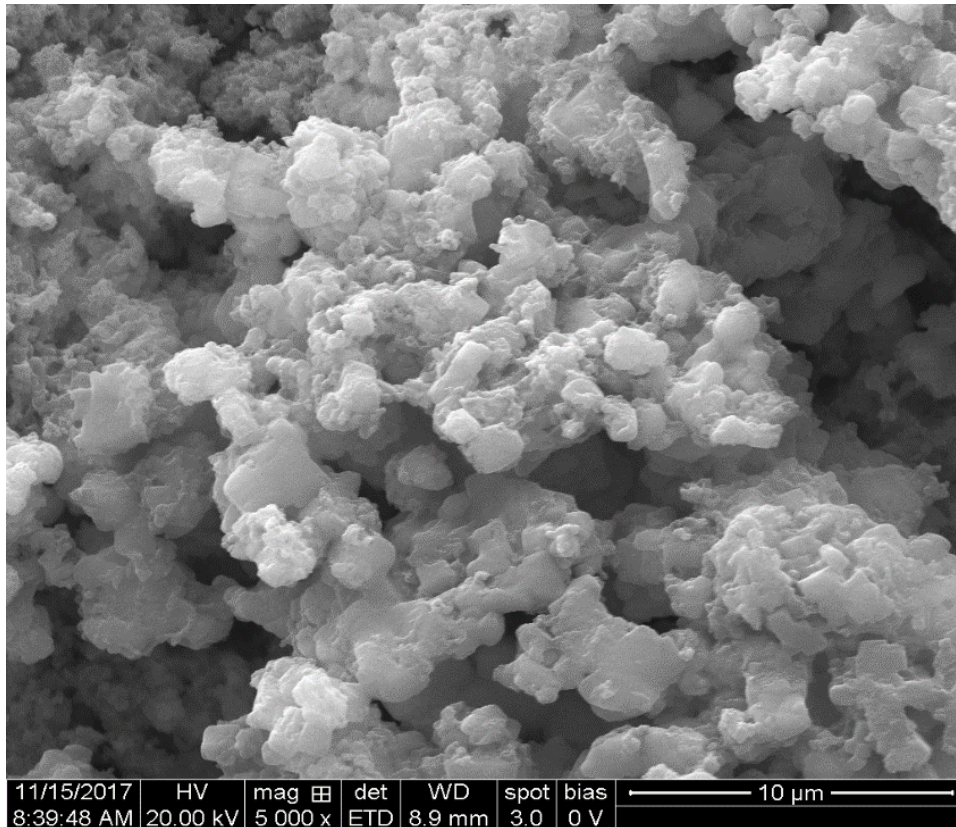


Fig. 65a: Representative photomicrograph of surface topography of Group II (Sandblasted) test sample under 5000x magnification.

Inference: Three week post-immersion SEM photomicrograph of Group II (Sandblasted) test sample revealed presence of dense, large, irregular, crystal-like deposits of calcium apatite particles of varying sizes, distribution and layer density. There is no observed evidence of uncovered zirconia substrate throughout the observed field.

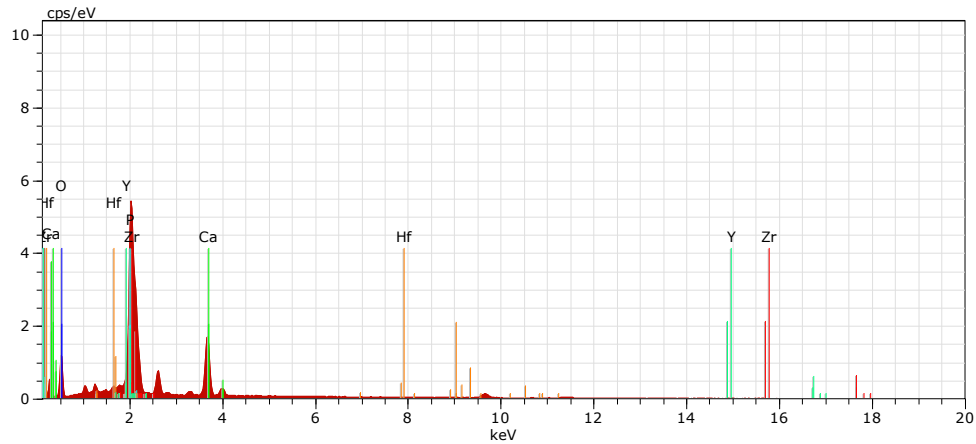


Fig. 65b: EDX spectrum of surface elemental analysis of the Group II (Sandblasted) test sample

El	AN	Series	unn. [wt.%]	C norm. [wt.%]	C Atom. [at.%]	C Error(1Sigma) [wt.%]
Zr	40	L-series	28.87	40.95	14.38	1.13
O	8	K-series	22.60	32.06	64.17	3.29
Ca	20	K-series	11.47	16.27	13.00	0.37
P	15	K-series	4.93	6.99	7.23	0.22
Y	39	L-series	2.15	3.04	1.10	0.12
Hf	72	L-series	0.48	0.69	0.12	0.06
Total:			70.51	100.00	100.00	Ca/P ratio=1.79

Inference: Three week post-immersion EDX spectrum of Group II (Sandblasted) test sample revealed surface elemental composition of Zirconium (14.38%), Oxygen (64.17%), Calcium (13%), Phosphorus (7.23%), Yttrium (1.10%) and Hafnium (0.12%), indicating that 3 week immersion in SBF after sandblasting surface treatment did not substantially degrade the original surface elemental composition of zirconia. Presence of calcium and phosphorus elements is indicative of the formation of hydroxyapatite. The calcium-phosphorus ratio was **1.79**.

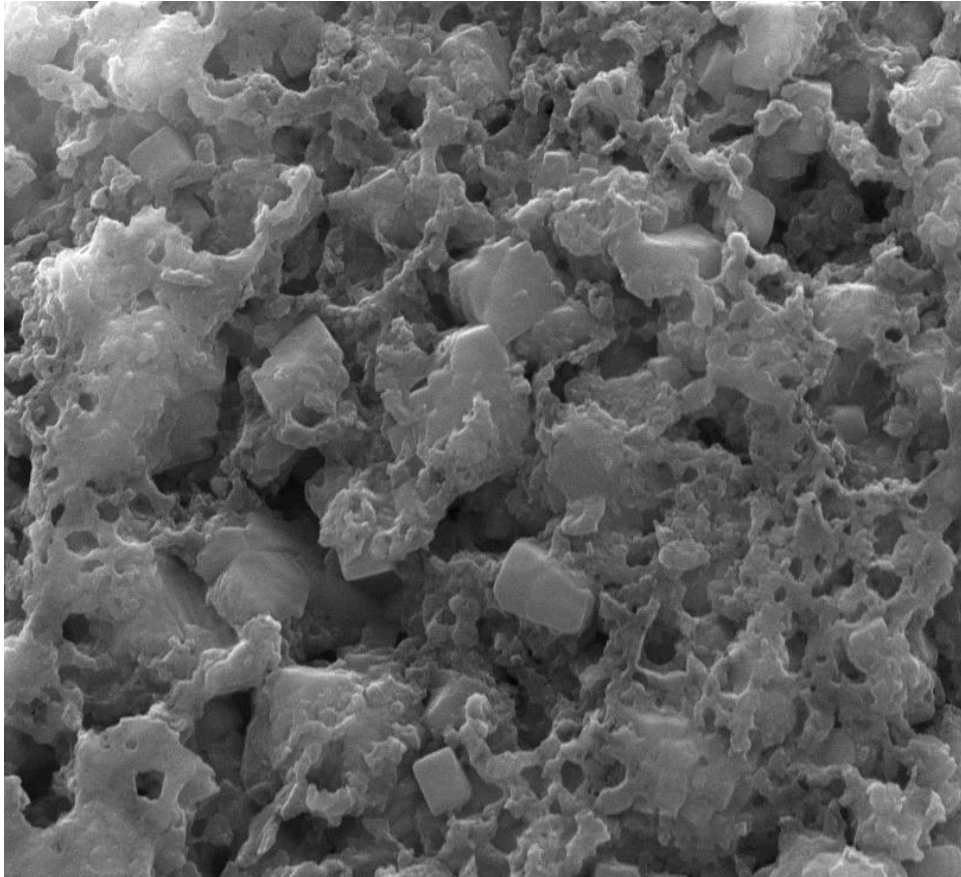


Fig. 66a: Representative photomicrograph of surface topography of Group III (UVP) test sample under 5000x magnification

Inference: Three week post-immersion SEM photomicrograph of Group III (UVP) test sample revealed presence of dense, continuous, profuse, well-formed, crystal-like apatite structures. The layer appears more uniform in density, crystal size and distribution. There is no observed evidence of uncovered zirconia substrate throughout the observed field.

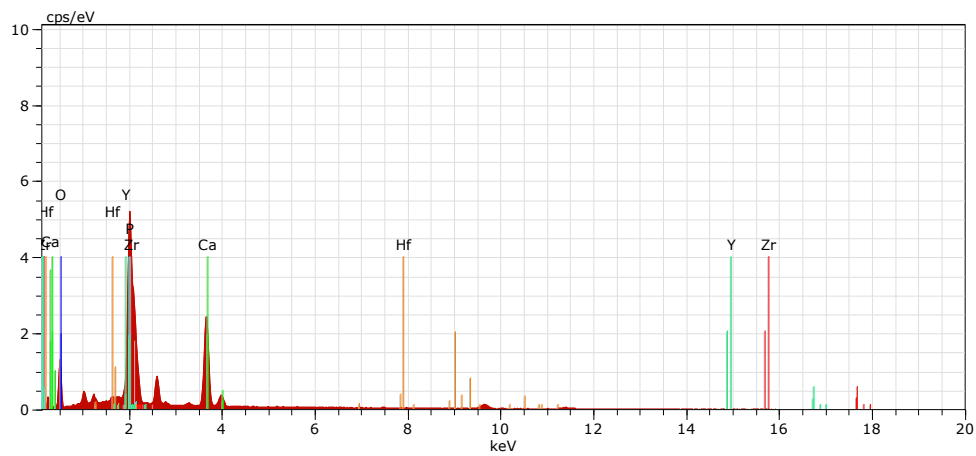


Fig. 66b: EDX spectrum of surface elemental analysis of the Group III (UVP) test sample

El	AN	Series	unn. [wt. %]	C norm. [wt. %]	C Atom. [at. %]	C Error(1Sigma) [wt. %]
Zr	40	L-series	22.54	32.28	10.56	0.89
O	8	K-series	24.04	34.42	64.19	3.47
Ca	20	K-series	15.37	22.01	16.39	0.48
P	15	K-series	5.70	Hf 8.16	7.86	0.25
Y	39	L-series	1.97	2.82	0.95	0.11
Hf	72	L-series	0.22	0.31	0.05	0.05
Total:			69.84	100.00	100.00	Ca/P ratio=2.08

Inference: Three week post-immersion EDX spectrum of Group III (UVP) test sample revealed surface elemental composition of Zirconium (10.56%), Oxygen (64.19%), Calcium (16.39%), Phosphorus (7.86%), Yttrium (0.95%) and Hafnium (0.05%), indicating that a 3 week immersion in SBF after UVP surface treatment did not substantially degrade the original surface elemental composition of zirconia. Presence of calcium and phosphorus elements is indicative of the formation of hydroxyapatite. The calcium phosphorus ratio was **2.08**.

Discussion

DISCUSSION

An increasing interest in aesthetics and concerns about toxic and allergic reactions to certain metals and alloys, led to ceramics, especially zirconia, being proposed as a popular alternative to titanium implants due to its low plaque affinity, tooth like colour and biocompatibility.^{1,26,48,60,72,82} Zirconia ceramics became a prevalent biomaterial in restorative dentistry and subsequently research for employing it as a non-metallic implant material is on the rise.^{1,14,19,25,26,30,38,44}

Zirconia ceramics can exist in cubic (c), tetragonal (t) and monoclinic (m) crystal phases that are temperature dependent. Above 2370°C, it exists in cubic form, and between 1170°C to 2370°C in the tetragonal phase and below 1170°C in the monoclinic phase.^{1,7,19,43,44,50,52,60} Thus, technically, pure zirconia at room and oral temperatures will revert to its monoclinic form due to low temperature degradation (LTD) or ageing.^{7,15,18,19,28,43} However, this monoclinic phase is mechanically unfavourable, and is prone to roughening and microcracking, resulting in increased wear and damage.⁷ Hence, oxides of elements such as yttrium, cerium, hafnium and aluminium are added to stabilize or dope the zirconia to retain its tetragonal crystal phase, by preventing t-m conversions.^{7,19,30,43,67,68} Thus the superior mechanical properties such as, low porosity, high density, higher resistance to bending, higher flexural strength and higher fracture resistance and resistance to LTD can be retained.^{30,43,52,60} This stabilized zirconia is referred to as Yttria stabilized Tetragonal Zirconia

Polycrystals (Y-TZP), and is currently the much investigated type of zirconia implant biomaterial. Although, Y-TZP is stabilized 't' zirconia with favourable mechanical properties, it does not bond readily with bone tissue due to its biological inertness, which can retard/impact osseointegration.^{27,30,34,52} Bioinert materials receive minimal biological response from the host tissues and are prone to form a non-adherent fibrous layer.²⁹

The surface properties of any implant biomaterial are reported to play a crucial role in promoting enhanced *in vivo* biological response, and is one of the key parameters influencing osseointegration according to Albrektsson and Zarb (1993)⁴ and other researchers.^{18,29,30,34} Surface roughness and wettability are considered crucial factors in promoting osseointegration.^{3,20,22,27,50,52,72} Given this significance and taking into consideration the bioinertness of zirconia, surface treatments to enhance its bioactivity by modifying the surface characteristics, such as, surface roughness (macro, micro and nano) and wettability (hydrophilicity), continue to be researched.^{3,20,22,27,29,49,50,52,72,82} Studies have also reported that surface treatments could also alter the surface characteristics and induce t-m phase transformations that could impact the *in vivo* longevity of zirconia.^{14,26,30} Hence, the focus of research is also on developing surface treatment methods that will enhance the bioactivity of zirconia, without inducing t-m phase transformation. Given the above perspectives, assessment of surface characteristics such as, type of crystal phase, surface roughness, wettability, topography and elemental composition following different surface treatments assumes significance and is frequently

carried out as an adjunct in bioactivity studies for implant biomaterials.^{9,12,18,20,22,33,75} XRD, 3D AFM, Contact angle goniometry and SEM-EDX are some of the recommended methods in the literature to ascertain crystal phase, surface roughness, wettability, topography and elemental composition, respectively.^{2,5,6,8,12,15,22,28,59,67,68,81}

Various additive and subtractive surface treatments of zirconia have been studied, with the view towards improving the surface characteristics and rendering the material more bioactive. These include, airborne particle abrasion (Sand blasting)^{9,56,65}, aerosol deposition¹⁶, acid etching with different acids and concentrations,^{18,22,47,71} airborne particle abrasion and acid etching,^{9,23,49} calcium apatite coatings,^{52,55,58} plasma spraying,^{32,75} cathodic arc deposition,⁴² micro arc oxidation,⁸¹ bioactive glass infiltration,^{33,66} Er,Cr: YSGG laser application^{37,47}, fusion sputtering²² and recently, Ultra-violet light Photofunctionalization (UVP).^{6,49,59,67,68,75}

Sandblasting (airborne particle abrasion) is a subtractive method and is employed to improve the surface area available for bonding. The major advantage of sandblasting is that it not only cleans organic contaminants from zirconia surface but also modifies its energy, wettability, microroughness, thus increasing bonding area and promoting osseointegration.^{20,56} However, studies exploring sandblasting as a surface treatment method have yielded mixed results. The main shortcoming with sandblasting is the appearance of flaws, pits, microcracks on the surface that can induce t—m phase changes.^{28,80,82} These shortcomings can be overcome by using low blasting pressure, low particle size

and short blasting distances.^{22,28} Controlled sandblasting technique results in micro-roughened surface that has been suggested to improve the osseointegration potential. Most studies have tested bioactivity of zirconia by coupling sandblasting with acid-etching.^{9,23,49} Studies focusing on the effect of sandblasting alone on improving the bioactivity of zirconia are sparse^{9,24,48,65} and hence merit further investigation.

Recently, researchers have turned their focus on the development of UV photofunctionalization (UVP) for surface modification of zirconia. It has been suggested as a simple and inexpensive surface treatment modality to enhance the osseointegration potential of zirconia without compromising its structural changes.^{12,59,67,68,78,81} It not only imparts changes in the surface roughness and topography, but also makes the zirconia surface "superhydrophilic" by reducing the hydrocarbon contamination of surfaces to very low levels, which are prime factors for bioactivity and enhanced osseointegration.^{12,46,59,67,68,78} The improved wettability due to UV treatment in zirconia is reported to actively promote the attachment, proliferation and differentiation of human osteoblast-like cells.⁷⁶ Hydrophilicity presents major advantages during the initial stages of wound healing and during the cascade of events that occurs during osseointegration, facilitating bone integration.^{49,75} Studies comparing the influence of both sandblasting and UVP, on the influence of bioactivity of zirconia tested in a single experimental design, are lacking.

Assessment of bioactivity of a test material under *in vitro* conditions has been performed using standalone or combination of bioactivity tests such as,

apatite formation following immersion in Simulated Body Fluid (SBF), protein adsorption assays, alkaline phosphatase activity, fibroblast/osteoblast cell culture studies, experimental animal studies.^{5,6,9,18,22,32,38,65,69,76} Although cell culture works well for controlled experimental design, its limitation is the difficulty to extrapolate the results to the clinical situation.

According to Kokubo and Takadama³⁹ and other researchers, evaluation of bioactivity using SBF is a reliable method.^{18,39,51,69,73} Simulated Body Fluid is a solution prepared under *in vitro* conditions, with ion concentrations similar to that of human blood plasma, but not its organic component.³⁴ Kokubo³⁹ had reported that *in vivo* apatite formation could be replicated appreciably under *in vitro* conditions by immersing samples in SBF at physiologic temperature (37°C). In such studies, the calcium content of freshly-prepared SBF prior to immersion of test samples and the post-immersion calcium content in SBF is assessed. The extent of calcium depletion in SBF is indicative of the test sample's bioactive potential. This method is also referred to as the 'biomimetic' method.¹⁸ The bioactivity findings are also corroborated by surface characteristics analysis of test samples to assess apatite formation, topography, composition., etc for correlation of test results.^{18,69}

In light of the above, the present *in vitro* study was conducted to comparatively evaluate the effect of two different surface treatments, namely, sandblasting and UV photofunctionalization (UVP) on the bioactivity of zirconia. The null hypothesis of the present study was that there would be no

significant difference in bioactivity as a result of the two different surface treatment methods.

Commercially available Y-TZP was used as the test material in the present study due to previously mentioned attributes of this material. Test sample preparation procedures were performed by a single operator to avoid operator-based errors. All test samples employed were procured by copy-milling a customised resin pattern to ensure standardised sample dimensions.

All test samples were randomly assigned into three test groups, to avoid bias prior to carrying out any further surface treatments. The untreated samples acted as the control to aid in comparative interpretation of study results. Sandblasting and UVP were chosen as the two test surface treatment methods because of aforementioned reasons.

Sandblasting was done using 50 μ m sizes alumina, since particle sizes >100 μ m are reported to cause reduction in flexural strength, induce t-m phase transformation and material loss.²² The blasting procedure was carried out as per recommendations in the literature.^{9,11,19,24,28,53,65}

UVP can be accomplished by Ultraviolet A (UVA) and Ultraviolet C (UVC) types of irradiation. In the present study, UVC irradiation was selected as it has been reported to enhance the bioactivity by altering the biological properties without compromising the physical characteristics and mechanical properties. UVC irradiation works through photolytic degradation mechanism/concept unlike the photocatalytic degradation in UVA treatment.^{6,81} The UVP protocols in the present study was as per those stated in literature.^{12,59}

Surface characteristic analysis of test samples has been reported in literature as an adjunct procedure in bioactivity studies, given their significance on the osseointegration potential and to aid in correlation and interpretation of results.^{3,17,22} Surface crystal phase,^{18,69} surface roughness,^{34,69} surface topography⁶, wettability^{6,78} and elemental composition³⁴ are major variables that can affect the bioactivity as previously mentioned.^{5,12,16,29,47,59} Hence, in the present study, the above surface characteristics were assessed on representative samples of each test group to obtain better insights of the untreated and treated zirconia surfaces.

Possible crystalline phase t-m transformations of untreated and treated zirconia surfaces is very significant because any phase change implies that the material is more prone to surface degradation. Thus assessment of crystal phase after surface treatments and comparison with that of the untreated surface assumes importance. X-Ray Diffraction (XRD) analysis was employed to assess the types of crystalline phase on the zirconia surfaces as recommended in the literature.^{33,47,59,68}

Surface texture or roughness, is an important parameter affecting osseointegration. *In vitro* studies have demonstrated increased osteoblast proliferation^{6,48} and apatite formation⁶⁵ on roughened surfaces. Surface roughness at a micrometre resolution has been studied in previous studies for various implant biomaterials.^{22,47,78} However, the implant surface 3-D topography at a nanolevel has been suggested to be important in determining the extent of bioactivity, as well as to eliminate implant rejection.^{6,12,26,29,42,67,68}

Hence, in the present study, surface roughness evaluation was performed by Atomic Force Microscopy (AFM) to obtain 3-D, nanoresolution qualitative and quantitative data.

Contact angle measurements of a surface are significant as they denote wettability (hydrophilicity) of a material. Hydrophilic property is considered a necessary condition for osseointegration in biomaterial science.⁶ More the hydrophilicity, higher the surface energy of the material and hence greater the bioactivity.^{12,60,61,75} Zirconia being a bioinert material, is rendered bioactive by surface treatments which are said to induce apatite enucleation by increasing the surface energy. Surface treatment by UVP is reported to render the surface more hydrophilic^{6,12,61,67,68,75} or “superhydrophilic”. Hence, in the present study, wettability of untreated and treated test samples were measured by contact angle goniometry, as recommended in the literature.^{6,61,75}

Scanning Electron Microscopy coupled with Energy Dispersive X-ray Spectroscopy (SEM-EDX) is performed to assess the surface topography at high magnifications and to assess the surface elemental composition, respectively. Such interpretations are critical in understanding study results. Hence, in the present study, representative samples of each test group were analysed using SEM-EDX.^{6,29,34,53,65,71,79}

The effect of surface treatments of zirconia on its bioactivity was evaluated in the present study, by employing the Simulated Body Fluid (SBF) method, due to previously mentioned advantages of testing bioactivity in SBF, by following the recommended protocols.^{32,33,35,42,72,77} Considering the impact

of the composition and preparation of SBF on test outcomes, the guidelines for the same as recommended in the literature were strictly adhered to.³⁹ In the preparation of SBF, it has been reported that apatite nucleation can be induced at the surface of a glass container or the edge of scratches in such containers, which could mask the actual test results.³⁹ Hence, new plastic containers and polypropylene test tubes with smooth surfaces were used for preparation and immersion of the test samples in SBF. All test samples were individually immersed in test tubes containing equal volumes of SBF and incubated at 37°C for 3 weeks to ensure standardised study conditions.¹⁸

In the present study, calcium content in SBF was assessed by Inductively Coupled Plasma Mass Spectrometry (ICP-MS),^{51,79} since this equipment has an accuracy to detect and automatically compute the percentage of any given ion concentration in a known quantity of a solution, from a 1 ml sample dose. Multiple measurements of the calcium ion concentration in SBF were randomly done in the present study to ascertain the standardisation of SBF preparation procedure and the mean pre-immersion Ca-content was obtained and kept as the reference value for comparison with the post-immersion calcium content.

Different studies have tested bioactivity of zirconia in SBF by employing various periods of immersion ranging from 2 days to several weeks.^{18,32-34,69} In a related pilot study, a 2 weeks immersion protocol was initially tested. However, there was no appreciable calcium depletion in SBF or formation of apatite on the test samples of all test groups at the end of this period. This could perhaps be caused due to inherent bioinert nature of zirconia.

Hence, in the present study, the immersion of test samples was done for a period of 3 weeks, which has also been considered as the minimum immersion time in previous studies.^{18,33,72,79} The respective mean post-immersion calcium content in SBF was derived and compared with the pre-immersion calcium value to arrive at each group's bioactivity potential. The respective mean post-immersion calcium contents in SBF of the test groups were compared to determine if there were any significant differences in their bioactivity with respect to each other. Additionally, the surface characteristics of post-immersion test samples of each group were assessed to see the impact of immersion ageing and apatite formation on the zirconia surfaces. The crystal phase was rechecked using XRD to determine whether immersion ageing had resulted in any t-m transformation.^{33,34,70} SEM-EDX was used to analyse the post-immersion surface topography and elemental composition to evaluate apatite formation on the surfaces and Ca/P ratio.^{33,34,69} The Ca-SBF analysis results, in correlation with the SEM-EDX findings is useful in assessment of bioactivity.

Pre-immersion XRD revealed strong tetragonal (t) peaks of zirconia with negligible 'm' phase in representative diffractograms of all test groups (Figs.56 a, b & c). The highest peak of ZrO₂ appeared at 30° (2θ-Theta value), indicating no phase transformation due to either sandblasting or UVP. These results are suggestive of maintenance of the mechanically superior 't' zirconia crystal phase following either surface treatments and are in agreement with that observed in previous reports.^{59,67,68,72,78}

Surface roughness evaluation on a nanoscale by AFM of representative samples of all test groups revealed average surface roughness of 41.83 nm for Group I (Untreated), 115.65 nm for Group II (Sandblasted) and 102.43 nm for Group III (UVP) (Table 1; Graph 1). Both types of surface treatments resulted in significantly higher surface roughness as compared to the untreated sample ($p < 0.05$) (Tables 2 & 3; Graph 1). Although, the surface roughness achieved by sandblasting was slightly higher than that achieved by UVP, this difference was found to be statistically insignificant ($p > 0.05$). These results were correlated with the respective 2-D and 3-D images (Fig. 57a to Fig. 58c), which revealed a uniform surface texture with lesser number of isolated shallow peaks and valleys for Group I (Untreated) sample, a non-uniform texture with greater number of very high and well-defined peaks for Group II (Sandblasted) sample, and a non-uniform texture of roughened plains with several deep grooves along with some clusters of well-defined peaks and valleys for Group III (UVP) sample. These findings indicate that both types of surface treatments improve the surface roughness similarly.^{37,49,59,67,68,75} Previous standalone studies employing sandblasting or UVP have reported significant increase in surface roughness as compared to untreated surfaces and the results obtained in the present study is in line with these findings.^{9,12,24,28,57,59,67,68} Comparative studies on surface roughness caused by these surface treatments are lacking and hence, further correlations on this aspect of the present study results cannot be drawn.

The mean contact angles of 98.26° for Group I (Untreated) samples, 86.77° for Group II (Sandblasted) samples and 68.03° for Groups III (UVP) samples, respectively were obtained in the present study (Figs. 59a, 59b & 59c; Table 4; Graphs 2-4). On comparison, these differences were found to be highly significant (p -value < 0.01) between all the three test groups (Tables 5 & 6; Graph 5). These results indicate that both types of surface treatments significantly improve the surface wettability as compared to that of the untreated surface, and is in accordance with that reported in the literature.^{5,6,12,59,67,68,78,80}

The mechanism of improving the wettability due to surface treatments by lowering the surface energy has been previously mentioned. Surface wettability of 90° and more have been categorised as hydrophobic and “superhydrophobic”. Contact angles $< 90^\circ$ have been said to hydrophilic and those that are between 0 - 30° are said to be highly hydrophilic or “superhydrophilic”. It has been reported that UVP treatment renders the surface “superhydrophilic”. In such studies, a wide range of contact angles after UVP treatment, ranging from 0 - 34° , has been reported.^{5,6,12,59,67,68,78,80} The literature reported range is considerably lower than the wettability angles observed after UVP treatment in the present study, and hence the present study values can be termed as hydrophilic behaviour, instead of superhydrophilic. This could be attributed to differences in study environment and the number of samples tested in the present study and merits further investigation. However, the fact that UVP significantly improved the hydrophilicity as compared to untreated and

sandblasted surfaces is established here, which is in line with that stated in previous studies.^{12,59,67,68,78}

In this study, SEM photomicrographs revealed significant variations in the microtopographies of the untreated and treated samples. Group I (Untreated) sample (Fig. 60a) exhibited flattened areas with isolated patches of moderately roughened surface, while Group II (Sandblasted) sample (Fig. 61a) showed non-uniform, irregular surface with accentuated peaks and valleys and Group III (UVP) sample (Fig. 62a) showed uniformly roughened surface with a coral-like appearance. Both the surface treated groups were marked by absence of flattened areas as observed with the untreated sample. These observations indicated that surface topography is altered due to both types of surface treatments and UVP resulting in a more uniformly textured surface, which are in line with that observed in previous studies.^{12,13,22,26,42,59} Respective EDX spectrums revealed the presence of the elements, Zr (32.66- 40.26%), O₂ (53.59- 61.31 %), Y (5.28-5.71%), Al (0.13-0.38%) and Hf (0.16-0.19%) in all test groups (Figs. 60b, 61b & 62b), indicating that both surface treatments do not alter the elemental composition of zirconia, as compared to the untreated sample. Thus, the stabilizing elements added by the manufacturer have been retained even after the surface treatment procedures. These findings are in line with those reported in previous EDX spectrum reports.^{29,34,47,82}

The mean pre-immersion Ca-content of SBF was found to be 159 mg/L (Table 7; Graph 6) and this was used as the reference value for calculating bioactivity. Previous bioactivity studies employing SBF have reported a mean

calcium content of 100-160 mg/L in freshly prepared SBF.^{33,40,42,46,72} The reference value obtained in the present study was within the literature reported range. Group I (Untreated) showed a mean post-immersion Ca-content of 70.10 mg/L (Table 8; Graph 7), Group II (Sandblasted) showed a mean post-immersion Ca-content of 60.80 mg/L (Table 9; Graph 8) and Group III (UVP) showed a mean post-immersion Ca-content of 56.20 mg/L (Table 10, Graph 9) at the end of 3 weeks. The difference between the mean pre- and post-immersion Ca-contents in SBF that is observed, is due to the precipitation of calcium-rich apatite phase on the zirconia test surfaces. The lower the post-immersion Ca-content in SBF, the higher the bioactivity for that particular test group.

On comparison, the respective mean post-immersion Ca-content in SBF for all the three test groups showed statistically significant calcium depletion when compared with the pre-immersion Ca-content, indicating highly significant bioactivity for untreated as well as both the surface test groups (Table 11; Graph 10) (p -value < 0.01). Although, the results of the present study indicates significant bioactive potential for untreated zirconia by virtue of the calcium depletion observed after immersion, this bioactivity was found to be significantly lesser as compared to that of both the surface treated groups (p -value < 0.01) (Tables 12 & 13; Graph 11). On comparison between the two types of surface treatments, Group II (Sandblasted) had lesser post-immersion calcium depletion in SBF, than that of Group III (UVP). However, this difference was found to be statistically insignificant (p -value > 0.05) (Tables 12

& 13; Graph 11), indicating similar bioactive potential for both the types of surface treatments employed in the present study.

Thus, despite being categorized as a bioinert ceramic, there is a definite apatite forming tendency on untreated zirconia at the end of a 3 week immersion period.^{18,33,69,70} However, this apatite layer formed on the untreated sample was found to be a poorly-defined, discontinuous layer of bone-like apatite in the form of scattered crystals, with evidence of uncovered zirconia substrate at certain locations, as evidenced in the post-immersion SEM image (Fig. 64a). The post-immersion SEM images for Groups II and III also corroborate this finding of superior bioactivity, in that, their apatite layer was made of denser, larger crystals with a continuous surface topography and the zirconia substrate was not visible in any of the observed fields. Group II (Sandblasted) sample exhibited dense, large, irregular, crystal-like calcium apatite deposits of irregular density and distribution, and Group III (UVP) exhibited profuse, rectangular crystal-like calcium apatite deposits with greater uniformity in size, density and distribution (Figs. 65a, 66a). Moreover, the post-immersion EDX results revealed a higher Ca/P ratio for both the surface treated groups as compared to the untreated group (Figs. 64b, 65b & 66b). Group III (UVP) exhibited the highest Ca/P ratio of 2.08, followed by Group II (Sandblasted) and Group I (Untreated) with ratios of 1.79 and 1.15, respectively. It has been reported in the literature that Ca/P ratio of 1.50 indicates apatite formation similar to trabecular bone, whereas, values upwards of 1.60 indicate cortical bone-like apatite formation.^{39,41} When viewed in this perspective, the low Ca/P

ratio for the untreated group is indicative of trabecular bone formation, whereas, both surface treated groups in this study had Ca/P ratios indicative of cortical bone formation, indicating their superiority as surface treatment methods. All these findings suggest that surface treatment of zirconia serves to significantly enhance its bioactive potential and also results in apatite layer of superior quality as compared to an untreated surface. These findings are echoed in the results of previous studies that have evaluated the bioactivity of zirconia following surface treatment by either sandblasting or UVP.^{18,33,42,69,70} These results are also in agreement with literature quoting that untreated zirconia surfaces also attract the calcium present in SBF, but to a diminished extent as compared to any type of surface treatment.³⁴ Surface treatments are said to promote bioactivity, since they remove impurities, reduce surface hydrocarbons, increase surface energy, thereby, providing improved surface characteristics such as roughness and wettability, that are critical in promoting cell adhesion and calcium apatite formation. Previous studies evaluating efficacy of sandblasting and UVP surface treatments have reported improved cell adhesion and osseointegration.^{43,48,71} The results of superior bioactivity in SBF obtained after these two types of surface treatments in the present study complement the results obtained from previous cell culture studies.^{9,48,59,65,67,75}

Further, post-immersion x-ray diffractograms revealed that there was no detectable crystalline phase change from tetragonal to monoclinic (t-m transformation), following a 3 week immersion (Figs. 63a, 63b & 63c). The post-immersion EDX (Figs. 64b, 65b & 66b) revealed presence of all the surface

elements that were detected in the pre-immersion EDX (Figs. 60b, 61b & 62b), and additionally calcium and phosphorus were also detected attributable to apatite formation. This prevention of t-m transformation even after immersion, can be attributed to the maintained presence of the stabilizing elements like yttrium and hafnium that were added by the manufacturer. Thus, even after a 3 week immersion or ageing, there was no detectable low temperature degradation (LTD), which is usually the area of concern with using zirconia ceramic as an implant biomaterial. The results obtained with the present study serve as an encouragement for use of zirconia as an implant biomaterial, with respect to this finding.

Both sandblasting and UVP surface treatments resulted in insignificant differences with respect to their bioactivity in SBF, in the present study and hence, the null hypothesis of the present study is validated. Therefore, it can reasonably be assumed within the limitations of the present study, either of these surface treatments can be employed to significantly and probably, similarly improve the bioactivity of zirconia. This is especially so, given that both these types of surface treatments significantly improved surface roughness and wettability, without deleteriously affecting their surface crystalline phase ('t' phase) and their elemental composition. Although, superior surface wettability was observed after UVP as compared to sandblasting, the bioactivity of the UVP samples was only marginally and insignificantly higher in comparison, in the present study. Wettability has been repeatedly emphasized as one of the key determinants in deciding the bioactive potential of a material, both with respect

to the apatite forming ability as well as for improving cellular adhesion.^{12,59,61,67,78} Hence, the apparent lack of a significantly superior bioactive potential after UVP surface treatment, over that obtained after sandblasting surface treatment needs to be considered, especially given the fact that UVP treated samples showed significantly superior wettability as compared to the sandblasted samples. This can be attributed to the lesser number of samples that were investigated in the present study and merits further investigation. Moreover, bioactivity studies in SBF comparing these type of surface treatments are lacking in the literature and hence, further correlations with the results obtained in the present study cannot be drawn to arrive at better conclusions. Though it is well accepted that chemical and topographical aspects of surface texture are important in playing a vital role in osseointegration,^{41,64,65,72} the exact effect of this aspect on bioactivity is still the object of investigation by researchers.

The present study had certain limitations. The effect of a single grit size of alumina and a single wavelength of UVC, on the bioactivity of zirconia was studied. Different grit sizes of alumina particles as well as different UV wavelengths and duration also merit investigation. Further, for assessing bioactivity, other parameters such as, alkaline phosphatase activity, cell culture, cell migration, protein adsorption assays should also be concomitantly investigated along with assessments using SBF, employing larger sample sizes and different immersion durations to enhance the results obtained with the present study.

Conclusion

CONCLUSION

The following conclusions were drawn from the data obtained in the present *in vitro* study that was conducted to comparatively evaluate the effects of two different surface treatments, namely, sandblasting and UV Photofunctionalization (UVP) on the bioactivity of zirconia:

1. X-Ray diffractograms of Group I (Untreated), Group II (Sandblasted) and Group III (UVP) zirconia samples revealed presence of tetragonal (t) zirconia peaks, with negligible monoclinic (m) phase, indicating no phase transformation after both the surface treatments.
2. 2-D and 3-D AFM images revealed, a relatively uniform surface texture with fewer isolated and shallow peaks and valleys for Group I (Untreated) sample, a non-uniform surface texture with greater number of high and well-defined peaks throughout the surface for Group II (Sandblasted) sample, and a non-uniform surface texture of roughened plains and clustered areas of well-defined peaks and valleys for Group III (UVP) sample.
3. The mean surface roughness for all the three test groups was found to be, **41.83nm** for Group I (Untreated), **115.65nm** for Group II (Sandblasted), and **102.43nm** for Group III (UVP).
4. On comparison, the mean surface roughnesses of Group II (Sandblasted) and Group III (UVP) were found to be significantly higher (p-value <0.01) than that of Group I (Untreated). Group II (Sandblasted) exhibited a marginally higher mean surface roughness when compared to that of Group III (UVP) that was found to be statistically insignificant (p-value > 0.05).

- **Surface Roughness: Group I <* Group II & Group III** (* denotes significance)
 - Group III < Group II** (Not significant)
5. The wettability (hydrophilicity) measurements of the three test groups revealed, mean contact angles of **98.26°** for Group I (Untreated), **86.77°** for Group II (Sandblasted) and **68.03°** for Group III (UVP).
 6. On comparison, all the three test groups revealed statistically significant differences between their respective mean contact angle measurements (p-value < 0.01), with Group III (UVP) having the least contact angle, followed by Group II (Sandblasted) with a relatively higher contact angle and Group I (Untreated) with the maximum contact angle.
- **Wettability (Hydrophilicity): Group I <* Group II <* Group III** (* denotes significance)
7. SEM photomicrographs of representative samples of all three test groups revealed considerable variations in the microtopographies of the untreated and treated surfaces. Group I (Untreated) surface showed presence of flattened areas interspersed with patches of moderately roughened surface. Group II (Sandblasted) surface showed presence of non-uniform, irregular surface, with accentuated peaks and valleys with absence of flattened areas. Group III (UVP) surface showed presence of uniformly roughened surface with a coral-like appearance and absence of flattened areas.
 8. EDX spectrum of representative samples of Group I (Untreated), Group II (Sandblasted) and Group III (UVP) revealed similar surface elemental

composition consisting of Zr (32.66-40.26%), O₂ (53.59-61.31%), Hf (0.16-0.19%), Y (5.28-5.71%) and Al (0.13-0.38%).

9. The mean calcium-ion content in freshly prepared Simulated Body Fluid (SBF), prior to immersion of the test samples, as determined by Inductively Coupled Plasma Mass Spectrometry (ICP-MS), was found to be **159 mg/L**.
 10. The mean post-immersion calcium-ion content in SBF of Group I (Untreated) samples, was found to be **70.10 mg/L**.
 11. The mean post-immersion calcium-ion content in SBF of Group II (Sandblasted) samples, was found to be **60.80 mg/L**.
 12. The mean post-immersion calcium-ion content in SBF of Group III (UVP) samples, was found to be **56.20 mg/L**.
 13. On comparison, the mean post-immersion Ca-content in SBF for all the three test groups showed statistically significant calcium depletion when compared with the pre-immersion Ca-content in SBF, indicating significant bioactivity for all the three test groups (p-value < 0.05).
 14. On comparison, the mean post-immersion Ca-content in SBF of Group II (Sandblasted) and Group III (UVP), showed significantly higher calcium depletion when compared with that of Group I (Untreated) (p < 0.05). The mean post-immersion Ca-content in SBF of Group III (UVP) was found to be lesser than that of Group II (Sandblasted), but these were found to be statistically insignificant with respect to each other (p-value > 0.05).
- **Bioactivity: Group II and Group III >* Group I** (* denotes significance)
Group III > Group II (Not significant)

15. X-Ray diffractograms of Group I (Untreated), Group II (Sandblasted) and Group III (UVP) representative post-immersion test samples revealed presence of tetragonal (t) zirconia peaks, with negligible monoclinic (m) phase, indicating no phase transformation following a 3 weeks immersion period in SBF.
16. SEM photomicrographs of representative post-immersion test samples of all the three test groups revealed considerable variations in the apatite layer, indicative of different degrees of bioactivity. Group I (Untreated) surface exhibited low precipitation of poorly-defined, discontinuous layer of apatite with bare zirconia visible at some locations. Both Group II (Sandblasted) and Group III (UVP) surfaces exhibited dense, continuous, large, crystal-like calcium apatite, with no evidence of uncovered zirconia. The apatite formation on Group III (UVP) surface was relatively uniform in crystal size and distribution.
17. EDX spectrum of representative post-immersion samples of Group I (Untreated), Group II (Sandblasted) and Group III (UVP) revealed similar surface elemental composition following a 3 week immersion, consisting of Zr (10.56-14.38%), O₂ (47.85-64.19%), Hf (0.05-0.12%), Y (0.95-1.69%), Ca (13-21 %) and P (7.23-18.18 %). There was an increasing Ca/P ratio of **1.15** for Group I (Untreated), **1.79** for Group II (Sandblasted) and **2.08** for Group III (UVP), indicative of calcium apatite formation.

Summary

SUMMARY

The present *in vitro* study was conducted to comparatively evaluate the effects of two different surface treatments, namely, sandblasting and UV Photofunctionalization (UVP) on the bioactivity of zirconia.

33 samples of dimensions 10mm x 2mm, were obtained from zirconia blanks and randomly divided into three groups (n=11). Group I samples were left untreated, Group II and Group III samples were surface treated by sandblasting with alumina and UVP, respectively. Surface characteristics of representative samples from test groups were analysed using XRD, AFM, Contact angle Goniometry, SEM and EDX, to evaluate crystal phase, surface roughness, wettability, topography and elemental composition, respectively. Simulated Body Fluid (SBF) was prepared and the mean pre-immersion Ca-content was assessed by Inductively Coupled Plasma Mass Spectrometry (ICP-MS). Test samples were incubated in SBF and mean post-immersion Ca-content was assessed after 3 weeks. The respective mean post-immersion Ca-content in SBF of test groups was compared with the mean pre-immersion value and with respect to each other to assess bioactivity. Post-immersion representative samples were subjected to XRD, SEM and EDX. Data analysis was done using One-way ANOVA, Post-hoc Tukey's HSD test and Students' paired t-test.

After surface treatments, tetragonal zirconia phase was observed for all test groups, indicating no phase transformation. Surface roughness for both Groups II and III was statistically similar and significantly superior as compared to Group I. Group I showed the least wettability, Group II showed moderate

wettability and Group III showed highest wettability and these values were found to be statistically significant with respect to each other. SEM revealed that Group I had a relatively flat surface, Group II an irregularly roughened surface, and Group III a uniformly roughened surface. EDX for all groups revealed Zr, O₂, Y, Hf and Al.

The Ca-content in SBF of all three groups showed statistically significant depletion from the pre-immersion Ca-content. Both Groups II and III exhibited superior and statistically significant Ca depletion as compared to Group I. Group III showed a marginally higher, but statistically insignificant Ca depletion when compared to Group II. These findings were corroborated by the presence of dense, Ca apatite crystals on both surface treated test samples as seen by SEM, when compared to the low precipitation of poorly-defined, scattered apatite layer for the untreated sample. EDX revealed Zr, O₂, Hf, Y, Ca and P and an increasing Ca/P ratio from untreated to sandblasted to UVP groups. XRD revealed no phase change following immersion in SBF for all test groups.

In the present study, surface treatments with sandblasting and UVP did not significantly affect the bioactivity of zirconia and hence, the null hypothesis is validated. This superior bioactivity was in line with the respective improved SEM-EDX observations. Both surface treatments improve the *in vitro* bioactivity of zirconia significantly, but similarly, suggestive of a favourable *in vivo* response. Further studies, employing larger sample sizes, coupled with cell culture and animal studies are recommended to enhance the results of the present study.

Bibliography

BIBLIOGRAPHY

1. **Abd El-Ghany OS, Sherief AH.** Zirconia based ceramics, some clinical and biological aspects: Review. *Future Dental Journal* 2016; 2:55-64.
2. **Abi-Rached FO, Martins SB, Campos JA, Fonseca RG.** Evaluation of roughness, wettability, and morphology of an yttria-stabilized tetragonal zirconia polycrystal ceramic after different airborne-particle abrasion protocols. *J Prosthet Dent* 2014; 6 (112):1385-1391.
3. **Albrektsson T, Wennerberg A.** Oral implant surfaces: Part 1—Review Focusing on topographic and chemical properties of different surfaces and in vivo responses to them. *Int J Prosthodont* 2004;17(5):536–543.
4. **Albrektsson T, Zarb GA.** Current Interpretations of the osseointegrated response: clinical significance. *Int J Prosthodont* 1993; 6(2):95-105.
5. **Altmann B, Kohal RJ, Steinberg T, Tomakidi P, Bachle-Haas M, Wennerberg A, Att W.** Distinct cell functions of osteoblasts on UV-functionalized titanium- and zirconia-based implant materials are modulated by surface topography. *Tissue Eng Part C. Methods* 2013; 19:850-863.
6. **Al Qahtani MS, Wu Y, Spintzyk S, Krieg P, Killinger A, Schweizer E, Stephan I, Scheideler L, Geis-Gerstorfer J, Rupp F.** UV-A and UV-C light induced hydrophilization of dental implants. *Dent Mater* 2015; 31(8):e157-67.

7. **Anusavice KJ, Shen C, Rawls HR.** Phillips' Science of Dental Materials, ed 12. Elsevier, 2013: 418-473, 499-518.
8. **Att W, Takeuchi M, Suzuki T, Kubo K, Anpo M, Ogawa T.** Enhanced osteoblast function on ultraviolet light-treated zirconia. *Biomaterials* 2009; 30:1273–1280.
9. **Bächle M, Butz F, Hübner U, Bakalinis E, Kohal RJ.** Behavior of CAL72 osteoblast-like cells cultured on zirconia ceramics with different surface topographies. *Clin. Oral Implants Res.* 2007;18(1): 53–59.
10. **Best S.M., Porter A.E., Thian E.S., Huang. J.** Bioceramics: Past, Present and for the Future. *J. Eur. Ceram. Soc.* 2008; 28:1319-1330.
11. **Borges GA, Sophr AM, de Goes MF, Sobrinho LC, D.C.N. Chan.** Effect of etching and airborne particle abrasion on the microstructure of different dental ceramics. *J Prosthet Dent* 2003; 89(5):479–488.
12. **Brezavscek M , Fawzy A , Bächle M , Tuna T , Fischer J, Att W.** The Effect of UV Treatment on the Osteoconductive Capacity of Zirconia-Based Materials. *Materials* 2016; 9: 958-977.
13. **Casucci A, Osorio E, Osorio R, Monticellic F, Toledano M, Mazzitellia C, Ferraria M.** Influence of different surface treatments on surface zirconia frameworks. *Journal of Dentistry* 2009; 37(11):891–897.
14. **Chevalier J.** “What future for zirconia as a biomaterial?” *Biomaterials* 2006; 27(4):535–543.

- 15. Chintapalli RK, Marro FG, Jimenez-Pique E, Anglada M.** Phase transformation and subsurface damage in 3Y-TZP after sandblasting. *Dent Mater* 2013; 29(5):566-72.
- 16. Cho Y, Hong J, Ryoo H, Kim D, Park J, Han J.** Osteogenic responses to zirconia with hydroxyapatite coating by aerosol deposition. *J Dent Res* 2015; 94(3):491-9.
- 17. Curtis AR, Wright AJ, Fleming GJ.** The influence of surface modification techniques on the performance of a Y-TZP dental ceramic. *J Dent* 2006; 34(3):195-206.
- 18. Dehestani M, Ilver L, Adolfsson E.** Enhancing the bioactivity of zirconia and zirconia composites by surface modification. *J Biomed Mater Res Part B* 2012; 100B: 832–840.
- 19. Della Bona A, Donassollo TA, Demarco FF, Barrett AA.** Characterization and surface treatment effects on topography of a glass-infiltrated alumina/zirconia-reinforced ceramic. *Dent Mater* 2007; 23(6):769–775.
- 20. Depprich R, Zipprich H, Ommerborn M, Naujoks C, Wiesmann HP, Kiattavorncharoen S, Lauer HC, Meyer U, Kübler NR, Handschel J.** Osseointegration of zirconia implants compared with titanium: an in vivo study. *Head Face Med* 2008; 11(3):40-55.
- 21. Eliades G, Eliades T, Brantley WA, Watts DC.** Dental Materials in Vivo: Aging and Related Phenomena *Quintessence* 2003: 35-45.

- 22. Ewais OH, Al Abbassy F, Ghoneim MM, Aboushelib MN.** Novel zirconia surface treatments for enhanced osseointegration: Laboratory characterization. *Int J Dent* 2014; 203940-203948.
- 23. Ferguson SJ, Langhoff JD, Voelter K.** Biomechanical comparison of different surface modifications for dental implants. *Int J Oral Maxillofac Implants* 2008; 23(6):1037–1046.
- 24. Gahlert M, Gudehus T, Eichhorn S, Steinhauser E, Kniha H, Erhardt W.** Biomechanical and histomorphometric comparison between zirconia implants with varying surface textures and a titanium implant in the maxilla of miniature pigs. *Clin. Oral Implants Res* 2007; 18: 662–668.
- 25. Garvie RC, Hannink RH, Pascoe RT.** “Ceramic steel?” *Nature* 1975; 258 (5537):703–704.
- 26. Gupta S.** A Recent Updates on Zirconia Implants: A Literature Review. *Dent Implants Dentures* 2016; 1: 113.
- 27. Hafezeqoran A, Koodaryan R.** Effect of Zirconia Dental Implant Surfaces on Bone Integration: A Systematic Review and Meta-Analysis. *BioMed Res. Int.*2017; 9246721:1-12.
- 28. Hallmann L, Ulmer P, Reusser E, Hämmerle C.** Effect of blasting pressure, abrasive particle size and grade on phase transformation and morphological change of dental zirconia surface. *Surface and Coatings Technology* 2012; 206(19):4293-4302.

- 29. Han J, Hong G, Matsui H, Shimizu Y, Zheng G, Lin H, Sasaki K.**
The surface characterization and bioactivity of NANOZR in vitro. Dent. Mater. J. 2014; 33(2):210–219.
- 30. Hisbergues M, Vendeville S, Vendeville P.** Zirconia - Established facts and perspectives for a biomaterial in dental implantology. J Biomed Mater Res. B: Appl Biomater 2009; 88:519-529
- 31. Hoffmann O, Angelov N, Zafiropoulos GG, Andreana S.**
Osseointegration of zirconia implants with different surface characteristics: An evaluation in rabbits. Int J Oral Maxillofac implants 2012; 27:352-358
- 32. Karamian E, Khandan A, Reza M, Kalantar K, Mirmohammadi H.**
Surface Characteristics and Bioactivity of a Novel Natural HA/Zircon Nanocomposite Coated on Dental Implants. BioMed Res Int 2014;Article ID 410627;2014: 627-638.
- 33. Ke J, He F, Ye J.** Enhancing the Bioactivity of Yttria-Stabilized Tetragonal Zirconia Ceramics via Grain-Boundary Activation. ACS Appl Mater Interfaces 2017; 9(19):16015–16025.
- 34. Kenawy MH, El-Hadad AA, Soliman IE, Ereiba KMT.** Bioactivity and **Characterization.** Study of Synthetic Zirconia-Silicate Sol-Gel Glass Powder. Middle East Journal of Applied Sciences 2016: 6(2): 329-340.

- 35. Kim YH, Koak J, Chang I, Wennerberg A, Heo S. A.** Histomorphometric Analysis of the Effects of Various Surface Treatment Methods on Osseointegration. *Int J Oral Maxillofac Implants* 2003; 18: 349-356.
- 36. Kim S.E, Lim J.H, Lee S. C, Nam S-C, Kang H-G., Choi J:** Anodically nanostructured titanium dioxides for implant applications. *Electrochimica Acta* 2008;53:4846-4851
- 37. Kirmali O, Kustarci A, Kapdan A.** Surface roughness and morphologic changes of zirconia: effect of different surface treatment. *Niger J Clin Pract.* 2015;18(1):124-9
- 38. Kohal RJ, Wolkewitz M, Hinze M, Han JS, Bachle M, Butz F.** Biomechanical and histological behavior of zirconia implants: an experiment in the rat. *Clin Oral Implants Res.* 2009; 20:333-339.
- 39. Kokubo T, Takadama H.** How useful is SBF in predicting in vivo bone bioactivity? *Biomaterials* 2006; 27(15):2907-2915.
- 40. Lakshmi R, Sasikumar S.** Influence of needle-like morphology on the bioactivity of nanocrystalline wollastonite-an in vitro study. *Int J Nanomedicine* 2015; 10:129-136.
- 41. Li J, Liao H, Sjostrom M.** Characterization of calcium phosphates precipitated from simulated body fluid of different buffering capacities. *Biomaterials* 1997; 18:743-747.

- 42. Liu X, Huang A, Ding C, Chu PK.** Bioactivity and cytocompatibility of zirconia (ZrO₂) films fabricated by cathodic arc deposition. *Biomaterials* 2006; 27(21):3904-3911.
- 43. Lugh V, Sergio V.** Low temperature degradation – ageing of zirconia: A critical review of the relevant aspects in dentistry. *Dent. Mater* 2010; 26:807-820.
- 44. Madfa AA, Al-Sanabani FA, Al-Qudami NH, Al-Sanabani JS, Amran AG.** Use of Zirconia in Dentistry: An Overview. *The Open Biomaterials Journal* 2014; 5:1-9.
- 45. Miyazaki T, Nakamura H, Matsumura S, Ban T, Kobayashi E.** “Current status of zirconia restoration,” *Journal of Prosthodontic Research* 2013;57(4):236–261.
- 46. Mohamed I. El.G, , El-Dyn S.M., Abd El- moniem B.M., Al-Ashkar E, Saleh S, Tolba, E, Soliman I.** Synthesis and Microstructure Characterization of Novel Sr-HA Prepared by Co-precipitation with Enhanced Bioactivity. *Egypt. J. Biophys. Biomed. Engng* 2012; 13:73-85.
- 47. Moura CG, Pereira R. Buciumeanu, M, Carvalho O, Bartolomeu, F, Silva FS.** Effect of laser surface texturing on primary stability and surface properties of zirconia implants. *Ceramics International* 2017; 43(17):15227-15236.
- 48. Nguyen, Thi TP, Jeong OG, Pil LH, Dug YK, Won KJ, Thi VV, Chan P, Jae B, Yang S, Seo H, Won PS.** 2017. Evaluation of Sandblasting on

Mechanical Properties and Cell Response of Bioactive Glass Infiltrated Zirconia. *J. Nanosci. Nanotechnol.* 2017; 17(4):2740-2742.

- 49. Noro A, Kaneko M, Murata I, Yoshinari M. 2013.** Influence of surface topography and surface physicochemistry on wettability of zirconia (tetragonal zirconia polycrystal). *J Biomed Mater Res Part B* 2013;101B:355–363.
- 50. Osman R, Swain M V.** A critical Review of Dental Implant Materials with an Emphasis on Titanium *versus* Zirconia. *Materials* 2015; 8:932-958.
- 51. Oyane A, Kim HM, Furuya T, Kokubo T, Miyazaki T, Nakamura T.** Preparation and assessment of revised simulated body fluids. *J Biomed Mater Res A* 2003; 65A:188-195.
- 52. Ozkurt Z, Kazazoğlu E.** Zirconia dental implants: a literature review. *J Oral Implantol* 2011; 37 (3):367–376
- 53. Paes PNG, Bastian FL, Jardim PM.** The influence of Y-TZP surface treatment on topography and ceramic/resin cement interfacial fracture toughness. *Dent Mater* 2017; 33 (9):976-989.
- 54. Piconi C, Maccauro G.** Zirconia as a ceramic biomaterial. *Biomaterials* 1999; 20(1):1–25.
- 55. Ponche A, Biggerelle M, Anselme K.** Relative influence of surface topography and surface chemistry on cell response to bone implant

materials. Part 1: Physico-chemical effects. Proc Inst Mech Eng. 2010; 224: 1471–1486.

56. Ponche A, Bigerelle M, Anselme K. Relative influence of surface topography and surface chemistry on cell response to bone implant materials. Part II: Biological effects. Proc Inst Mech Eng. 2010; 224:1487–1507.

57. Queiroz JRC, Paulo GPM, Ozcan M, Nogueira Jr.L. “Effect of airborne particle abrasion protocols on surface topography of Y-TZP ceramic” *Ceramica* 2012; 58(346):253–261.

58. Rocchietta I, Fontana F, Addis A, Schupbach P, Simon M. Surface-modified zirconia implants: Tissue response in rabbits. *Clin. Oral Implants Res* 2009; 20: 844–850.

59. Roy M, Pompella A, Kubacki J, Piosik A, Psiuk B, Klimontko J, Szade J, Roy RA, Hedzelek W. Photofunctionalization of dental zirconia oxide: Surface modification to improve bio-integration preserving crystal stability. *Colloids and Surfaces B: Biointerfaces* 2017; 156:194–202.

60. Saini M, Singh Y, Arora P, Arora V, Jain K. Implant biomaterials: A comprehensive review. *World J Clin Cases* 2015; 3(1):52-57.

61. Sartoretto SC, Alves AT, Resende RF, Calasans-Maia J, Granjeiro JM, Calasans-Maia MD. Early osseointegration driven by the surface chemistry and wettability of dental implants. *J Appl Oral Sci* 2015; 23(3):279-287.

- 62. Schliephake H, Hefti T, Schlottig F, Gédet P, Staedt H.** Mechanical anchorage and peri-implant bone formation of surface-modified zirconia in minipigs. *J. Clin. Periodontol* 2010; 37: 818–828.
- 63. Sennerby L, Dasmah A, Larsson B, Iverhed M.** Bone tissue responses to surface-modified zirconia implants: A histomorphometric and removal torque study in the rabbit. *Clin Implant Dent Relat Res* 2005; 7(1): S13- 20.
- 64. Shibata Y, Tanimoto Y.** A review of improved fixation methods for dental implants. Part I: Surface optimization of rapid osseointegration. *J Prosthodont Res.* 2015; 59:20-33.
- 65. Strickstroek M, Rothe H, Grohmann S, Hildebrand G, Zylla I, Liefelth K.** 2017. Influence of surface roughness of dental zirconia implants on their mechanical stability, cell behavior and osseointegration. *BioNanoMat* 2017; 18(1-2): 1-13.
- 66. Tuladhar SL, Parajuli U, Wang H.** Response of MC3T3-E1 cells on microroughen bioactive glass coated zirconia. *JCMS Nepal* 2017; 13(3):350-356.
- 67. Tuna T, Wein M, Swain M, Fischer J, Atta W.** Effect of ultraviolet photofunctionalisation on the cell attractiveness of zirconia implant materials. *Eur Cell Mater* 2015; 29:82-96.

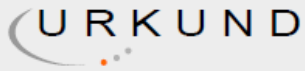
- 68. Tuna T, Wein M, Swain M, Fischer J, Atta W.** Influence of ultraviolet photofunctionalization on the surface characteristics of zirconia-based dental implant materials. *Dent Mater* 2015; 31:e14–e24.
- 69. Uchida, Kokubo T, Kawashita M, Neo M.** Apatite-Forming Ability of Zirconia / Alumina Composite Induced by Chemical Treatment. *J Biomed Mater Res* 2002; 60: 277–282.
- 70. Uchida M, Kim HM, Kokubo T, Fujibayashi S, Nakamura T.** Bonelike Apatite Formation Induced on Zirconia Gel in a Simulated Body Fluid and Its Modified Solutions. *J. Am. Ceram. Soc.* 2001; 84(9) 2041-2044.
- 71. Van Thi Vu, Gye-Jeong Oh, Kwi-Dug Yun, Hyun-Pil Lim, Ji-Won Kim, Thao Phuong Thi Nguyen, and Sang-Won Park.** Acid etching of glass-infiltrated zirconia and its biological response. *J Adv Prosthodont* 2017; 9(2): 104–109.
- 72. Wang G, Meng F, Ding C, Chu PK, Liu X.** Microstructure, bioactivity and osteoblast behavior of monoclinic zirconia coating with nanostructured surface. *Acta Biomater* 2009; 6:990-1000.
- 73. Wang X.-X., Yan W., Hayakawa S., Tsuru K., Osaka A.** Apatite deposition on thermally and anodically oxidized titanium surfaces in a simulated body fluid. *Biomaterials* 2003; 24:4631-4637.
- 74. Wennerberg A(1), Albrektsson T** On implant surfaces: a review of current knowledge and opinions. *Int J Oral Maxillofac Implants* 2010; 25(1):63-74.

- 75. Watanabe H, Saito K, Kokubun K, Sasaki H, Yoshinari M.** Change in surface properties of zirconia and initial attachment of osteoblast like cells with hydrophilic treatment. *Dent Mater J* 2012; 31: 806-814.
- 76. Wu CC, Wei CK, Ho CC and Ding SJ.** Enhanced Hydrophilicity and Biocompatibility of Dental Zirconia Ceramics by Oxygen Plasma Treatment. *Materials* 2015; 8:684-699.
- 77. Yan Y, Han Y.** Structure and bioactivity of micro-arc oxidized zirconia films *Surface & Coatings Technology* 2007; 201:5692–5695.
- 78. Yang Y, Zhou J, Liu X, Zheng M, Yang J, Tan J.** Ultraviolet light-treated zirconia with different roughness affects function of human gingival fibroblasts in vitro: The potential surface modification developed from implant to abutment. *J Biomed Mater Res Part B* 2015;103B:116-124.
- 79. Yoshida E, Hayakawa T.** Quantitative Analysis of Apatite Formation on Titanium and Zirconia in a Simulated Body Fluid Solution Using the Quartz Crystal Microbalance Method. *Advances in Materials Science and Engineering* 2017; 928379:1-9.
- 80. Zhang Y, Lawn BR, Rekow ED, and Thompson VP.** Effect of sandblasting on the long term performance of dental ceramics. *J. Biomed. Mater. Res. B Appl Biomater*; 71:381–386.

- 81. Zhang Z, Wang K, Bai C, Li X, Dang X, Zhang C.** The influence of UV irradiation on the biological properties of MAO-formed ZrO₂. *Colloids Surf B Biointerfaces* 2012; 89:40-47.
- 82. Zinelis S, Thomas A, Syres K, Silikas N, Eliades G.** Surface characterization of zirconia dental implants. *Dent. Mater.* 2010; 26:295–305.

ANNEXURE VII

PLAGIARISM REPORT



Urkund Analysis Result

Analysed Document: DOC PLAGIARISM.docx (D35079392)
Submitted: 1/28/2018 8:20:00 AM
Submitted By: agayathree@yahoo.com
Significance: 2 %

Sources included in the report:

EBINU.pdf (D34322169)
HA thesis.docx (D32588246)
Sakthipriya M.phil physics.docx (D30474385)
Prem Ananth. K.docx (D29710685)
janani plagiarism.docx (D34389163)
Ranjitha M.phil physics.docx (D30474531)

Instances where selected sources appear:

14